

# Machine Learning for Predicting Chaotic Systems

Christof Schötz<sup>\*1,2</sup>, Alistair White<sup>†1,2</sup>, Maximilian Gelbrecht<sup>‡1,2</sup>, and Niklas Boers<sup>§1,2,3</sup>

<sup>1</sup>Potsdam Institute for Climate Impact Research

<sup>2</sup>Technical University of Munich

<sup>3</sup>University of Exeter

## Abstract

Predicting chaotic dynamical systems is critical in many scientific fields, such as weather forecasting, but challenging due to the characteristic sensitive dependence on initial conditions. Traditional modeling approaches require extensive domain knowledge, often leading to a shift towards data-driven methods using machine learning. However, existing research provides inconclusive results on which machine learning methods are best suited for predicting chaotic systems. In this paper, we compare different lightweight and heavyweight machine learning architectures using extensive existing benchmark databases, as well as a newly introduced database that allows for uncertainty quantification in the benchmark results. In addition to state-of-the-art methods from the literature, we also present new advantageous variants of established methods. Hyperparameter tuning is adjusted based on computational cost, with more tuning allocated to less costly methods. Furthermore, we introduce the cumulative maximum error, a novel metric that combines desirable properties of traditional metrics and is tailored for chaotic systems. Our results show that well-tuned simple methods, as well as untuned baseline methods, often outperform state-of-the-art deep learning models, but their performance can vary significantly with different experimental setups. These findings highlight the importance of aligning prediction methods with data characteristics and caution against the indiscriminate use of overly complex models.

## Contents

<b>1</b>	<b>Introduction</b>	<b>2</b>
<b>2</b>	<b>Methodology</b>	<b>4</b>
2.1	Data . . . . .	4
2.1.1	DeebLorenz . . . . .	4
2.1.2	Dysts . . . . .	4
2.2	Prediction Task and Evaluation . . . . .	7
2.3	Estimation Methods . . . . .	8
2.4	Cumulative Maximum Error – CME . . . . .	10
2.5	Hyperparameter Tuning . . . . .	12
<b>3</b>	<b>Results and 10 Key Insights</b>	<b>12</b>
3.1	Lightweight Methods Outperform Heavyweight Methods . . . . .	13
3.2	Polynomial Fits to Noise-free Data Are Accurate Emulators . . . . .	13
3.3	Method Selection and Hyperparameter Optimization Are Essential . . . . .	13
3.4	Noise and Timestep Design Influence Absolute and Relative Performance . . . . .	20

<sup>\*</sup>math@christof-schoetz.de,  0000-0003-3528-4544

<sup>†</sup>alistair.white@tum.de,  0000-0003-3377-6852

<sup>‡</sup>maximilian.gelbrecht@tum.de,  0000-0002-0729-6671

<sup>§</sup>n.boers@tum.de,  0000-0002-1239-9034

3.5	Repeating Experiments is Crucial for a Robust Evaluation . . . . .	20
3.6	Evaluation Lacks Robustness When Only Assessing a Fixed System . . . . .	21
3.7	The Functional Form of a Parametric Method Should Fit the System . . . . .	21
3.8	Choosing the Right Variant of Propagators Improves Performance . . . . .	21
3.9	Using The Cumulative Maximum Error Is Advantageous . . . . .	22
3.10	Scarce Validation Data Can Lead to Over-Tuning . . . . .	22
<b>4</b>	<b>Conclusion</b>	<b>22</b>
<b>A</b>	<b>The Databases</b>	<b>25</b>
A.1	<i>Dysts</i> . . . . .	25
A.2	<i>DeebLorenz</i> . . . . .	25
<b>B</b>	<b>Methods</b>	<b>26</b>
B.1	Implementation . . . . .	26
B.2	Normalization . . . . .	26
B.3	Different Variants of Methods . . . . .	27
B.4	Hand-Tuning and Hyperparameter Grids . . . . .	27
B.5	<i>Analog</i> . . . . .	27
B.6	<i>Node1</i> , <i>Node32</i> . . . . .	27
B.7	<i>PgGp*</i> . . . . .	28
B.8	<i>PgNet*</i> . . . . .	28
B.9	<i>PgLl*</i> . . . . .	28
B.10	<i>Lin*</i> . . . . .	29
B.11	<i>LinPo4</i> , <i>LinPo6</i> , <i>LinPo4T</i> , <i>LinPo6T</i> . . . . .	29
B.12	<i>RaFe*</i> . . . . .	29
B.13	<i>Esn*</i> . . . . .	30
B.14	<i>Trafo*</i> . . . . .	30
B.15	<i>PwNn</i> . . . . .	30
B.16	<i>SpNn</i> . . . . .	31
B.17	<i>LlNn</i> . . . . .	31
B.18	<i>SpPo</i> . . . . .	31
B.19	<i>SpPo2</i> , <i>SpPo4</i> . . . . .	31
B.20	<i>SpGp</i> . . . . .	32
B.21	<i>GpGp</i> . . . . .	32
B.22	<i>SINDy</i> , <i>SINDyN</i> . . . . .	32
B.23	<i>Rnn*</i> , <i>Lstm*</i> , <i>Gru*</i> . . . . .	33
<b>C</b>	<b>On The Symmetric Mean Absolute Percent Error</b>	<b>33</b>
<b>D</b>	<b>Further Details of the Results</b>	<b>34</b>

# 1 Introduction

Chaos is a ubiquitous phenomenon in nature and technology, arising from nonlinearities, complex interactions, or feedbacks within the system [Ott02; Str24]. Predicting the behavior of such dynamical systems is a critical goal in many scientific disciplines. Chaotic systems are characterized by their sensitive dependence on initial conditions, making them notoriously difficult to predict and posing a significant challenge to researchers studying them.

A traditional approach to addressing this problem involves using domain knowledge to model the dynamical system. However, this approach requires detailed understanding of the specific system that is often not be available. In recent years, system-agnostic, data-driven approaches have emerged as a viable alternative. These methods, which leverage techniques from statistics and machine learning, are trained on observational data to predict the future behavior of the system.

These algorithms range from relatively simple and computationally inexpensive methods, such as fitting polynomials, to highly sophisticated models that utilize complex neural network architectures, demanding significant computational power for training. To evaluate these approaches, various comparison studies have been conducted.

For instance, [Han+21] focus on complex machine learning models with mostly classical neural network architectures. They do not include the sophisticated transformer model [Vas+17], which has gained popularity due to its effectiveness for large language models. Such models are surveyed in [Wen+23], where different variants of transformer models for time series forecasting are reviewed. Remarkably, [Zen+23] demonstrate how simple linear methods can outperform these complex models. Additionally, [Vla+20] compare reservoir computers (RCs) and recurrent neural networks (RNNs), favoring RNNs, whereas [SFC22] conduct a similar comparison, adding further machine learning methods and concluding that RCs are preferable.

Previous studies typically compare methods on a limited number of systems. However, [Gil21; Gil23] emphasize the need to use extensive databases and benchmarks to evaluate the performance of different methods. They introduce a database of more than 130 different chaotic dynamical systems and, in their comparison study, find that the sophisticated NBEATS method [Ore+20] performs best. Hyperparameter tuning in this study is minimal, despite its importance for algorithm performance.

All in all, there is no consensus in the literature on which method should be preferred. Even a distinction in the quality of results between lightweight and heavyweight methods is not clear. Apart from using only a few systems (and often different data in each study), the lack of robustness of existing comparisons may stem from an inherent randomness in the evaluations. The results of the error metrics used may vary when different initial conditions are applied. If experiments are repeated only a few times with randomly drawn initial conditions, the results may still not be robust. If there is only one trial, then uncertainty cannot even be judged.

With this work, we aim to address several questions left open in previous studies. We compare various lightweight and heavyweight algorithms, including simple statistical methods that have shown promising performance but have received limited attention [RH17]. We also present modifications of algorithms based on propagator map estimates, such as RCs, where we target the increment instead of the next state, and show the advantages of these for certain prediction tasks. We tune hyperparameters guided by the computational cost of each algorithm, allowing a broader exploration of hyperparameter sets for lightweight methods to facilitate a fairer comparison with heavyweight models.

As one source of synthetic data, we use the *Dysts* database of [Gil21], allowing tests on a wide range of chaotic systems and direct comparison with the results in [Gil23]. Additionally, we introduce a new database, *DeebLorenz*, which encompasses three variations of the well-known Lorenz63 system [Lor63], allowing for an easy comparison with other studies on the Lorenz63 system. Our database includes 100 repetitions of simulated time series for each system to increase the robustness of results and to allow uncertainty quantification. The database also features a nonparametric version of Lorenz63 to assess the performance of polynomial-based fitting algorithms on non-polynomial targets. All the systems studied have state-space dimensions ranging from 3 to 10, categorizing them as low-dimensional. Different observation schemes are used for each system to examine the impact of noise and time step intervals on performance. Furthermore, we propose a new error metric for forecasting tasks on dynamical systems, the cumulative maximum error (CME). It combines the benefits of integrated error metrics (as used in, e.g., [Gil23; God+21]) and measures of forecast horizon, such as the valid time [Ren+09; Pat+18].

Our study demonstrates significantly better performance of various tuned and untuned simple methods compared to complex machine learning models on forecasting tasks for low-dimensional chaotic systems. Additionally, we find that the relative performance of methods is highly dependent on the experimental setup, though some trends, such as the strong performance of simple methods, remain consistent. Notably, introducing random time steps between consecutive observations dramatically alters performance. In this case, a Gaussian process-based method [RW05; Hei+18] that ranks mid-tier under constant time steps, outperforms all other methods.

The remaining parts of the paper are structured as follows: Section 2 describes the databases, the forecasting task, the methods compared, the CME error metric, and the hyperparameter tuning. The results and key insights of the simulation study are described in Section 3, followed by a short

conclusion in Section 4. Appendix A provides additional details on the databases, followed by a discussion of the estimation methods in Appendix B. Finally, additional tables and plots detailing the simulation study results are available in Appendix D.

## 2 Methodology

### 2.1 Data

We use two different databases: *DeebLorenz*<sup>1</sup>, a database created specifically for this study, and the *Dysts* database<sup>2</sup> from [Gil21]. An overview of their structure is given in Figure 1, and further details are described below.

Both databases consist of solutions  $u: \mathbb{R} \rightarrow \mathbb{R}^d$  of autonomous, first-order ordinary differential equations (ODEs), i.e.,  $\dot{u}(t) = f(u(t))$ , where  $\dot{u}$  is the derivative of  $u$  and  $f: \mathbb{R}^d \rightarrow \mathbb{R}^d$  is the vector field of the ODE describing the dynamics of the system. All considered systems are chaotic, i.e., they exhibit a sensitive dependence on initial conditions, an aperiodic long-term behavior, and a fractal structure in the state space [Ott02; Str24].

The two databases are complementary in nature. *Dysts* consists of many different chaotic systems with only one time series per system and dataset, and only a rather small amount of samples per time series. *DeebLorenz* focuses on different versions of the Lorenz63 system, using multiple different observation schemes and an order of magnitude more samples per time series than *Dysts*. This allows for a more detailed case study of forecasting chaotic systems, specifically using the Lorenz63 system, and enables the investigation of the effects of different settings under directly comparable conditions. As 100 time series per system and observation scheme are available with randomly drawn initial conditions, system parameters, and noise values, an evaluation of methods can be made robust in a statistical sense. To obtain any kind of robustness in the evaluation using *Dysts*, we have to aggregate over all of its different systems, which makes the results depend strongly and somewhat obscurely on the systems chosen for *Dysts*.

#### 2.1.1 DeebLorenz

All three systems considered in *DeebLorenz* are related to the Lorenz63 system [Lor63], in which  $f: \mathbb{R}^3 \rightarrow \mathbb{R}^3$  is a sparse polynomial of degree 2 with 3 parameters. In LORENZ63STD, the parameters are fixed to their default values used in the literature. In LORENZ63RANDOM the parameters are drawn randomly. In LORENZ63NONPAR the parameters change with the state using a random nonparametric function drawn from a Gaussian process. See Figure 2 for examples of ground truth data from these systems. Notably, LORENZ63NONPAR introduces a novel approach to randomly sampling nonpolynomial dynamical systems, all of which appear to exhibit chaotic behavior.

The data are generated under different observation schemes: In all cases, initial conditions  $u(0)$  are drawn randomly from the attractor of the system. For times  $t_1, \dots, t_n \in [0, T]$ ,  $T \in \mathbb{R}_{>0}$ , the state  $u(t_i)$  is recorded either directly as  $Y_i = u(t_i)$  or with random measurement error  $\varepsilon_i$ , i.e.,  $Y_i = u(t_i) + \varepsilon_i$ . The observation times  $t_i$  either have a constant timestep so that  $t_i = iT/n$  or timesteps are drawn randomly from an exponential distribution  $t_{i+1} - t_i \sim \text{Exp}(\lambda)$ ,  $\lambda = n/T$ . All combinations of these timestep and measurement options make up the four different observation schemes for *DeebLorenz*.

For each combination of the three systems and four observation schemes, the generation of the training data  $(t_i, Y_i)_{i=1, \dots, n}$ ,  $t_i \in [0, T]$ , with  $n = 10^4$  (in expectation if time steps are random), and of the (noise-free) testing data  $(t_j, u(t_j))_{j=n+1, \dots, n+m}$ ,  $t_j \in [T, T+S]$ ,  $S \in \mathbb{R}_{>0}$ , with  $m = 10^3$ , is repeated with different random seeds to create a validation dataset (10 repetitions) and a testing dataset (100 repetitions). Further details can be found in Appendix A.2.

#### 2.1.2 Dysts

The *Dysts* [Gil21] database consists of 133 chaotic systems with dimensions between 3 and 10, observed with constant timesteps, i.e.,  $t_i = iT/n$ , and two different noise settings: one without

<sup>1</sup>Differential Equation Estimation Benchmark – Lorenz, available at <https://doi.org/10.5281/zenodo.12999941>

<sup>2</sup><https://github.com/williamgilpin/dysts>, [https://github.com/williamgilpin/dysts\\_data](https://github.com/williamgilpin/dysts_data)

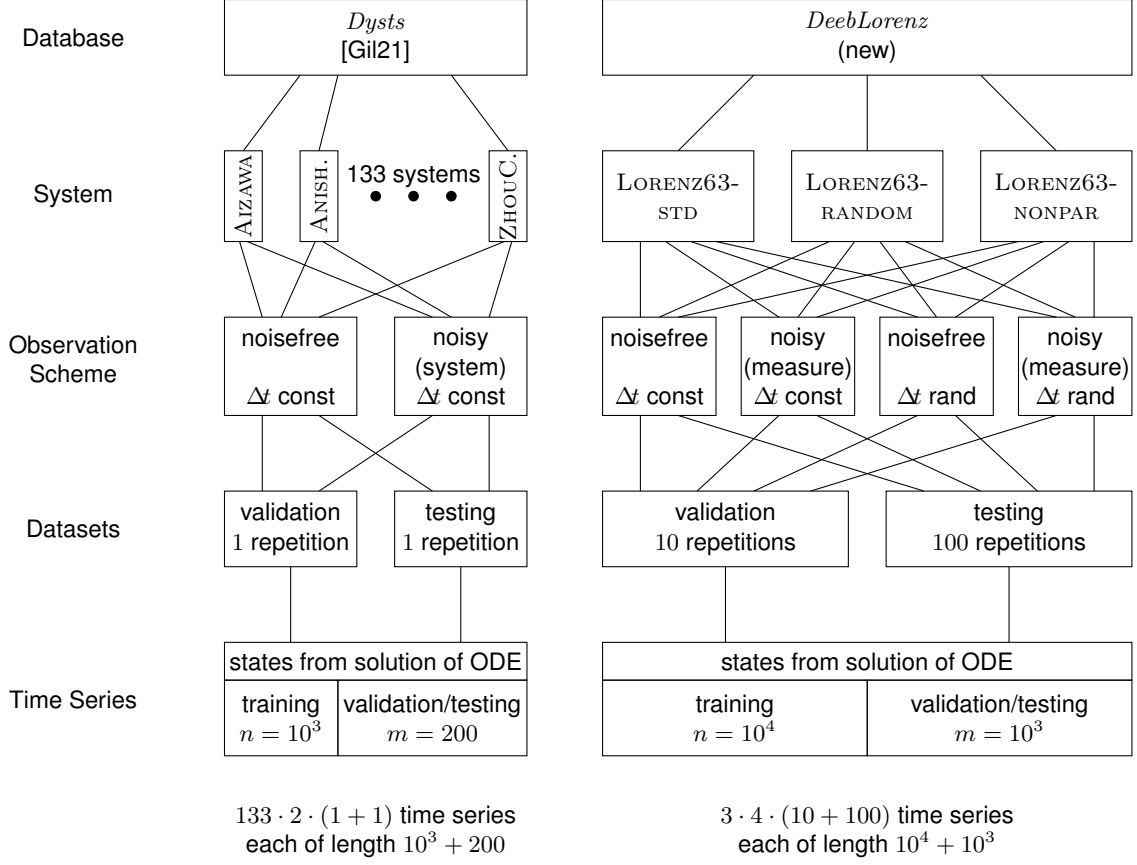


Figure 1: Visual overview over the databases used in this study. We consider two different databases, *Dysts* and *DeebLorenz*. Each database consists of different (dynamical) systems (133 for *Dysts*, 3 for *DeebLorenz*). Systems may come with parameters, including the initial conditions. After random initialization of the parameters, ground truth data is generated by solving the differential equations numerically. From ground truth data, we generate synthetic 'observation' time series using different observations schemes (with or without noise; constant or random timestep  $\Delta t$ ). In *Dysts*, noise is treated as system noise, i.e., it influences the evolution of the state of the system; in *DeebLorenz*, the noise is treated as measurement noise, i.e., the noisy data is observed but the system is evolved based on the ground truth. For each system and observation scheme, we create two different datasets: a validation dataset for hyperparameter tuning and a testing dataset for evaluation of performance. Each dataset consists of one (*Dysts*) or several (*DeebLorenz*) time series. Each time series is divided into two parts: the first part is designated as training data, while the second part serves different purposes depending on the dataset. For time series in the validation dataset, the second part is used as validation data, and for time series in the testing dataset, it is used as testing data. It is important to note that we use the terms 'testing' and 'validation' both to differentiate between datasets and to distinguish between data used for training and ground truth data to which the predictions are compared. In this setup, the training data from the validation dataset, the validation data from the validation dataset, the training data from the testing dataset, and the testing data from the testing dataset are all mutually exclusive.

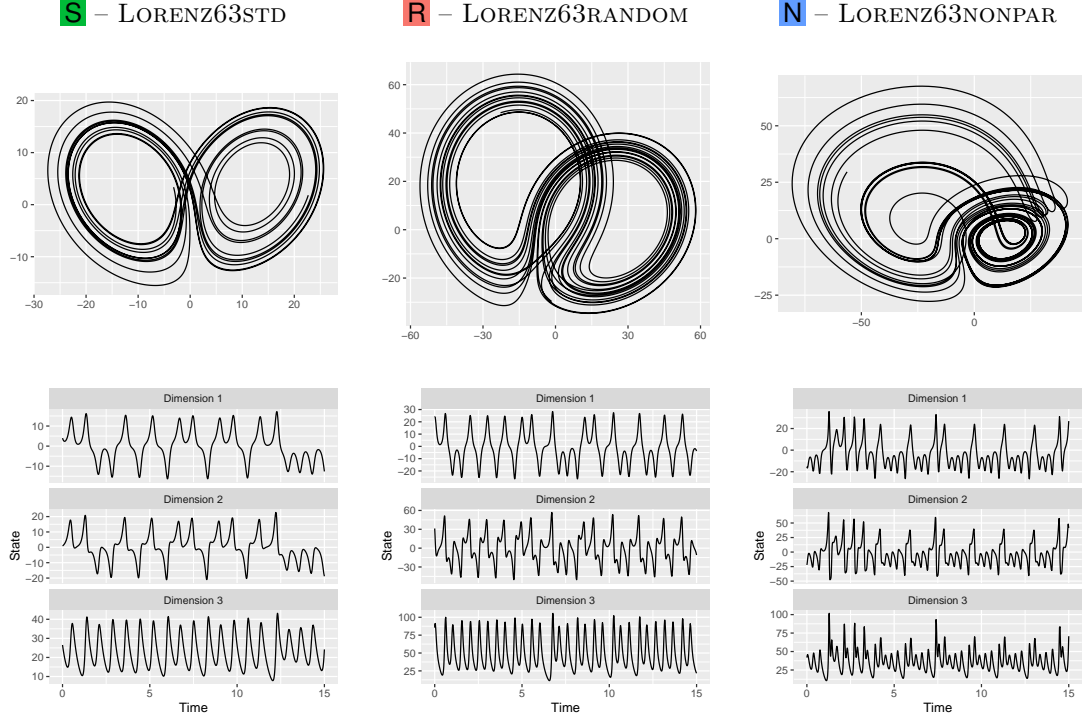


Figure 2: The three systems of the database *DeebLorenz*. The plots show one example of a ground truth for each of the systems for an interval of 15 time units. The top row illustrates the attractor for each system in a 2D-projection of the state space. The bottom row shows individual time series plots for the three dimensions of the state space. All three systems are related to the Lorenz63 system [Lor63], which can be described with a sparse polynomial of degree two as vector field  $f$ . The vector field  $f$  has three parameters, which are set to the default values found in the literature for LORENZ63STD. In LORENZ63RANDOM, for each time series, we sample those three parameters from a probability distribution centered around the default values. In LORENZ63NONPAR, the parameter values have a functional dependence on the state that, for each time series, is drawn randomly from a Gaussian process.

noise  $Y_i = u(t_i)$ ,  $\dot{u}(t) = f(u(t))$ ; the other with system noise, i.e.,  $Y_i = u(t_i)$  with

$$du(t) = f(u(t))dt + \sigma dB(t), \quad (1)$$

where  $B(t)$  is a standard Brownian motion and  $\sigma \in \mathbb{R}_{>0}$  is the scale of the noise. For both observation schemes, data are available in a validation dataset and a testing dataset, which each consist of one repetition of generated training data  $(t_i, Y_i)_{i=1, \dots, n}$  with  $n = 10^3$  and testing data  $(t_j, u(t_j))_{j=n+1, \dots, n+m}$  with  $m = 200$  for each of the 133 systems.

## 2.2 Prediction Task and Evaluation

For all systems, observation schemes, datasets, and repetitions, we impose the following task: Given the observations of the past,  $(t_i, Y_i)_{i=1, \dots, n}$  in the time interval  $t_i \in [0, T]$  (training time), and the true current state  $u(T)$ , predict the future states  $u(t_j)$  at given times  $t_j \in [T, T + S]$  (prediction time) for  $j = 1, \dots, m$ .

Allowing the forecasting methods to know the true current state  $u(T)$  — even in the case of otherwise noisy observations — eliminates the dependence of our simulation results on the (random) specific noise value of the final observation. This is crucial to increase the reliability of our comparison study, since prediction errors in chaotic systems typically grow exponentially with time. Additionally, it allows us to concentrate solely on the forecasting task (predicting future states) rather than on the data assimilation task (estimating the true value of a nosily observed state).

We apply and compare different statistical and machine learning methods on this task. The methods are described below in Section 2.3. For a given method, we first tune its hyperparameters on the validation dataset for each system individually: For each time series in the validation dataset, we train a given method and hyperparameter combination on the training data and calculate the error metrics described below on the validation data. We select the hyperparameter combination with the best (lowest) mean cumulative maximum error (CME, see Section 2.4), which creates the tuned method. Then, for each time series of the testing dataset, we judge performance the same way as in the validation dataset: We train the (tuned) method on the training data and create the predictions  $\hat{u}(t_j)$  for the prediction time. The predictions are compared with the ground truth  $u(t_j)$  using different metrics.

We calculate the following three metrics for comparing an estimate  $\hat{u}(t)$  with the ground truth  $u(t)$  in the prediction time  $t \in [T, T + S]$ :

- The *valid time*  $t_{\text{valid}}$ , e.g., [Ren+09; Pat+18], for a given threshold  $\kappa \in \mathbb{R}_{\geq 0}$  is defined as the duration such that the normalized error stays below  $\kappa$ , i.e.,

$$t_{\text{valid}}(\hat{u}, u) := \inf \left\{ t \in [T, T + S] \left| \frac{\|\hat{u}(t) - u(t)\|_2}{\text{sd}(u)} > \kappa \right. \right\} - T \quad (2)$$

where  $\|\cdot\|_2$  denotes the Euclidean norm and  $\text{sd}(u)$  is the standard deviation of  $u$  in the interval  $[T, T + S]$ , i.e.,

$$\text{sd}(u) := \sqrt{\frac{1}{S} \int_T^{T+S} \|u(t) - \mu(u)\|_2^2 dt}, \quad \mu(u) := \frac{1}{S} \int_T^{T+S} u(t) dt. \quad (3)$$

If the threshold is not reached, we set  $t_{\text{valid}} = S$ . In our evaluation, we set the threshold as  $\kappa = 0.4$ . Note that the normalization, i.e., division by  $\text{sd}(u)$ , is sometimes done differently in the literature: [Ren+09] do not integrate but normalize by  $\|u(t)\|_2$ , and [Pat+18] do not remove the mean  $\mu(u)$  in (3). However, only the version described in (2) and (3) is translation invariant, which is an advantage as described in Section 2.4 below.

- The *symmetric mean absolute percent error* sMAPE, e.g., [Gil23; God+21], is defined as

$$\text{sMAPE}(\hat{u}, u) := \frac{2 \cdot 100}{S} \int_T^{T+S} \frac{\|\hat{u}(t) - u(t)\|_2}{\|\hat{u}(t)\|_2 + \|u(t)\|_2} dt. \quad (4)$$

It is the standard mean absolute error, symmetrically normalized with respect to both the forecast and ground truth, and expressed as a percentage. A sMAPE of 0 represents a perfect forecast and a forecast that diverges to infinity approaches a sMAPE value of 200, see Appendix C.

- For this study, we design a new error metric, the cumulative maximum error CME. It is defined as

$$\text{CME}(\hat{u}, u) := \frac{1}{S} \int_T^{T+S} \max_{s \in [T, t]} \min \left( 1, \frac{\|\hat{u}(s) - u(s)\|_2}{\text{sd}(u)} \right) dt \quad (5)$$

with  $\text{sd}$  as in (3). It combines the advantages of  $t_{\text{valid}}$  and sMAPE, see Section 2.4 for details.

In practice, the canonical discrete-time versions of these metrics are applied, i.e., integrals are replaced by suitable sums.

## 2.3 Estimation Methods

We apply a wide range of different methods. Additionally, for the noise-free version of the *Dysts* database, we also include the methods evaluated in [Gil23] in our benchmark (pre-calculated predictions are not available for the noisy version). Names of these reference methods start with an underscore, e.g., `_NBEAT`. In this section, we provide a high-level description of the methods specifically applied for this study. A more detailed description can be found in Appendix B.

The methods can be separated into *propagators*, *recurrent architectures*, *solution smoothers*, and other methods that do not belong to any of the first three groups.

We start with the last category, which also contains our baselines:

- **ConstM** (*constant mean*, also called *climatology*): The prediction  $\hat{u}(t)$  is the constant mean of the observed states, i.e.,  $\frac{1}{n} \sum_{i=1}^n Y_i$ .
- **ConstL** (*constant last*, also called *persistence*): In our prediction task, the noise-free true state at time  $T$  is always available to the methods, even in an observation scheme with noise. For this method, we set  $\hat{u}(t) := u(T)$  for all  $t$ .
- **Analog**: For the method of the analog, we find the observed state  $Y_{i_0}$  with the closest Euclidean distance to  $u(T)$  and predict  $\hat{u}(T + k\Delta t) = Y_{i_0+k}$ , or a linear interpolation thereof if timesteps are not constant.
- **Node1, Node32**: For the neural ODE [Che+18], a neural network  $f_\theta$  is fitted to the data such that solving the ODE  $\dot{u}(t) = f_\theta(\hat{u}(t))$  minimizes the error  $\|\hat{u}(t_i) - Y_i\|_2$ .
- **Trafo, TrafoT**: A transformer network [Vas+17] is applied that uses attention layers to compute the next state from a sequence of previous states. The suffix **T** in **TrafoT** indicates that the timestep  $t_{i+1} - t_i$  is appended to the observation vector  $Y_i$ , which is relevant if timesteps are non-constant.

The methods **ConstM**, **ConstL**, and **Analog** can be treated as trivial baselines as no fitting or learning is required.

Next, we consider the group of *propagators*: For these methods, the basic idea is to find an estimate for the so-called propagator map

$$\mathcal{P}_{\Delta t}: u(t) \mapsto u(t + \Delta t) \quad \text{or equivalently} \quad \mathcal{P}_{\Delta t}: \mathbb{R}^d \rightarrow \mathbb{R}^d, x \mapsto u_x(\Delta t), \quad (6)$$

where  $u_x$  solves the initial value problem  $\dot{u}_x(t) = f(u_x(t))$ ,  $u_x(0) = x$ . This task can be formulated as a regression problem on the data  $(Y_i, Y_{i+1})_{i=1, \dots, n-1}$  assuming constant timesteps  $t_{i+1} - t_i = \Delta t$ . After the propagator is estimated, recursive application yields the predictions

$$\hat{u}(T + k\Delta t) = \underbrace{\mathcal{P}_{\Delta t}(\dots \mathcal{P}_{\Delta t}(u(T)) \dots)}_{k \text{ times}}. \quad (7)$$



All methods listed next are variations on this basic idea. Several of them come in different flavors marked by the suffix S, D, and/or T in their name: S indicates the next state as a target, see (6), whereas D means that the difference quotient

$$x \mapsto \frac{u_x(\Delta t) - x}{\Delta t} \quad (8)$$

is estimated and the prediction formula is adapted suitably. The latter approach is analogous to residual learning commonly used in the deep learning literature. If T is part of the suffix, the timestep  $t_{i+1} - t_i$  is available for the method as an input for the prediction of  $u(t_{i+1})$ . This is not useful for constant timesteps, but crucial for random timesteps. The symbol \* below indicates that a method is available in different variants denoted with the suffixes T, S, D, or a combination thereof.

- **PgGp\***, **PgNet\***, **PgLl\***: Fit  $\mathcal{P}_{\Delta t}$  with a Gaussian process [RW05], a feed-forward neural network [RHW86], or a local linear estimator [RW94], respectively.
- **Lin\***: The propagator  $\mathcal{P}_{\Delta t}$  is estimated via ridge regression [Has+09, chapter 3.4.1] using polynomial features. For a prediction of  $u(t_{i+1})$ , state values at times  $t_{i-sk}$ ,  $k = 0, \dots, K$  for a fixed  $s \in \mathbb{N}$  are available as inputs to the polynomial features. This method is also called a *nonlinear vector autoregressive model* [Gau+21].
- **LinPo4**, **LinPo6**, **LinPoLinPo4T**, **LinPo6T**: Tuning-free versions of **LinD** and **LinDT** with linear regression (ridge penalty parameter equal to 0), without past states as predictors ( $K = 0$ ), and with the polynomial degree fixed to 4 and 6, respectively.
- **RaFe\***: For *Random Features* [RR08], features are created from the predictors (the current state variables) by applying a once randomly created and untrained neural network. Then ridge regression [Has+09, chapter 3.4.1] is applied to estimate the mapping from features to targets (the next state).

The *recurrent architectures* are similar to the propagators, as they essentially also estimate the propagator map  $P_{\Delta t}$ . But instead of viewing the task purely as a standard regression problem, where the ordering of the data  $(Y_i, Y_{i+1})_{i=1, \dots, n-1}$  has no influence of the result, these methods keep an internal state that is updated while processing the data sequentially, ordered by time. The internal state influences the prediction of the next system state.

- **Esn\***: The Echo State Network (ESN) [Jae01] is a specific type of *reservoir computer*. It is similar to *Random Features*, but features of the previous timestep are also inputs for the feature calculation of the current timestep. This structure creates an internal state, allowing the ESN to retain memory of the information from previous inputs.
- **Rnn**, **RnnT**: The Recurrent Neural Network (RNN) [She20] has cyclic connections of neurons, allowing information from previous inputs to persist for future predictions.
- **Lstm**, **LstmT**: The Long Short-Term Memory network (LSTM) [HS97] is a variation of the standard RNN designed to capture long-term dependencies in sequential data by using gating mechanisms to regulate the flow of information and prevent issues like vanishing gradients.
- **Gru**, **GruT**: A Gated Recurrent Unit (GRU) [Cho+14] is a simplified variant of LSTM that uses gating mechanisms to control the flow of information, but with fewer parameters, making it more efficient while still addressing the vanishing gradient problem in sequential data.

The final category of methods are the *solution smoothers* [RH17, chapter 8]. In certain settings (that are slightly different from our experiments), these methods are shown to be optimal, see [Sch24, section 4] and [SS24, section 4]. Solution smoothers work in three steps: First, estimate  $u(t)$  in the observation time  $[0, T]$  with a regression estimator  $\hat{u}(t)$ . Then, view the data  $(\hat{u}(t), \dot{\hat{u}}(t))_{t \in [0, T]}$  as observations of  $(x, f(x))$  and use a second regression estimator to obtain an estimate  $\hat{f}$ . Lastly, solve the ODE  $\dot{u}(t) = \hat{f}(\hat{u}(t))$  on the time interval  $[T, T + S]$  with initial conditions  $\hat{u}(T) = u(T)$ .

- **PwNn**: The observed solution is interpolated with a piece-wise linear function  $\tilde{u}$ , from which  $\hat{f}$  is generated by a nearest neighbor interpolation.
- **SpNn**: As **PwNn**, but  $\tilde{u}$  is cubic spline interpolation [For+77].
- **L1Nn**: As **PwNn**, but  $\tilde{u}$  is local linear regression [Fan93].
- **SpPo**: As **SpNn**, but  $\hat{f}$  is ridge regression [Has+09, chapter 3.4.1] with polynomial features.
- **SpPo2**, **SpPo4**: Tuning-free version of **SpPo** with linear regression (ridge penalty parameter equal to 0) and with fixed polynomial degree 2 and 4, respectively.
- **SpGp**: As **SpNn**, but  $\hat{f}$  is Gaussian process regression [RW05].
- **GpGp**: As **SpGp**, but  $\tilde{u}$  is also Gaussian process regression. The method is similar to the one proposed in [Hei+18].
- **SINDy**, **SINDyN**: As **SpPo** without  $L_2$ -penalty, but sparsity is enforced for the polynomial  $\hat{f}$  via thresholding [BPK16]. As for all other methods, data normalization is applied before the actual estimation method for **SINDyN**. Only for **SINDy** it is turned off to not destroy potential sparsity in the original data. The name **SINDy** is short for *Sparse Identification of Nonlinear Dynamics*.

In the following, we will additionally classify the methods according to their central computational concept:

- **Direct**: Predictions for **ConstL**, **ConstM**, **Analog** are computed directly from the observations.
- **Gradient Descent**: **Node\***, **Trafo\***, **PgNet\***, **Rnn\***, **Lstm\***, **Gru\*** are trained using a variant of gradient descent.
- **Fit Propagator**: **Lin\***, **LinPo2**, **LinPo4**, **RaFe\***, **Esn\***, **PgGp\***, **PgLl\*** fit the propagator map by solving a system of linear equations.
- **Fit Solution**: **PwNn**, **SpNn**, **L1Nn**, **SpPo**, **SpPo2**, **SpPo4**, **SpGp**, **GpGp**, **SINDy**, **SINDyN** fit the solution and/or the vector field  $f$  by solving a system of linear equations.

## 2.4 Cumulative Maximum Error – CME

Although different error metrics are calculated to evaluate the results of this simulation study, we focus on the CME (5), which we newly introduce for this study. If time is discrete, (5) becomes

$$\text{CME}_m(\hat{u}, u) := \frac{1}{m} \sum_{j=1}^m \max_{k=1, \dots, j} \min \left( 1, \frac{\|\hat{u}(t_k) - u(t_k)\|_2}{\text{sd}_m(u)} \right). \quad (9)$$

where

$$\text{sd}_m(u) := \sqrt{\frac{1}{m} \sum_{j=1}^m \|u(t_j) - \mu_m(u)\|_2^2}, \quad \mu_m(u) := \frac{1}{m} \sum_{j=1}^m u(t_j). \quad (10)$$

Similar to the sMAPE, errors are integrated over time, and similar to  $t_{\text{valid}}$ , the time and error of the worst prediction so far are essential for the value of the overall error metric. The CME has many desirable properties:

- It is translation and scale invariant, in contrast to sMAPE and the version of the valid time used in [Ren+09; Pat+18], but similar to our definition of  $t_{\text{valid}}$ . This is desirable as every ODE system can be modified — without adding complexity — to create any translation and scaling of its solutions. Thus, the evaluation of an estimator  $\hat{u}$  should not depend on the location and scale of the system.

- (ii) We focus on a task that involves evaluating the precise state within a near-future time interval, as in weather forecasting. In contrast, one could also consider a task where the long-term behavior of the prediction should resemble the ground truth, without emphasizing the error at any single point in time, as in climate modeling. For the former task, predictive power deteriorates quickly over time due to the chaotic nature of the systems considered. Therefore, if the prediction interval  $[T, T + S]$  is long, we are primarily interested in the early times when accurate prediction is possible. Accurate predictions at the beginning of the interval should not be discounted by divergence at the end, where accurate predictions are not possible anyway. This requirement is captured by CME and, to some extent, by  $t_{\text{valid}}$ , but not by sMAPE.
- (iii) The value of the CME is always between 0 and 1, where 0 is only achieved by perfect prediction. In contrast, the scale of  $t_{\text{valid}}$  depends strongly on the system's time scale and the best value  $t_{\text{valid}} = S$  can be achieved for imperfect predictions.
- (iv) Dealing with missing values when calculating the CME is canonical: If  $\hat{u}(t)$  is not available for some  $t$ , we set the value of the minimum in (5) to 1. Consistently, if all of the prediction is missing, we set the CME to 1.
- (v) The CME is parameter-free in contrast to  $t_{\text{valid}}$ , where the threshold  $\kappa$  has to be specified.
- (vi) If time is discrete,  $t_{\text{valid}}$  can only attain a finite number of values. In contrast, for all values in  $[0, 1]$  there is a prediction  $\hat{u}$  such that  $\text{CME}_m(\hat{u}, u)$  attains this value. Furthermore,  $\hat{u}_1$  and  $\hat{u}_2$  may have the same  $t_{\text{valid}}$ , but  $\|\hat{u}_1(t) - u(t)\|_2 < \|\hat{u}_2(t) - u(t)\|_2$  for all  $t \in [T, T + t_{\text{valid}}]$ . If time is discrete, we can even have  $\|\hat{u}_1(t) - u(t)\|_2 < \|\hat{u}_2(t) - u(t)\|_2$  for all  $t \in [T, T + S]$  while  $t_{\text{valid}}(\hat{u}_1, u) = t_{\text{valid}}(\hat{u}_2, u)$ . This cannot happen with CME: If  $\|\hat{u}_1(t) - u(t)\|_2 < \|\hat{u}_2(t) - u(t)\|_2$  for all  $t \in [T, t^*]$  for some  $t^* > T$  and  $\|\hat{u}_1(t) - u(t)\|_2 \leq \|\hat{u}_2(t) - u(t)\|_2$  for all  $t \in [t^*, T + S]$ , we have  $\text{CME}(\hat{u}_1, u) < \text{CME}(\hat{u}_2, u)$ .

Let us also describe potential drawbacks of the CME.

- (i) The CME is not symmetric,  $\text{CME}(\hat{u}, u) \neq \text{CME}(u, \hat{u})$  in general, in contrast to sMAPE. But in our use case, the relationship between its two arguments  $\hat{u}$  and  $u$  is also not symmetric. Thus, there does not seem to be a benefit to symmetry.
- (ii) If  $u$  is constant, then  $\text{sd}(u) = 0$  and (5) is not valid. In this case, a reasonable definition is to set CME to 1 for all  $\hat{u}$  except the perfect prediction  $\hat{u} = u$  in which case 0 is the appropriate value. Note that  $t_{\text{valid}}$  (and to some extent sMAPE) also suffers from this *division by zero*-problem.
- (iii) If a prediction gets far away from  $u(t)$  but recovers at a later point in time, the recovery is not accredited in CME. As future states in our dynamical systems are independent of the past given the present (Markov property), a time point with a good forecast following a previous time point with a poor forecast should be considered spurious and attributed to chance rather than skill. This is especially true in chaotic systems, where the dependence of the future on the present is particularly strong. But note that the same distance  $\delta = \|\hat{u}(t_0) - u(t_0)\|_2$  can translate to different future predictability at times  $t > t_0$  for different states  $u(t_0) = x_1$  or  $u(t_0) = x_2$ ,  $x_1 \neq x_2$ . I.e., we can have

$$\|u_{x_1}(t) - u_{x_1'}(t)\|_2 \neq \|u_{x_2}(t) - u_{x_2'}(t)\|_2 \quad (11)$$

for  $t > t_0$  even if  $\|x_1 - x_1'\|_2 = \|x_2 - x_2'\|_2$ .

- (iv) On one hand, the value 1 in the min-term of (5) could be replaced by a threshold parameter  $\kappa$  as in  $t_{\text{valid}}$ , removing the advantage of being parameter-free for the CME. On the other hand,  $\kappa = 1$  is a natural choice for the CME (in contrast to  $t_{\text{valid}}$ ), as the trivial baseline **ConstM**,  $\hat{u}(t) = \frac{1}{n} \sum_{i=1}^n Y_i$ , achieves  $\|\hat{u}(s) - u(s)\|_2 / \text{sd}(u) = 1$  on average. Furthermore, for every constant prediction there is a finite time point  $s_0$  such that  $\|\hat{u}(s) - u(s)\|_2 / \text{sd}(u) \geq \kappa$  for  $\kappa = 1$ , and  $\kappa = 1$  is the largest value with this property.

- (v) The value of the CME depends on the testing duration  $S$  (similar to sMAPE, but in contrast to  $t_{\text{valid}}$ ). This could be mitigated by setting  $S = \infty$  and multiplying the integrand in (5) by a weighting function  $w(t - T)$ , e.g.,  $w(\tau) = \exp(-\alpha\tau)$ , but this introduces a new parameter choice  $\alpha \in \mathbb{R}_{>0}$ . To make the weighting choice-free and time-scale adaptive,  $\alpha$  needs to be set depending on  $u$ , e.g., to the inverse correlation time.

## 2.5 Hyperparameter Tuning

Each pair of a dynamical system and an observation scheme comes as a *validation* dataset and a *testing* dataset. For hyperparameter tuning only the *validation* dataset is used. Each such dataset consists of 1 (*Dysts*) or 10 (*DeebLorenz*) repetitions/time series. Each repetition consists of training and validation data.

For a given method  $\hat{u}_{\mathbf{a}}$  with hyperparameters  $\mathbf{a}$ , we train it, predict, and calculate the CME for different  $\mathbf{a}$ . Let us denote the average CME of all repetitions by  $\text{CME}(\mathbf{a})$  and the best hyperparameters among the tested ones as  $\mathbf{a}^* = \arg \min_{\mathbf{a}} \text{CME}(\mathbf{a})$ . Then  $\hat{u}_{\mathbf{a}^*}$  is applied to the testing dataset for the final results presented in Section 3. See Appendix B for a description of the tuned hyperparameters for each method.

To decide which hyperparameters  $\mathbf{a}$  to evaluate, we follow a local grid search procedure: For a given estimation method, decide on which parameters should be tuned  $\mathbf{a} = (a_1, \dots, a_\ell)$ . Each parameter  $a_j$  has a domain of possible values  $\mathcal{A}_j$ . The domain can be *categorical* or *scalar*. For categorical parameters, decide whether they are *persistent* (always evaluate all options) or *yielding* (only evaluate best). For scalar parameters, decide on a *linear* or *exponential scale* and a *stepsize*  $s_j \in \mathbb{R}_{>0}$ . Decide on finite sets of initial hyperparameter values  $A_{0,j}$ . Now, for step  $k \in \mathbb{N}_0$  in the optimization procedure, evaluate all elements of the grid of hyperparameters  $(a_1, \dots, a_\ell) \in A_{k,1} \times \dots \times A_{k,\ell}$  that have not been evaluated before. If there are none, stop the search. Denote the best hyperparameter combination evaluated so far as  $(a_{k,1}^*, \dots, a_{k,\ell}^*)$ . Generate  $A_{k+1,j}$  from  $a_{k,j}^*$  as follows: If the  $j$ -th variable is categorical, set  $A_{k+1,j} = A_{0,j}$  for persistent parameters and  $A_{k+1,j} = \{a_{k,j}^*\}$  for yielding ones. If the  $j$ -th variable is scalar, set  $A_{k+1,j} = \{a_{k,j}^* - s_j, a_{k,j}^*, a_{k,j}^* + s_j\} \cap \mathcal{A}_j$  if it has a linear scale and  $A_{k+1,j} = \{a_{k,j}^*/s_j, a_{k,j}^*, s_j a_{k,j}^*\} \cap \mathcal{A}_j$  if the scale is exponential.

The local grid search finds locally optimal hyperparameter combinations with a reasonable amount of evaluations assuming the number of tuned hyperparameters  $\ell$  is small enough. In this study, the algorithm is applied to  $\ell \leq 4$  hyperparameters to limit the computational costs. We tune more parameters in case of methods with low computational demand and limit to one categorical variable (no adaptive search) for the most expensive methods. See the main results Tables 1 to 3 in the next section (column **Tune**) for the computational cost of hyperparameter tuning. By adjusting the number of evaluated hyperparameters, we try to make the comparison fairer regarding total computational costs. The resulting total compute time can still be rather different between methods. This is partially due to the adaptive nature of the local grid search algorithm (i.e., the total number of predictions cannot be known beforehand) and partially due to the lack of meaningful tunable hyperparameters for some methods (in particular for very simple methods that typically have low computational costs). Furthermore, perfect fairness does not seem achievable, as the choice of hyperparameters to be tuned, the choice of initial hyperparameters, and the design of the scales all influence the result.

In contrast to our approach, [Gil23] tune one hyperparameter for each method, independent of computational cost. The parameter selected is always related to the number of past time series elements that are inputs for the prediction of the next step. Note that in theory only the current state is required to predict a future state (Markov property) if there is no measurement noise, and as long as one has access to all system variables.

## 3 Results and 10 Key Insights

Examples of training data and the prediction of the best methods are shown in Figure 3 for *DeebLorenz*. The results of the simulation study in terms of the error metric CME are depicted in Table 1 for *DeebLorenz* with constant timestep, in Table 2 for *DeebLorenz* with random timestep, and in Table 3 for the *Dysts* database. Additional details including score values and ranks for

the error metrics CME, sMAPE, and  $t_{\text{valid}}$  can be found in the appendix Tables 7 to 14. Finally, Figure 4 shows the results for noiseless and noisy test data with constant timestep  $\Delta t$  of system LORENZ63RANDOM from database *DeebLorenz*. Below, we describe 10 key insights these results provide. Further details on the results can be found in Appendix D.

### 3.1 Lightweight Methods Outperform Heavyweight Methods

In all settings, almost all of the best methods (top 5) are comparably simple (e.g., **SpPo**, **LinS**, **EsnS**) and have low computational costs, as they do not rely on gradient descent learning. In contrast, computationally more complex learning methods (e.g., **Node\***, **Trafo**, **Rnn**) perform rather poorly. The only exceptions are **Gru** and **Trafo** for the noisy *Dysts* data and **Node1** for LORENZ63RANDOM and LORENZ63NONPAR in the noisy setting with random time steps. Nonetheless, in these select cases, simple methods with similar or better performance are also available. See also Figure 4 for an illustration of this distinction on LORENZ63RANDOM with constant timestep. Furthermore, Table 17 shows that lightweight methods also outperform heavyweight methods under different sample sizes (at least on the system LORENZ63STD with constant timestep).

Even some of the tuning-free methods (**SpPo2**, **SpPo4**, **PwNn**, **SpNn**, **LinPo4**, **LinPo6**) have mostly lower errors than heavyweight algorithms. We recommend using at least some of these methods as baselines for tasks similar to those shown in this study, as these methods are conceptually simple, easy to implement, have negligible computational costs, and good performance.

Altogether, performance, computational demand, and implementation complexity clearly favor lightweight methods. This calls into question the use of complex machine learning algorithms for the prediction of low-dimensional chaotic dynamical systems.

### 3.2 Polynomial Fits to Noisefree Data Are Accurate Emulators

**LinPo6** applied to the noisefree data of LORENZ63STD delivers near-perfect forecasts, achieving a CME of  $6.6 \cdot 10^{-6}$  (see Table 7). This method employs a degree-6 polynomial to approximate the propagator map  $u(t) \mapsto u(t + \Delta t)$ . Our results are in line with the experiments on the Lorenz63 system shown in [Gau+21] from which **LinS** (fitting polynomial propagator with time-delay) is adapted, even though **LinPo6** does not use time delay. **LinS** achieves a CME of  $1.9 \cdot 10^{-4}$  in our setting.

While the vector field  $f$  of the ODE in LORENZ63STD is a degree-2 polynomial, the propagator map itself is not necessarily polynomial. However, since the propagator is derived from solving an ODE with smooth vector field, it is a smooth function. Taylor’s theorem ensures that polynomials can provide increasingly accurate approximations to such smooth functions. Note that we obtain our ground truth trajectory  $u(t)$  using a 4th order Runge-Kutta solver with constant solver timestep  $\Delta t/10$ , where  $\Delta t$  is the observation timestep, to ensure the higher order terms are present in  $u(t)$ . If we were to use the Euler method with solver timestep equal to  $\Delta t$  instead, the propagator would indeed be a degree-2 polynomial.

In Figure 5, we demonstrate that **LinPo6** performs essentially as well as directly solving the ODE for LORENZ63STD starting from initial conditions specified with 9 significant digits. This shows that **LinPo6** surpasses the accuracy of 32-bit single-precision machine arithmetic, which provides between 7 and 8 significant digits of accuracy. Moreover, as our simulation study stores data in CSV files with only 8 digits written after the decimal point, **LinPo6** is close to achieving the best possible accuracy given the limitations of the data (for noisefree LORENZ63STD).

### 3.3 Method Selection and Hyperparameter Optimization Are Essential

Compared to the results of [Gil23] (the method names starting with an underscore in Table 3), several of the methods considered here have much lower errors: For the noisefree *Dysts* data, the median CME of **\_NBEAT**, the best performing method in [Gil23], is 0.56. The lowest error achieved in our simulations is 0.0041 (**SpPo**, Table 14).

One reason for the improved performance is the more extensive hyperparameter tuning in our study compared to [Gil23], where only a single parameter was optimized for each method. For methods with low computational costs, we optimize several parameters. To illustrate the effect, we

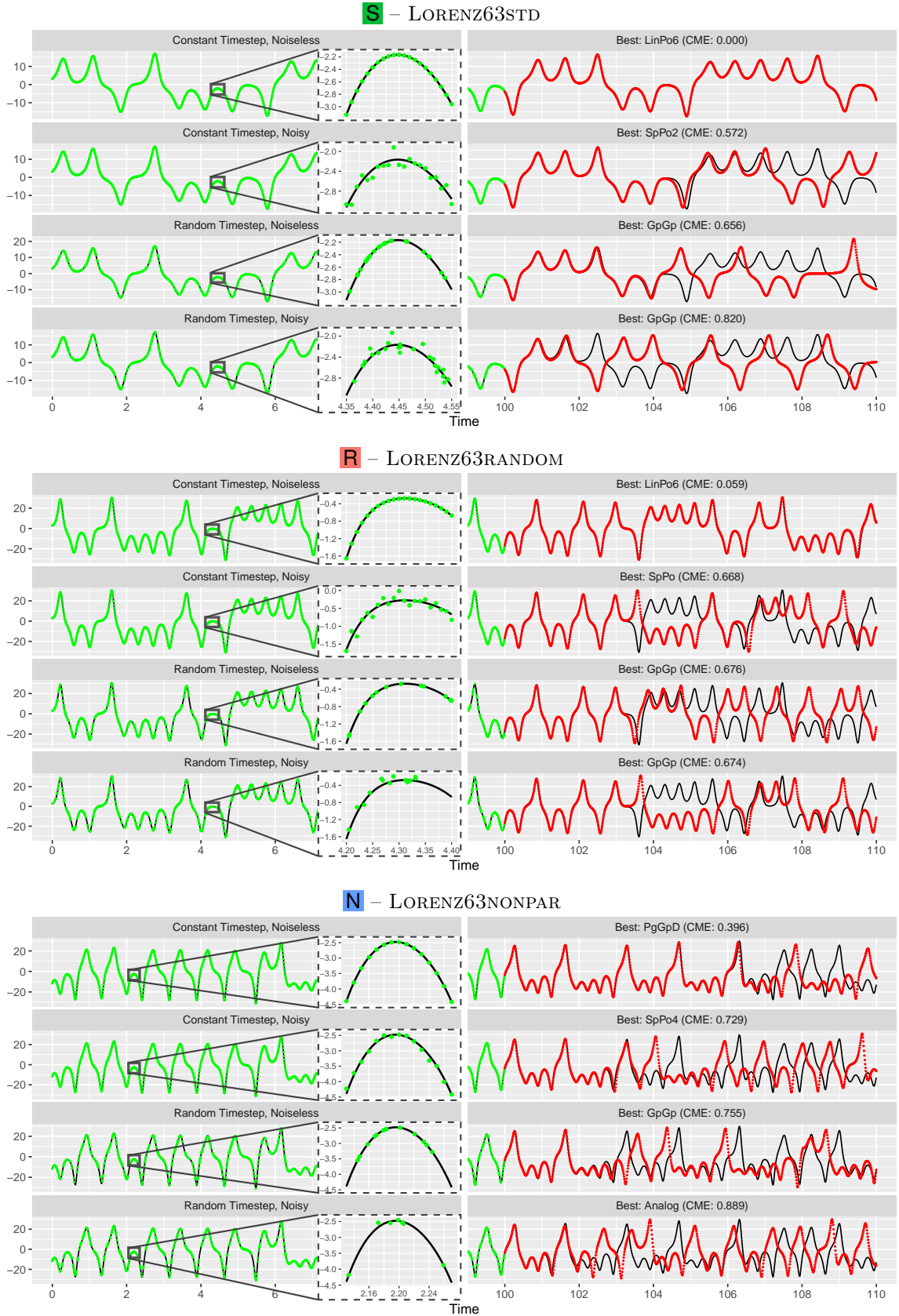


Figure 3: The plots show one example (out of 100) of train and test data from the testing dataset of *DeebLorenz*. Only the first state dimension (out of three) is shown. Observations are drawn in green, predictions of the best method in red, and the ground truth in black. As the noise is relatively small, a part of the observation time series is zoomed in to make it visible.

Cumulative Maximum Error for Test Data of *DeebLorenz* with Constant Timestep

Method				Compute		Noisefree						Noisy					
Name	Class	Model	Variant	Test	Tune	S#	R#	N#	0	CME 0.5	1	S#	R#	N#	0	CME 0.5	1
LinPo6	Fit Prop.	Lin	Poly6	1s		1	1	8				15	14	15			
LinD	Fit Prop.	Lin	D	7s	17m	2	3	2				4	5	6			
LinS	Fit Prop.	Lin	S	4s	17m	3	2	4				5	4	4			
SpPo4	Fit Solu.	Spline	Poly4	4s		4	6	14				9	3	1			
SpPo	Fit Solu.	Spline	Poly	5s	3m	5	5	7				2	1	5			
SINDy	Fit Solu.	SINDy		6s	51s	6	8	11				11	9	2			
SpPo2	Fit Solu.	Spline	Poly2	2s		7	9	28				1	1	26			
PgGpD	Fit Prop.	GP	D	9s	17m	8	4	1				14	20	19			
SINDyN	Fit Solu.	SINDy	norm	5s	1m	9	11	16				10	10	8			
LinPo4	Fit Prop.	Lin	Poly4	1s		10	15	15				13	13	12			
EsnD	Fit Prop.	ESN	D	5s	27m	11	13	9				8	6	7			
PgGpS	Fit Prop.	GP	S	15s	28m	12	7	3				24	18	17			
RaFeD	Fit Prop.	RandFeat	D	5s	27m	13	10	6				6	11	9			
EsnS	Fit Prop.	ESN	S	6s	32m	14	14	10				7	7	3			
RaFeS	Fit Prop.	RandFeat	S	5s	28m	15	12	5				3	8	11			
GpGp	Fit Solu.	GP	GP	19s	18m	16	17	13				12	12	10			
SpGp	Fit Solu.	Spline	GP	10s	3m	17	16	12				19	17	18			
PgNetD	Gr. Desc.	NeuralNet	D	7m	23m	18	20	17				22	26	22			
PgL1D	Fit Prop.	LocalLin	D	8s	5m	19	19	19				17	15	13			
PgL1S	Fit Prop.	LocalLin	S	8s	5m	20	18	18				16	16	14			
PgNetS	Gr. Desc.	NeuralNet	S	6m	11m	21	21	22				29	28	27			
L1Nn	Fit Solu.	LocalLin	NN	1m	9m	22	24	21				20	22	21			
SpNn	Fit Solu.	Spline		3s		23	22	20				25	21	20			
Node32	Gr. Desc.	NODE	bs32	11m	1h	24	23	26				21	23	24			
Pw1Nn	Fit Solu.	PwLin	NN	10s		25	26	23				23	24	23			
Node1	Gr. Desc.	NODE	bs1	1h	10h	26	25	25				27	25	25			
Analog	Direct	Analog		<1s		27	27	24				18	19	16			
Gru	Gr. Desc.	GRU		44m	2h	28	28	27				28	29	29			
Trafo	Gr. Desc.	Transformer		57m	4h	29	29	29				26	27	28			
Rnn	Gr. Desc.	RNN		14m	59m	30	30	31				31	30	31			
Lstm	Gr. Desc.	LSTM		46m	2h	31	31	30				30	31	30			
ConstL	Direct	Const	Last	<1s		32	32	32				32	32	32			
ConstM	Direct	Const	Mean	<1s		33	33	33				33	33	33			

Table 1: Results on the *DeebLorenz* database with constant timestep. In the first four columns, the methods are described by abbreviated names, their **Class** (Direct, Gradient Descent, Fit Propagator, Fit Solution), **Model** and **Variant** (see Section 2.3). The average **Compute** time of the tuned method for training and testing on one time series (**Test**) and of hyperparameter tuning per time series (**Tune**) are shown. Missing tune times indicate methods that are not tuned. The last columns describe the results for each tuned method applied to the testing dataset based on the Cumulative Maximum Error (CME) with forecasting horizon  $S = 10$  system time units: S# (green), R# (red), N# (blue) indicate the rank of the mean CME over 100 repetitions for the systems LORENZ63STD, LORENZ63RANDOM, and LORENZ63NONPAR, respectively. The column right after the ranks shows plots of the mean CME of 100 repetitions, with 95% confidence intervals (color coded as in the rank column titles).

Cumulative Maximum Error for Test Data of *DeebLorenz* with Random Timestep

Method				Compute		Noisefree							Noisy						
Name	Class	Model	Variant	Test	Tune				CME						CME				
						S#	R#	N#	0	0.5	1	S#	R#	N#	0	0.5	1		
GpGp	Fit Solu.	GP	GP	19s	16m	1	1	1					1	1	2				
SpPo2	Fit Solu.	Spline	Poly2	2s		2	2	19					21	21	25				
SpPo4	Fit Solu.	Spline	Poly4	4s		3	4	3					20	19	24				
SpPo	Fit Solu.	Spline	Poly	5s	3m	4	3	6					22	20	23				
SINDy	Fit Solu.	SINDy		6s	53s	5	6	4					23	22	22				
SINDyN	Fit Solu.	SINDy	norm	5s	47s	6	8	5					24	24	21				
SpGp	Fit Solu.	Spline	GP	10s	3m	7	5	2					18	12	17				
PgGpDT	Fit Prop.	GP	DT	8s	32m	8	7	8					28	28	28				
LinDT	Fit Prop.	Lin	DT	4s	6m	9	14	12					25	30	20				
LinPo4T	Fit Prop.	Lin	Poly4T	1s		10	10	10					29	26	30				
LinPo6T	Fit Prop.	Lin	Poly6T	2s		11	12	18					32	31	26				
EsnDT	Fit Prop.	ESN	DT	5s	28m	12	17	16					4	5	5				
PgNetDT	Gr. Desc.	NeuralNet	DT	6m	17m	13	13	11					26	25	29				
SpNn	Fit Solu.	Spline		3s		14	9	7					16	14	15				
PgL1DT	Fit Prop.	LocalLin	DT	7s	7m	15	18	15					30	29	31				
RaFeDT	Fit Prop.	RandFeat	DT	5s	27m	16	15	14					3	6	3				
Node1	Gr. Desc.	NODE	bs1	1h	9h	17	11	13					7	4	4				
LinST	Fit Prop.	Lin	ST	12s	12m	18	19	23					5	2	8				
PwLNn	Fit Solu.	PwLin	NN	10s		19	20	17					12	11	11				
PgGpST	Fit Prop.	GP	ST	15s	31m	20	21	22					10	8	7				
Analog	Direct	Analog		<1s		21	16	9					6	3	1				
L1Nn	Fit Solu.	LocalLin	NN	1m	9m	22	23	21					8	10	10				
PgNetST	Gr. Desc.	NeuralNet	ST	9m	23m	23	22	20					11	9	9				
RaFeST	Fit Prop.	RandFeat	ST	5s	30m	24	25	24					2	7	6				
PgL1ST	Fit Prop.	LocalLin	ST	9s	5m	25	24	26					13	16	14				
EsnST	Fit Prop.	ESN	ST	6s	29m	26	26	25					9	13	12				
TrafoT	Gr. Desc.	Transformer	T	1h	6h	27	28	28					15	17	16				
GruT	Gr. Desc.	GRU	T	44m	2h	28	27	27					14	15	13				
RnnT	Gr. Desc.	RNN	T	15m	58m	29	29	29					17	18	18				
LstmT	Gr. Desc.	LSTM	T	52m	2h	30	30	30					19	23	19				
ConstL	Direct	Const	Last	<1s		31	31	31					27	27	27				
ConstM	Direct	Const	Mean	<1s		32	32	32					31	32	32				

Table 2: Same as Table 1 but with the observation schemes that have random timesteps. Where applicable, we show the variants of the methods that incorporate the timestep as an input (marked with T). For the Neural ODE, we include only the variant with a batch size of 1 (**Node1**) and exclude the variant with a batch size of 32 (**Node32**). This exclusion is due to the requirement of equal computational steps across all elements within a batch, which is not feasible when varying timesteps are used.



Cumulative Maximum Error for Test Data of *Dysts*

Method				Compute		Noisefree				Noisy					
Name	Class	Model	Variant	Test	Tune	#	medi	CME			#	medi	CME		
								0	0.5	1			0	0.5	1
SpPo	Fit Solu.	Spline	Poly	3s	2m	1	0.00				9	0.78			
LinS	Fit Prop.	Lin	S	<1s	49s	2	0.01				6	0.77			
LinD	Fit Prop.	Lin	D	<1s	48s	3	0.01				8	0.77			
SpPo4	Fit Solu.	Spline	Poly4	5s		4	0.01				21	0.85			
RaFeD	Fit Prop.	RandFeat	D	<1s	3m	5	0.02				19	0.84			
EsnD	Fit Prop.	ESN	D	1s	3m	6	0.02				1	0.73			
RaFeS	Fit Prop.	RandFeat	S	<1s	3m	7	0.03				15	0.80			
EsnS	Fit Prop.	ESN	S	1s	4m	8	0.03				3	0.76			
SINDy	Fit Solu.	SINDy		2s	3m	9	0.03				24	0.87			
LinPo4	Fit Prop.	Lin	Poly4	<1s		10	0.04				20	0.84			
SINDyN	Fit Solu.	SINDy	norm	2s	4m	11	0.12				25	0.87			
LinPo6	Fit Prop.	Lin	Poly6	2s		12	0.19				29	0.91			
SpPo2	Fit Solu.	Spline	Poly2	1s		13	0.21				10	0.79			
PgGpD	Fit Prop.	GP	D	3s	48s	14	0.22				26	0.88			
PgNetD	Gr. Desc.	NeuralNet	D	1m	4m	15	0.26				12	0.80			
Gru	Gr. Desc.	GRU		4m	19m	16	0.40				2	0.75			
Node1	Gr. Desc.	NODE	bs1	19m	1h	17	0.42				7	0.77			
Node32	Gr. Desc.	NODE	bs32	4m	29m	18	0.44				13	0.80			
PgGpS	Fit Prop.	GP	S	2s	47s	19	0.44				23	0.86			
PgNetS	Gr. Desc.	NeuralNet	S	1m	2m	20	0.46				11	0.80			
SpGp	Fit Solu.	Spline	GP	3s	35s	21	0.54				30	0.92			
_NBEAT	Dysts	NBEATS				22	0.56								
PgL1S	Fit Prop.	LocalLin	S	3s	10s	23	0.57				16	0.81			
Analog	Direct	Analog		<1s		24	0.60				17	0.81			
PwLnn	Fit Solu.	PwLin	NN	1s		25	0.60				18	0.83			
PgL1D	Fit Prop.	LocalLin	D	3s	10s	26	0.61				14	0.80			
SpNn	Fit Solu.	Spline		1s		27	0.62				22	0.85			
Rnn	Gr. Desc.	RNN		2m	7m	28	0.62				5	0.77			
Trafo	Gr. Desc.	Transformer		13m	1h	29	0.63				4	0.77			
GpGp	Fit Solu.	GP	GP	3s	2m	30	0.64				28	0.90			
_RaFo	Dysts	RandForest				31	0.69								
_NHITS	Dysts	NHiTS				32	0.70								
LlNn	Fit Solu.	LocalLin	NN	6s	19s	33	0.73				27	0.88			
_RNN	Dysts	RNN				34	0.76								
_Node	Dysts	NeuralOde				35	0.79								
_Esn	Dysts	Esn				36	0.79								
_Nvar	Dysts	Nvar				37	0.80								
_XGB	Dysts	XGB				38	0.81								
_Trafo	Dysts	Transformer				39	0.81								
_LinRe	Dysts	LinearReg				40	0.84								
_NLin	Dysts	NLinear				41	0.88								
_BlRNN	Dysts	BlockRNN				42	0.90								
_DLin	Dysts	DLinear				43	0.90								
Lstm	Gr. Desc.	LSTM		5m	16m	44	0.91				32	0.96			
_TCN	Dysts	TCN				45	0.94								
ConstL	Direct	Const	Last	<1s		46	0.96				31	0.96			
_Kalma	Dysts					47	0.98								
ConstM	Direct	Const	Mean	<1s		48	1.00				33	1.00			

Table 3: Results on the *Dysts* database. In the first four columns, the methods are described by abbreviated names, their **Class** (Direct, Gradient Descent, Fit Propagator, Fit Solution), **Model** and **Variant** (see Section 2.3). The average **Compute** time of the tuned method for training and testing (**Test**) and of hyperparameter tuning (**Tune**) are shown. For results from [Gil23] (class **Dysts**) this information is not available. For all other rows, missing tune times indicate methods that are not tuned. The last columns describe the results for each tuned method applied to the testing dataset, based on the Cumulative Maximum Error (CME) with forecast horizon of  $m = 200$  timesteps: # indicates the rank of the median (**medi** and black vertical line) over all systems. Each colored point corresponds to one system of *Dysts*. The colors are chosen according to the median CME over all applied methods.

Cumulative Maximum Error for Test Data of LORENZ63RANDOM with Constant Timestep

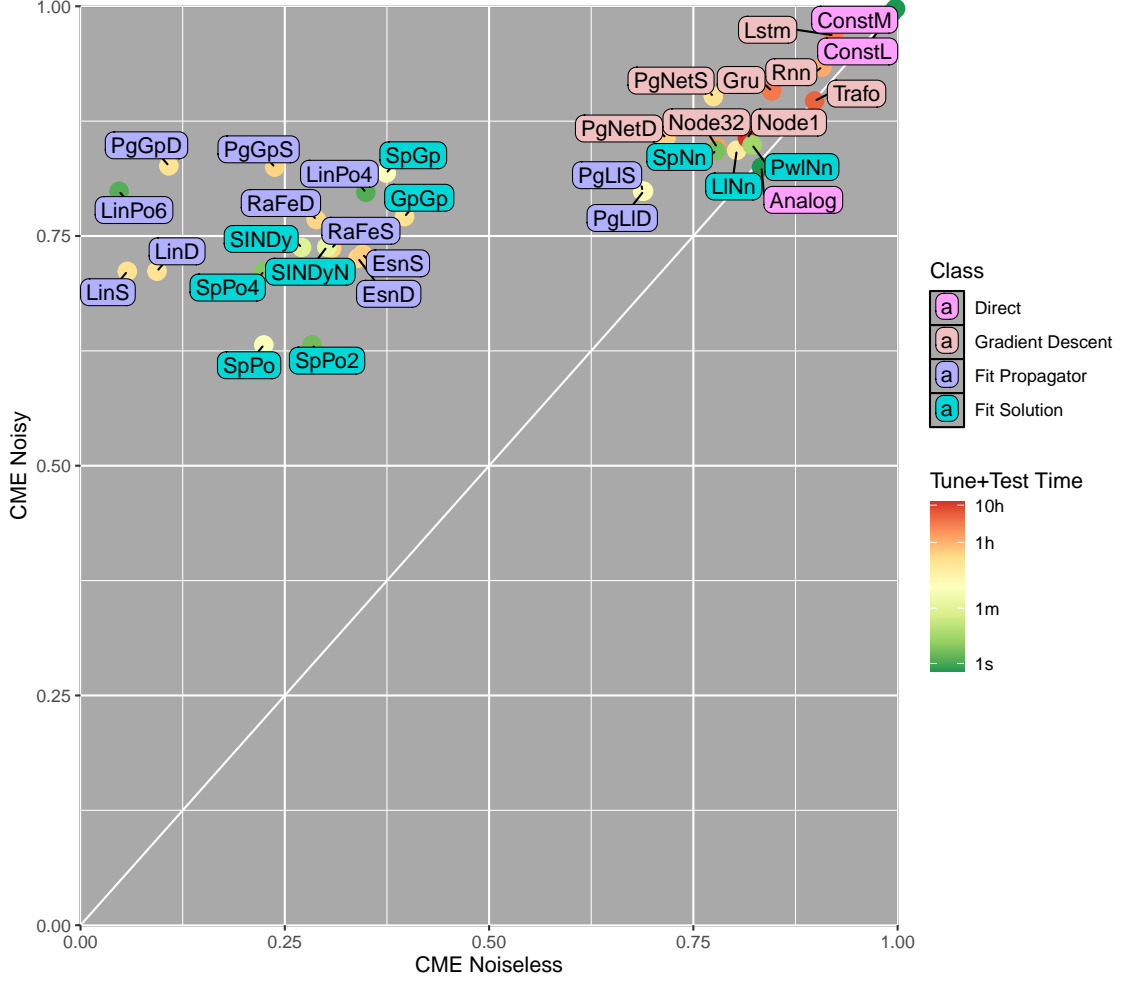
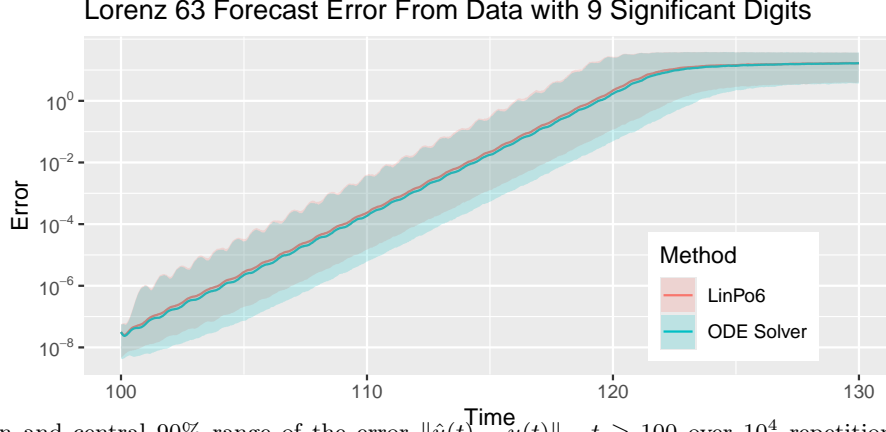
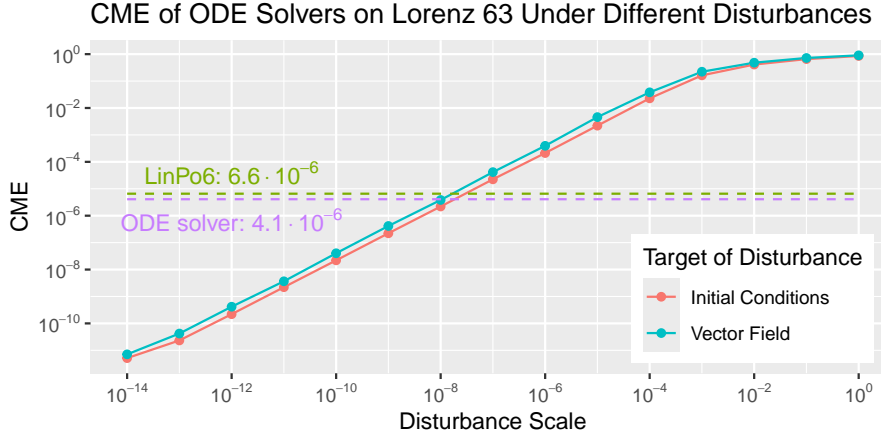


Figure 4: The Cumulative Maximum Error (CME) for noiseless and noisy test data with constant timestep  $\Delta t$  of system LORENZ63RANDOM from database *DeebLorenz*. The dots are colored according to the sum of average tune and test time of the respective method. Distance to the diagonal indicates sensitivity to noise. The plot shows clustering into a low error and a high error cluster, where all gradient descent based methods are in the high error group. The respective plots for the remaining system and timestep setting combinations are in the appendix, see Figures 9 to 13. Only some of them show a similarly clear clustering.



(a) Median and central 90% range of the error  $\|\hat{u}(t) - u(t)\|_2$ ,  $t \geq 100$  over  $10^4$  repetitions. The true trajectory  $u(t)$  is generated by a RK4 ODE solver (with constant timestep  $10^{-1}\Delta t$ ) with full double-precision accuracy (64 bit), starting from a random point on the attractor of LORENZ63STD and using the exact LORENZ63STD vector field. For the red curve,  $\hat{u}(t)$  is computed using a degree-six polynomial propagator (LinPo6) trained on  $\bar{u}(t_i)$  with  $i \in \{1, \dots, 10^4\}$ ,  $t_i = i\Delta t$ ,  $\Delta t = 10^{-2}$ . Here,  $\bar{u}(t_i)$  is obtained by rounding  $u(t_i)$  to 9 significant digits. Forecasting begins at  $t_n = 100$  with initial conditions  $\bar{u}(t_n)$ . For the blue curve,  $\hat{u}(t)$  is obtained by applying a RK4 ODE solver (double-precision) to the true LORENZ63STD vector field, starting from the same initial conditions  $\bar{u}(t_n)$ . The nearly identical errors of the polynomial propagator and the ODE solver demonstrate that at 9-digit accuracy, LinPo6 effectively emulates the ODE solver on the LORENZ63STD system.



(b) The Cumulative Maximum Error  $\text{CME}(\hat{u}, u)$  on a time range  $[0, S]$  with  $S = 10$  of LORENZ63STD for ODE solvers (median over  $10^3$  repetitions). The true trajectory  $u(t)$  is generated by a RK4 ODE solver (with constant timestep  $10^{-1}\Delta t$ ) with full double-precision accuracy (64 bit), starting from a random point on the attractor of LORENZ63STD and using the exact vector field. For the red curve,  $\hat{u}(t)$  is obtained by applying a RK4 ODE solver (double-precision) to the true LORENZ63STD vector field, starting from  $u(0) + \delta$ . Here,  $\delta$  is drawn uniformly at random from the sphere in  $\mathbb{R}^3$  centered at the origin with a radius specified on the  $x$ -axis. For the blue curve,  $\hat{u}(t)$  is obtained by applying a RK4 ODE solver (double-precision) to the true initial conditions  $u(0)$  with a perturbed version of the LORENZ63STD vector field. The perturbed dynamics are created by modifying the three parameters of LORENZ63STD,  $(\hat{\sigma}, \hat{\rho}, \hat{\beta}) = (\sigma, \rho, \beta) + \delta$ , where  $\sigma = 10$ ,  $\rho = 28$ ,  $\beta = 8/3$ , see Appendix A.2. Again,  $\delta$  is drawn uniformly at random from the sphere in  $\mathbb{R}^3$  with the radius specified on the  $x$ -axis. In our noise-free settings, all methods have only access to a rounded version  $\bar{u}(t)$  of  $u(t)$ , as we only write 8 digits after the decimal point in the CSV files that contain the training, validation, and testing data. The purple dashed line indicates the CME of a RK4 ODE solver applied to initial conditions from such a file format and using the true LORENZ63STD vector field. For comparison, the green dashed line shows the CME of LinPo6, the best performing method on LORENZ63STD.

Figure 5: Comparison between polynomial fit and ODE solver.

compare the median CME (in parenthesis) for selected methods on the noise-free testing dataset from *Dysts*, as shown in Table 3 and Table 14: The Nonlinear Vector Autoregression `_Nvar` (0.80) and the Echo State Network `_Esn` (0.79) from [Gil23] are essentially the same as our `LinS` (0.0054) and `EsnS` (0.030), respectively. Our simulations yield a median CME that is orders of magnitude lower than for the corresponding methods in [Gil23]. This indicates that optimizing key hyperparameters is critical for achieving good performance in these methods.

But note that `SpPo4` and `LinPo4` are tuning-free methods and achieve median CME’s of 0.0079 and 0.040, respectively. Furthermore, from all methods of [Gil23], only `_NBEAT` outperforms the baseline method `Analog`. This highlights the critical role of selecting appropriate methods and baselines for a given task.

### 3.4 Noise and Timestep Design Influence Absolute and Relative Performance

In the absence of noise, forecasting becomes an interpolation task, whereas noisy observations yield a regression problem. Generally, as expected, performance degrades across methods strongly when noise is added to the observations. Moreover, methods that are best for the noise-free interpolation task are typically not the best for the noisy regression task. This distinction is evident when comparing the noise-free and noisy columns in Tables 1 to 3.

The Echo State Network `Esn*` has access to states of the past, whereas the otherwise similar method Random Features `RaFe*` does not. Because of the Markovian nature of our dynamical systems, knowledge of the past is not required in the noise-free case as the next state is equal to the (true) propagator applied to the current state. This is reflected in our simulation results, where `RaFe*` tends to perform better than `Esn*` in noise-free settings and vice versa for the settings with measurement noise. As the noisy systems of *Dysts* are created with system noise, they are Markovian. Surprisingly, the `Esn*` seems to be at an advantage over `RaFe*` here, too.

Under noise, the lower degree polynomial solution smoother `SpPo2` performs relatively better than the higher degree polynomial `SpPo4`, and vice versa in the noise-free case. Overfitting to noise, which cannot happen in the noise-free case, seems to be the reason for this observation.

There is a noticeable difference in performances of methods between fixed and random timesteps (Tables 1 and 2). Generally, random timesteps for the training data make forecasting (at fixed timesteps) more difficult. But also the ranking of methods according to their CME changes: The Gaussian process based method `GpGp` takes the lead for random timesteps. For fixed timesteps, this method is only mediocre.

As expected, propagator methods that do not have the timestep as an input, do not fare well if the timestep is not constant. With the additional knowledge of the timestep (`*ST` and `*DT`), the performance improves (Table 15).

The combination of a random timestep with noisy observations seems to make the learning task extremely difficult. In the case of `LORENZ63RANDOM`, only `GpGp` (Gaussian process based solution smoother) and `LinST` (ridge regression fit of polynomial propagator) have better scores than the baseline `Analog`. For `LORENZ63NONPAR` no method beats `Analog`.

### 3.5 Repeating Experiments is Crucial for a Robust Evaluation

As there is only one time series per system available in the *Dysts* database, reported differences between the performance of methods might not be robust on the same system. Furthermore, confidence intervals based on the results on the 133 systems are hard to justify as one typically has to assume an independent, identical distribution of the considered values, whereas the selection of the specific systems for *Dysts* was a deterministic non-independent process. But note that the code for generating more data for *Dysts* is available at the respective repository.

In contrast, for *DeebLorenz*, experiments for the same system and observation scheme are repeated 100 times with randomly drawn initial conditions, noise values, and timesteps (if applicable). This allows us to judge whether reported differences in CME values are statistically significant. In Figure 7, we visualize the results of paired *t*-Tests for the null hypothesis  $\text{CME}(\text{Method1}) \geq \text{CME}(\text{Method2})$ . If the null can be rejected, it shows that `Method1` is significantly better `Method2` on the given system with the given observation scheme using the CME as error metric. We see

that the ranking of the algorithms as shown in Table 10 is mostly robust up to permutation of two or three consecutive ranks. In comparison, Figure 8 shows that only 10 repetitions would yield largely indistinguishable performances.

All in all, it seems prudent to repeat experiments to obtain more reliable results and be able to judge the confidence of these results.

### 3.6 Evaluation Lacks Robustness When Only Assessing a Fixed System

Although LORENZ63STD and LORENZ63RANDOM share the same functional form of the vector field  $f$ , differing only in their polynomial coefficients, the absolute errors and relative rankings of methods vary significantly between the two systems (Tables 1 and 2).

Tuning for LORENZ63RANDOM (and LORENZ63NONPAR) is hard in that the tuned hyperparameters must perform well across varying, randomly chosen system parameters. In contrast, LORENZ63STD has fixed dynamics, allowing not only the functional form of  $f$  but also the specific polynomial coefficients to be (partially) inferred during tuning.

Thus, a low error value for LORENZ63RANDOM is a more robust indicator of a method’s ability to generalize than a low error value for LORENZ63STD.

### 3.7 The Functional Form of a Parametric Method Should Fit the System

Most systems in *Dysts* and all systems but LORENZ63NONPAR in *DeebLorenz* have a vector field  $f$  that is a polynomial of low degree. Thus, it is not surprising that methods based on this assumption, such as SpPo (polynomial solution smoother) and SINDy (similar to SpPo, but assumes sparsity of target polynomial), perform well on these tasks. Note that a polynomial vector field  $f$  does not imply that the propagator  $\mathcal{P}_{\Delta t}$  for a given timestep  $\Delta t$  is also polynomial. Still, there might be a reasonable polynomial approximation, which would explain the good performance of Lin\* (ridge regression fit of polynomial propagator).

For LORENZ63STD and LORENZ63RANDOM, the vector field  $f$  is a quadratic polynomial. For these systems SpPo2, which fits such a polynomial, works very well (when excluding the extremely difficult combination of random timesteps and noisy observations). But the method shows poor performance for the non-polynomial LORENZ63NONPAR. The same is true in the noise-free, constant timestep setting for methods that can fit higher degree polynomials (SpPo, SpPo4, SINDy, SINDyN). In the noisy setting, where performance in general is worse, this effect is not visible, likely as a polynomial approximation (Taylor’s theorem) is accurate enough relative to the other methods.

The method SINDyN (with normalization) is usually worse than SINDy. This makes sense, as many systems studied here have sparse polynomial dynamics and normalization (which in our case includes a rotation) destroys sparsity.

All in all, low degree polynomial approximation works only well if the target function can be described sufficiently well as such a polynomial. Inherently nonparametric methods, such as GpGp or PgGp\*, which both fit Gaussian processes, seem to be more suitable if the target is non-polynomial.

### 3.8 Choosing the Right Variant of Propagators Improves Performance

As expected, the errors of propagators with and without timestep input (\*T, Table 15) are similar when the timestep is constant. An exception is observed with LinD, LinPo4, and LinPo6, which fit a polynomial propagator using ridge regression, in the noise-free case, where performance degrades when the timestep is (unnecessarily) included as an additional input. This decline is likely due to numerical issues arising from co-linear predictors. For random timesteps, however, providing timestep information improves the results in most cases.

Between the state (\*S\*) and the difference quotient (\*D\*) versions of the propagator estimators (Table 16), there is no clear overall winner. However, in the case of random timesteps without noise, difference-quotient based methods consistently yield lower errors. This may be due to the reduced dependence of the target on the timestep when estimating the difference quotient. Additionally, both PgGp\* and PgNet\*, which fit the propagator map using a Gaussian process and a neural network, respectively, exhibit a clear preference for the difference quotient as the target (except in the noisy setting with random timesteps).

To explain this preference, note that system states change smoothly over time, so one-step-ahead predictions should be close to persistence (where future states equal the current state). When the target is the state, persistence is achieved by the identity function as the propagator. When the target is the difference quotient, persistence corresponds to the constant zero function. The Gaussian Process **PgGp\*** has a prior centered at zero, biasing it toward persistence in the difference quotient setup. In contrast, when the state is the target, its predictions are biased toward the mean of observations (climatology), as the input data is normalized. For the neural network **PgNet\***, the constant zero function is easier to learn since only the weights in the last layer need suitable values, while the identity function requires appropriate weights across all layers. Thus, both the Gaussian process and the neural network are better suited to the difference quotient setup due to their inherent bias towards zero.

### 3.9 Using The Cumulative Maximum Error Is Advantageous

When ranking different methods based on their performance, the error metrics CME, sMAPE, and  $t_{\text{valid}}$  generally produce similar results. However, a notable difference arises with sMAPE for more challenging tasks, where strong initial performance can be overshadowed by a divergence of the forecast later on (instead of, e.g., defaulting to a constant), see Table 13. As seen from the explicit error values in Table 14,  $t_{\text{valid}}$  is less effective at distinguishing well-performing methods when the testing duration is too short or the threshold parameter is too lenient, as several methods can achieve the maximum valid time. The CME does not suffer from any of these limitations.

### 3.10 Scarce Validation Data Can Lead to Over-Tuning

Unsurprisingly, the error measures of tuned methods typically perform better on the validation dataset than on the testing datasets, see Table 14. For some methods, the difference is rather large (for the Echo State Network **EsnS**, we have a median CME of 0.0040 on the noise-free *Dysts* validation data and 0.030 on the test data). In combination with the high number of parameters tested for these methods (for **EsnS** on the noise-free *Dysts* data, 288.5 per system on average), this suggests that the hyperparameter tuning has the potential to introduce overfitting to the validation data. This affects *Dysts* more than *DeebLorenz* as there is much less tuning data for the former and no repetitions, making the validation errors less robust.

## 4 Conclusion

This study provides a comprehensive evaluation of various methods for time series prediction across several low-dimensional chaotic dynamical systems, demonstrating that lightweight, simple methods consistently outperform more complex, computationally intensive algorithms (see Figure 6). Methods based on the solution smoother approach or simple estimators of propagator maps showed both strong predictive performance and low computational costs. In contrast, more complex machine learning models that are trained using gradient descent generally underperformed.

Hyperparameter optimization is shown to be a key factor for improving accuracy in some methods, with optimized methods achieving errors several orders of magnitude lower than those reported in a previous study with limited tuning. Additionally, noise and random timestep designs were found to significantly impact performance, with different methods excelling under different conditions.

Furthermore, this work highlights the importance of robust evaluation practices. Repeating experiments is essential to ensure statistical significance. The use of appropriate error metrics, such as the newly introduced cumulative maximum error (CME), is necessary to capture relevant performance differences.

In general, meaningful evaluation of a method’s performance requires a carefully constructed study design that incorporates appropriate hyperparameter optimization, relevant baseline methods, informative error metrics, uncertainty quantification, and fair comparison practices. However, many existing studies fail to address one or more of these aspects, whereas we strive to adhere to these principles. Our findings challenge the increasing focus on complex, computationally intensive machine learning models and show that these models are often ill-suited for predicting

Median of Ranks vs Compute Time for *DeebLorenz*

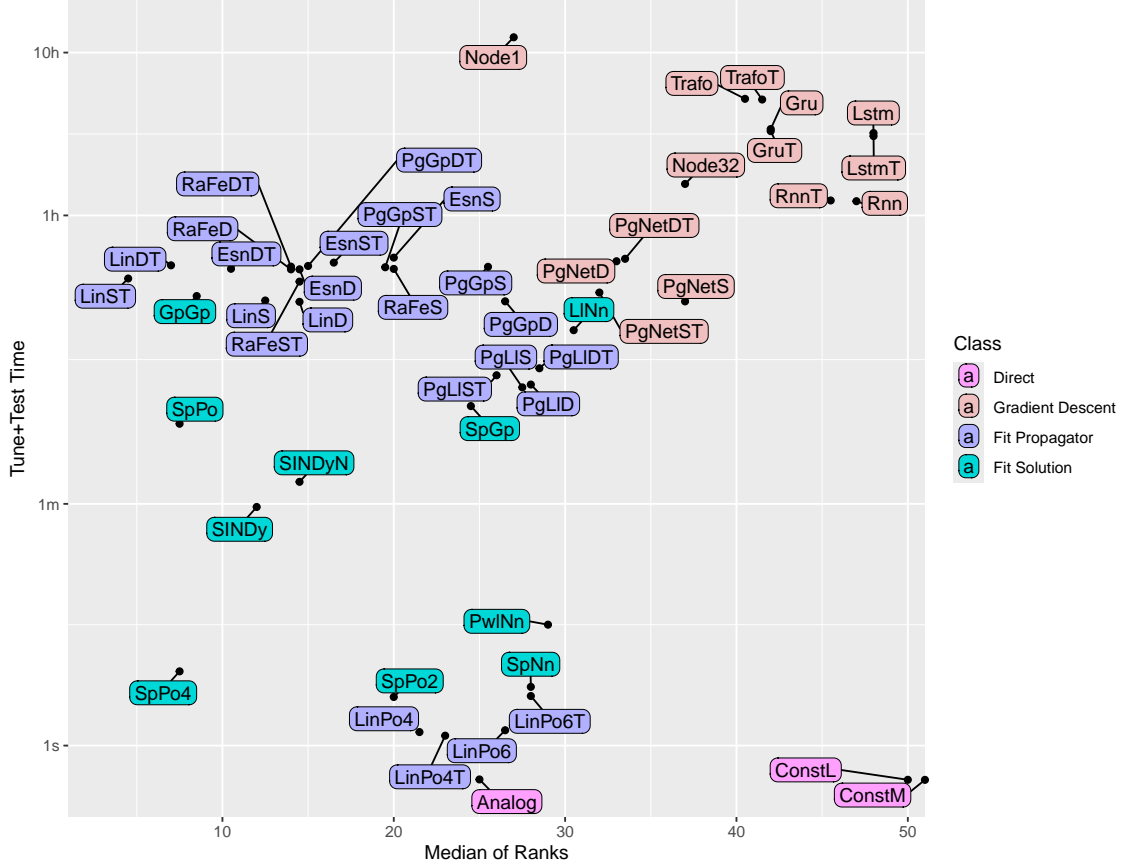


Figure 6: Overall comparison of the considered methods in terms of their ranks and computational efficiency. For the horizontal axis, for each method, we take the median over their ranks according to the Cumulative Maximum Error (CME) on the test data in the 12 different settings of *DeebLorenz* (3 systems with 4 observation schemes each), see Table 10. For the vertical axis, we take the sum over the tune and test time per time series and average it over 12 settings of *DeebLorenz*. Note that the median rank depends strongly on our specific selection of the 12 settings.

low-dimensional chaotic systems. Instead, simpler and more efficient approaches tailored to the specific problem domain, frequently deliver superior performance.



dimension	3	4	5	6	10
# systems	102	19	2	3	7

Table 4: Number of systems in *Dysts* with a given dimension.

## A The Databases

### A.1 *Dysts*

The *Dysts* database consists of 133 chaotic systems with state space dimension between 3 and 10, see Table 4. For a detailed description of the *Dysts* database, see [Gil21]. Here we comment on some peculiarities of the database, in particular the noisy version.

- (i) In the noisy version of the data, the system MACARTHUR is divergent (oscillating state values in the order of magnitude  $\pm 10^{100}$  and higher). Moreover, for CIRCADIANRHYTHM and DOUBLEPENDULUM, the variance of the solutions increases by multiple orders of magnitude between the noise-free and noisy version.
- (ii) Curiously, the oscillating behavior of MACARTHUR makes this system rather predictable in the noisy case with a best CME of 0.055 achieved by **EsnS**, which is lower than the best noise-free CME of 0.26 achieved by **PgNetD**.
- (iii) For the noise-free testing dataset, the most difficult to learn systems seem to be LIDDRIVEN-CAVITYFLOW, IKEDADELAY, DOUBLEPENDULUM, and FORCEDVANDERPOL. These all have values  $0.85 < \text{CME} < 0.96$  for the best methods in this study, while 100 out of 133 systems have a CME below 0.1 for the best method.
- (iv) For the following systems from the noisy testing dataset, learning seems impossible (best method with  $\text{CME} > 0.99$ ): ARNOLDBELTRAMICHILDRESS, ARNOLDWEB, BICKLEYJET. Out of 133 noisy systems, 21 have a CME below 0.1 and 14 have a CME above 0.9.

### A.2 *DeebLorenz*

The *DeebLorenz* database consists of three systems and four observation schemes and is separated into tuning and testing data with 10 and 100 replications, respectively.

Each system is described by an autonomous, first-order, three-dimensional ODE of the form

$$\dot{u}(t) = f(u(t)), \quad \text{for } t \in \mathbb{R},$$

where  $f: \mathbb{R}^3 \rightarrow \mathbb{R}^3$  is the vector field  $f$  and the solution  $u: \mathbb{R} \rightarrow \mathbb{R}^3$  describes the state of the system over time. For the three systems, the vector field  $f$  are created as follows:

- LORENZ63STD: The Lorenz63 system in its standard definition [Lor63], i.e.,

$$f(u) = \begin{pmatrix} \sigma(u_2 - u_1) \\ u_1(\rho - u_3) - u_2 \\ u_1u_2 - \beta u_3 \end{pmatrix} \quad (12)$$

with  $\sigma = 10$ ,  $\rho = 28$ ,  $\beta = 8/3$ .

- LORENZ63RANDOM: As LORENZ63STD, but for each replication, the three parameters are drawn uniformly at random from an interval,

$$\sigma \sim \text{Unif}([5, 15]), \quad \rho \sim \text{Unif}([20, 80]), \quad \beta \sim \text{Unif}([2, 6]). \quad (13)$$

These intervals are chosen so that the resulting systems exhibit chaotic behavior.

chroetz/DEEBdata	generation of DeebLorenz
chroetz/DEEBcmd	command line interface for the other packages
chroetz/DEEBesti	estimation methods
chroetz/DEEBeval	evaluate predictions
chroetz/DEEBtrajs	handling the csv-files containing observations and predictions
chroetz/DEEB.jl	the Julia implementation of the neural ODE
chroetz/ConfigOpts	handling the json-files containing settings for methods

Table 5: GitHub repositories containing the code used in this study.

- **LORENZ63NONPAR:** As **LORENZ63STD**, but the parameters depend on the state,  $\sigma = \sigma(u)$ ,  $\rho = \rho(u)$ ,  $\beta = \beta(u)$ . For each replication, the functions  $\sigma, \rho, \beta: \mathbb{R}^3 \rightarrow \mathbb{R}$  are sampled from a Gaussian process so that the (non-constant) parameter values are in (or at least close to) the intervals sampled from in (13). To make sure that the sampled vector fields lead to interesting systems, we reject results where the trajectory of given initial states seem to approach a fixed point. The resulting trajectories all seem to exhibit chaotic behavior.

Note that the vector fields of **LORENZ63STD** and **LORENZ63RANDOM** are polynomials of degree two with 23 out of 30 coefficients equal to zero, whereas instances of the vector fields of **LORENZ63NONPAR** cannot be described by a polynomial of finite degree.

To obtain one replication of one of the systems,  $f$  is set or sampled as described above. Then initial conditions  $u_0$  are sampled uniformly at random from the Lorenz63 attractor (as a proxy for the attractors of the other variations of the Lorenz63 system). The initial value problem  $\dot{u} = f(u)$ ,  $u(0) = u_0$  is solved using a fourth order Runge–Kutta (RK4) numerical ODE solver<sup>3</sup> with constant timestep of  $10^{-3}$  (one order of magnitude lower than the observation timesteps). If timesteps are random, they are sampled from an exponential distribution  $\Delta t_i \sim \text{Exp}(\lambda)$  with rate parameter  $\lambda = \Delta t_0^{-1}$  and  $\Delta t_0 = 10^{-2}$ . If the stepsize is constant, we set  $\Delta t_i = \Delta t_0$ . We set  $t_0 = 0$  and  $t_i = t_{i-1} + \Delta t_i$ . The last observation  $t_n$  is chosen such that  $t_{n+1} \geq T$  where  $T = 100$ . The number of observations is  $n = 10^4$  (exactly, for constant timesteps, and, in expectation, for random time steps). For noisy observations, we draw independent noise from a multivariate normal distribution,  $\epsilon_i \sim \mathcal{N}(0, \sigma^2 I_3)$  with standard deviation  $\sigma = 0.1$ , where  $I_3$  is the  $3 \times 3$  identity matrix. For the noise-free observation scheme, we set  $\epsilon_i = 0$ . Then the observations are  $Y_i = u(t_i) + \epsilon_i$ . For testing, we also record  $u(t_j)$ , where  $t_j = T + (j - n)\Delta t_0$ ,  $j = n + 1, \dots, n + m$ , and  $m = 10^3$ .

## B Methods

### B.1 Implementation

All methods are implemented in R [R C24], except for **Node**, which is implemented in Julia [Bez+17]. Furthermore, **PgNet\***, **Trafo\***, **Rnn\***, **Lstm\***, **Gru\*** use Keras [Cho+15] (via its R-interface). All methods were trained on CPUs (Intel Xeon Processor E5-2667 v3) with the exception of the indicated methods in Table 17, which utilize GPUs (NVIDIA H100). All code for running the methods is available in the public git repositories on GitHub as listed in Table 5. The predictions for the test and validation data are available at <https://doi.org/10.5281/zenodo.12999941>.

### B.2 Normalization

For all methods except **SINDy**, we calculate an affine linear normalization from the training data: Let  $\hat{\mu} = \frac{1}{n} \sum_{i=1}^n Y_i$  be the empirical mean and  $\hat{\Sigma} = \frac{1}{n-1} \sum_{i=1}^n (Y_i - \hat{\mu})(Y_i - \hat{\mu})^\top$  the empirical covariance matrix. Then the normalized data is

$$\bar{Y}_i := \hat{\Sigma}^{-\frac{1}{2}} (Y_i - \hat{\mu}) . \quad (14)$$

<sup>3</sup>The R function `deSolve::ode(..., method = "rk4")`.

It has mean zero and an identity covariance matrix. A prediction  $\bar{u}(t_j)$  from a given method trained on the normalized data is transformed back by

$$\hat{u}(t_j) := \hat{\Sigma}^{\frac{1}{2}} \bar{u}(t_j) + \hat{\mu}. \quad (15)$$

To not destroy potential sparsity, we only scale the inputs to SINDy by the inverse of the square root of  $\hat{\sigma}^2 = \frac{1}{n-1} \sum_{i=1}^n Y_i^\top Y_i$ .

### B.3 Different Variants of Methods

For propagator based methods, a mapping from the current state to the next one is learned. The target is either directly the next state (suffix S) or the increment scaled by the inverse of the time step (suffix D). Additionally to the current (and potentially past) state(s), the time step can also serves as a predictor (suffix T). See also Section 2.3.

### B.4 Hand-Tuning and Hyperparameter Grids

The hyperparameter grids presented below are selected to perform well across all systems while maintaining bounded computational costs. Many advanced machine learning models, such as transformers, recurrent networks, and neural ODEs, have numerous variants. In this study, we employ standard, out-of-the-box architectures for all methods, applying minimal manual adjustments and relying on automatic hyperparameter tuning, as detailed below. While extensive fine-tuning of specific model variants could potentially improve performance for individual systems, our approach prioritizes fairness in comparison across models. This design also caters to practitioners with limited time and computational resources when applying machine learning to data from dynamical systems.

### B.5 Analog

- Parameters: margin  $\omega \in \mathbb{N}$
- tuning: categorical, persistent:  $\omega \in \{1, 10, 100\}$ .
- Description: Initialize  $x \leftarrow u(T)$  and  $j_0 \leftarrow 0$ . Let  $k = \arg \min_{i \in \llbracket n-\omega \rrbracket} \|Y_i - x\|_2$ . Set  $\hat{u}(t_{j_0+j}) = Y_{k+j}$  for  $j \in \llbracket j_{\max} \rrbracket$ ,  $j_{\max} := \min(n-k, m)$ . If the prediction time series is not yet complete, repeat with  $x \leftarrow Y_{k+j_{\max}}$  and  $j_0 \leftarrow j_0 + j_{\max}$ .

### B.6 Node1, Node32

- Parameters:
  - number of hidden layers:  $L$
  - width of hidden layers:  $W$
  - activation function: swish
  - weight decay  $10^{-6}$
  - ODE solver steps for the loss:  $S$
  - batch size: 1 or 32 as indicated by the suffix of the method name (and one experiment marked by \* in Table 17 with 1024)
  - epochs: 400
  - Optimizer: AdamW
  - learning rate:  $10^{-3}$
  - internal training-validation to use weights with lowest validation error: 85% – 15%
- Tuning:
  - categorical, yielding:  $(L, W) \in \{(2, 32), (4, 32), (2, 128)\}$

- scalar, exponential (factor 2):  $S = 2, 4, S \in [2, 64]$
- Description: See [Che+18]. We use a Julia implementation.
- Note on Batch Size for Variable Timesteps: A batch size greater than 1 requires equal computational steps across all elements within the batch. When timesteps vary between different segments of the training time series, this requirement is not satisfied. Forcing training in such cases by setting the timestep to a constant value leads to significantly larger error values compared to using a batch size of one. Consequently, we do not report results for Node32 in the case of random timesteps.
- Note on Larger Networks: We evaluated wider and deeper networks using the validation dataset of LORENZ63STD. However, these larger architectures either resulted in increased errors or yielded error reductions that were not statistically significant ( $p > 0.1$ ).

## B.7 PgGp\*

- Parameters:
  - bandwidth:  $h$
  - kernel function:  $x \mapsto \exp(x^2/(2h^2))$
  - regularization:  $\lambda$
- Tuning:
  - scalar, exponential (factor 2):  $h = 0.05, 0.2, 0.8, 10^{-4} \leq h \leq 10$
  - scalar, exponential (factor 10):  $\lambda = 10^{-12}, 10^{-8}, 10^{-4}, 10^{-15} \leq \lambda \leq 10^2$
- Description: A propagator estimator (section B.3) using a Gaussian process [RW05].

## B.8 PgNet\*

- Parameters:
  - batch size: 32 (and one experiment marked by \* in Table 17 with 1024)
  - epochs: 1000,
  - training – validation split: 90% – 10%
  - architecture (tuple of layer width):  $w$
  - activation function: swish
  - learning rate  $2 \cdot 10^{-4}$
- Tuning: categorical, yielding:  $w = (32, 64, 64, 32), (128, 128), (64, 128, 64)$
- Description: A propagator estimator (section B.3) using a vanilla feed-forward neural network implemented using Keras.

## B.9 PgLl\*

- Parameters:
  - kernel function:  $x \mapsto \exp(x^2/h^2)$
  - bandwidth:  $h$
  - neighbors:  $k = 50$
- Tuning:
  - scalar, exponential (factor 2):  $h = 0.05, 0.2, 0.8, h \in [10^{-4}, 10]$
- Description: A propagator estimator (section B.3) using a local linear estimator. Locality is introduced by the kernel weights and a  $k$ -nearest neighbors restriction. The latter is used to keep the computational demand low.

## B.10 Lin\*

- Parameters:
  - past steps  $K$
  - skip steps  $s$
  - polynomial degree  $\ell$
  - penalty  $\lambda$
- Tuning:
  - scalar, linear (step 1):  $K = 0, 1, 4, 0 \leq K \leq 32$
  - scalar, linear (step 1):  $s = 1, 2, 1 \leq s \leq 9$
  - scalar, linear (step 1):  $\ell = 1, 4, 1 \leq \ell \leq 8$
  - scalar, exponential (factor 10):  $\lambda = 10^{-12}, 10^{-8}, 10^{-4}, 10^{-15} \leq \lambda \leq 10^2$
- Description: A propagator estimator (section B.3) using Ridge regression (linear regression with  $L_2$ -penalty with weight  $\lambda$ ) on polynomial features of degree at most  $\ell$  of the current at time  $t_i$  and past states  $t_{i-sk}$ ,  $k \in \llbracket K \rrbracket$ .

## B.11 LinPo4, LinPo6, LinPo4T, LinPo6T

- Parameters: as in section B.10 with  $K = 0$ ,  $\ell = 4$  and  $\ell = 6$ ,  $\lambda = 0$
- Tuning: none
- Description: As LinD and LinDT (section B.10), respectively, but with fixed hyperparameters.

## B.12 RaFe\*

- Parameters:
  - number of neurons: 400
  - input weight scale  $c$
  - penalty  $\lambda$
  - forward skip  $\psi$
  - random seed  $r$
- Tuning:
  - scalar, exponential (factor 2):  $c = 0.025, 0.1, 0.4, 10^{-7} \leq c \leq 10^2$
  - scalar, exponential (factor 10):  $\lambda = 10^{-12}, 10^{-8}, 10^{-4}, 10^{-15} \leq \lambda \leq 10^2$
  - scalar, exponential (factor 2):  $\psi = 0, 1, 1 \leq \psi \leq 64$
  - categorical, persistent:  $r = 1, 2, 3, 4$
- Description: A propagator estimator (section B.3) using random feature regression, i.e., Ridge regression on features created from an untrained vanilla feed forward neural network with 1 layer of  $\ell$  neurons. The forward skip  $\psi$  modifies the target to  $u(t) \mapsto u(t + (1 + \psi)\Delta t)$ , which can help in cases of high measurement noise and small stepsizes.

### B.13 Esn\*

- Parameters:
  - number of neurons: 400
  - node degree: 6
  - spectral radius: 0.1
  - input weight scale  $c$
  - penalty  $\lambda$
  - forward skip  $\psi$
  - random seed  $r$
- Tuning: same as **RaFe\*** (section B.12)
- Description: See [Jae01].

### B.14 Trafo\*

- Parameters:
  - context length:  $\ell$ ,
  - position dimension:  $d_{\text{pos}}$
  - head size:  $s_{\text{head}}$
  - number of heads:  $n_{\text{head}}$
  - number of blocks:  $n_{\text{block}} = 4$
  - number of neurons in the MLP-layers:  $n_{\text{mlp}}$
  - dropout parameter: 0.1
  - learning rate:  $\lambda$
  - training-validation split: 90% – 10%
  - epochs: 400
  - batch size: 32 (and one experiment marked by \* in Table 17 with 1024)
  - positional encoding: sinusoidal
  - loss: MSE
  - optimizer: Adam
- Tuning: We test the hyperparameter combinations  $(\ell, d_{\text{pos}}, s_{\text{head}}, n_{\text{head}}, n_{\text{mlp}}, \lambda)$  given in the rows of Table 6.
- Description: We use a Keras-implementation of a transformer network. As an input, we take the states at times  $t_{k-\ell+1}, \dots, t_k$  and add a sinusoidal positional encoding of dimension  $d_{\text{pos}}$  by appending it to each of the state vectors. The network consist of  $n_{\text{block}}$  consecutive blocks consisting of an attention layer (followed by layer normalization) and a dense MLP-layer with ReLu activation (followed by layer normalization). The attention layers have  $n_{\text{head}}$  heads of size  $s_{\text{head}}$ .

### B.15 PwNn

- Parameters: none.
- Tuning: none.
- Description: A solution smoother using piece-wise linear interpolation for estimating the solution  $u$  and a nearest neighbor interpolation for estimating the vector field  $f$ .

$\ell$	$d_{\text{pos}}$	$s_{\text{head}}$	$n_{\text{head}}$	$n_{\text{mlp}}$	$\lambda$
64	16	64	4	32	$10^{-3}$
32	8	32	16	32	$10^{-4}$
32	32	16	16	32	$10^{-4}$
32	8	16	16	32	$10^{-3}$
32	8	32	8	64	$10^{-4}$

Table 6: Hyperparameters for the Transformer **Trafo**.

### B.16 SpNn

- Parameters: none.
- Tuning: none.
- Description: A solution smoother using a cubic spline interpolation for estimating the solution  $u$  and a nearest neighbor interpolation for estimating the vector field  $f$ .

### B.17 L1Nn

- Parameters:
  - kernel function:  $x \mapsto \exp(x^2/h^2)$
  - bandwidth:  $h$
- Tuning:
  - scalar, exponential (factor 2):  $h = 0.05, 0.2, 0.8, 10^{-4} \leq h \leq 10$
- Description: A solution smoother using local linear regression for estimating the solution  $u$  and a nearest neighbor interpolation for estimating the vector field  $f$ .

### B.18 SpPo

- Parameters:
  - polynomial degree  $\ell$
  - penalty  $\lambda$
- Tuning:
  - scalar, linear (step 1):  $\ell = 2, 3, 4, 1 \leq \ell \leq 8$
  - scalar, exponential (factor 10):  $\lambda = 10^{-12}, 10^{-8}, 10^{-4}, 10^{-15} \leq \lambda \leq 10^2$
- Description: A solution smoother using a cubic spline interpolation for estimating the solution  $u$  and Ridge regression with polynomial features for estimating the vector field  $f$ .

### B.19 SpPo2, SpPo4

- Parameters: as in section B.18 with  $\ell = 2$  and  $\ell = 4, \lambda = 0$
- Tuning: none
- Description: As **SpPo\*** (section B.18), but with fixed hyperparameters.

## B.20 SpGp

- Parameters:
  - bandwidth:  $h$
  - neighbors:  $k = 50$
  - kernel function:  $x \mapsto \exp(x^2/(2h^2))$
  - regularization:  $\lambda$
- Tuning:
  - scalar, exponential (factor 2):  $h = 0.05, 0.2, 0.8, 10^{-4} \leq h \leq 10$
  - scalar, exponential (factor 10):  $\lambda = 10^{-12}, 10^{-8}, 10^{-4}, 10^{-15} \leq \lambda \leq 10^2$
- Description: A solution smoother using a cubic spline interpolation for estimating the solution  $u$  and Gaussian process regression for estimating the vector field  $f$ . To make the Gaussian process computationally efficient, we localize it by only considering the  $k$  nearest neighbors for an evaluation.

## B.21 GpGp

- Parameters:
  - bandwidth:  $h$
  - neighbors:  $k = 50$
  - kernel function:  $x \mapsto \exp(x^2/(2h^2))$
  - regularization:  $\lambda$
  - solution bandwidth: 0.1
  - solution regularization  $\mu$
- Tuning:
  - scalar, exponential (factor 2):  $h = 0.05, 0.2, 0.8, 10^{-4} \leq h \leq 10$
  - scalar, exponential (factor 10):  $\lambda = 10^{-12}, 10^{-8}, 10^{-4}, 10^{-15} \leq \lambda \leq 10^2$
  - scalar, exponential (factor 10):  $\mu = 10^{-12}, 10^{-8}, 10^{-4}, 10^{-15} \leq \mu \leq 10^2$
- Description: A solution smoother using Gaussian process regression for estimating the solution  $u$  and Gaussian process regression for estimating the vector field  $f$ . To make the second Gaussian process computationally efficient, we localize it by only considering the  $k$  nearest neighbors for an evaluation.

## B.22 SINDy, SINDyN

- Parameters:
  - polynomial degree: 5
  - thresholding iterations: 100
  - threshold  $\tau$
- Tuning:
  - scalar, exponential (factor 2):  $\tau = 0.04, 0.16, 0.64, 10^{-7} \leq \tau \leq 10^2$
- Description: A solution smoother using a cubic spline interpolation for estimating the solution  $u$  and sparse linear regression with polynomial features for estimating the vector field  $f$ . See [BPK16].



### B.23 Rnn\*, Lstm\*, Gru\*

- Parameters:
  - batch size: 32 (and one experiment marked by \* in Table 17 with 1024)
  - epochs: 100,
  - training – validation split: 90% – 10%
  - architecture (tuple of layer width):  $w$
  - activation function: swish
  - learning rate  $10^{-3}$
- Tuning: categorical, yielding:  $w = (128), (64, 64), (32, 64, 32)$
- Description: Recurrent neural network architectures implemented using Keras.

## C On The Symmetric Mean Absolute Percent Error

In this section, we show some mathematical properties of the symmetric mean absolute percent error, sMAPE.

Let  $S > 0$  and  $d \in \mathbb{N}$ . Let  $u, v: [0, S] \rightarrow \mathbb{R}^d$  be measurable functions such that there is no  $t \in [0, S]$  such that  $u(t) = 0 = v(t)$ . Then  $\text{sMAPE}(v, u)$  is defined as

$$\text{sMAPE}(v, u) := \frac{2 \cdot 100}{S} \int_0^S \frac{\|v(t) - u(t)\|_2}{\|v(t)\|_2 + \|u(t)\|_2} dt,$$

where  $\|\cdot\|_2$  denotes the Euclidean norm. Note that the case  $u(t) = 0 = v(t)$  has to be excluded so that there is no division by zero.

The sMAPE has following properties:

- (i)  $\text{sMAPE}(v, u) \in [0, 200]$
- (ii) Symmetry:  $\text{sMAPE}(v, u) = \text{sMAPE}(u, v)$
- (iii)  $\text{sMAPE}(v, u) = 0$  if and only if  $u(t) = v(t)$  for almost all  $t \in [0, S]$
- (iv)  $\text{sMAPE}(v, u) = 200$  if and only if there is  $\alpha: [0, S] \rightarrow (-\infty, 0]$  such that  $v(t) = \alpha(t)u(t)$  for almost all  $t \in [0, S]$
- (v) If  $v_n: [0, S] \rightarrow \mathbb{R}^d$  for  $n \in \mathbb{N}$  forms a sequence of functions with  $\lim_{n \rightarrow \infty} \inf_{t \in [0, S]} \|v_n(t)\|_2 = \infty$  and  $\sup_{t \in [0, S]} \|u(t)\|_2 < \infty$ , then  $\lim_{n \rightarrow \infty} \text{sMAPE}(v_n, u) = 200$

*Proof.*

- (i) Non-negativity and triangle inequality of the Euclidean norm.
- (ii) Trivial.
- (iii) Clearly,  $\text{sMAPE}(v, u) = 0$  if and only if  $\|v(t) - u(t)\|_2 = 0$  for almost all  $t \in [0, S]$ .
- (iv) On one hand, if such a function  $\alpha$  exists, we have  $\|v(t) - u(t)\|_2 = (1 + \alpha(t))\|u(t)\|_2 = \|v(t)\|_2 + \|u(t)\|_2$ . Thus,  $\text{sMAPE}(v, u) = 200$ . On the other hand, if  $\text{sMAPE}(v, u) = 200$ , we must have  $\|v(t) - u(t)\|_2 = \|v(t)\|_2 + \|u(t)\|_2$  for almost all  $t \in [0, S]$ . As the triangle inequality can only be an equality for linearly dependent vectors, there must be  $\alpha(t) \in \mathbb{R}$  such that  $v(t) = \alpha(t)u(t)$ . Furthermore,  $\alpha(t)$  must be non-positive, as we require  $|\alpha(t) - 1| = |\alpha(t)| + 1$ .
- (v) Let  $a_n := \inf_{t \in [0, S]} \|v_n(t)\|_2$  and  $B := \sup_{t \in [0, S]} \|u(t)\|_2$ . Then

$$\lim_{n \rightarrow \infty} \text{sMAPE}(v_n, u) \geq 200 \lim_{n \rightarrow \infty} \frac{a_n - B}{a_n + B} = 200.$$

□

## D Further Details of the Results

In this section we list additional tables and plots that show the results of the simulation study in more detail. Mean error values (CME, sMAPE,  $t_{\text{valid}}$ ) for *DeebLorenz* are shown in Tables 7 to 9. The respective rankings are displayed in Tables 10 to 12. Furthermore, Table 13 shows the ranks for all error metrics side by side and highlights the strongest disagreement. For *Dysts*, the median error values over all systems are shown in Table 14. These tables also include the values of the error metrics on the tuning data. Table 15 and Table 16 detail the performances of the different variants of propagator based methods. Results of statistical tests for distinguishing the performances of methods on *DeebLorenz* are shown in Figure 7 and Figure 8. Figures 9 to 13 show variants of Figure 4 for the other systems and observation schemes of *DeebLorenz*. Finally, Table 17 displays results for the system LORENZ63STD of *DeebLorenz* with reduced and increased data size.

## References

- [Bez+17] J. Bezanson, A. Edelman, S. Karpinski, and V. B. Shah. “Julia: A fresh approach to numerical computing”. In: *SIAM review* 59.1 (2017), pp. 65–98. DOI: 10.1137/141000671.
- [BPK16] S. L. Brunton, J. L. Proctor, and J. N. Kutz. “Discovering governing equations from data by sparse identification of nonlinear dynamical systems”. In: *Proceedings of the National Academy of Sciences* 113.15 (Mar. 2016), pp. 3932–3937. DOI: 10.1073/pnas.1517384113.
- [Che+18] R. T. Q. Chen, Y. Rubanova, J. Bettencourt, and D. Duvenaud. “Neural Ordinary Differential Equations”. In: *Proceedings of the 32nd International Conference on Neural Information Processing Systems*. NIPS’18. Montréal, Canada: Curran Associates Inc., 2018, pp. 6572–6583.
- [Cho+14] K. Cho, B. van Merriënboer, Ç. Gülçehre, D. Bahdanau, F. Bougares, H. Schwenk, and Y. Bengio. “Learning Phrase Representations using RNN Encoder-Decoder for Statistical Machine Translation”. In: *Proceedings of the 2014 Conference on Empirical Methods in Natural Language Processing, EMNLP 2014, October 25-29, 2014, Doha, Qatar, A meeting of SIGDAT, a Special Interest Group of the ACL*. Ed. by A. Moschitti, B. Pang, and W. Daelemans. ACL, 2014, pp. 1724–1734. DOI: 10.3115/V1/D14-1179.
- [Cho+15] F. Chollet et al. *Keras*. <https://keras.io>. 2015.
- [Fan93] J. Fan. “Local linear regression smoothers and their minimax efficiencies”. In: *Ann. Statist.* 21.1 (1993), pp. 196–216. DOI: 10.1214/aos/1176349022.
- [For+77] G. E. Forsythe et al. *Computer methods for mathematical computations*. Prentice-hall, 1977.
- [Gau+21] D. J. Gauthier, E. Bollt, A. Griffith, and W. A. S. Barbosa. “Next generation reservoir computing”. In: *Nature Communications* 12.1 (Sept. 2021). DOI: 10.1038/s41467-021-25801-2.
- [Gil21] W. Gilpin. “Chaos as an interpretable benchmark for forecasting and data-driven modelling”. In: *Proceedings of the Neural Information Processing Systems Track on Datasets and Benchmarks 1, NeurIPS Datasets and Benchmarks 2021, December 2021, virtual*. Ed. by J. Vanschoren and S. Yeung. 2021.
- [Gil23] W. Gilpin. “Model scale versus domain knowledge in statistical forecasting of chaotic systems”. In: *Phys. Rev. Res.* 5 (4 2023), p. 043252. DOI: 10.1103/PhysRevResearch.5.043252.
- [God+21] R. W. Godahewa, C. Bergmeir, G. I. Webb, R. Hyndman, and P. Montero-Manso. “Monash Time Series Forecasting Archive”. In: *Thirty-fifth Conference on Neural Information Processing Systems Datasets and Benchmarks Track (Round 2)*. 2021.
- [Han+21] Z. Han, J. Zhao, H. Leung, K. F. Ma, and W. Wang. “A Review of Deep Learning Models for Time Series Prediction”. In: *IEEE Sensors Journal* 21.6 (2021), pp. 7833–7848. DOI: 10.1109/JSEN.2019.2923982.

- [Has+09] T. Hastie, R. Tibshirani, J. H. Friedman, and J. H. Friedman. *The elements of statistical learning: data mining, inference, and prediction*. Vol. 2. Springer, 2009.
- [Hei+18] M. Heinonen, C. Yildiz, H. Mannerström, J. Intosalmi, and H. Lähdesmäki. “Learning unknown ODE models with Gaussian processes”. In: *Proceedings of the 35th International Conference on Machine Learning*. Ed. by J. Dy and A. Krause. Vol. 80. Proceedings of Machine Learning Research. PMLR, 2018, pp. 1959–1968.
- [HS97] S. Hochreiter and J. Schmidhuber. “Long Short-Term Memory”. In: *Neural Computation* 9.8 (Nov. 1997), pp. 1735–1780. DOI: 10.1162/neco.1997.9.8.1735.
- [Jae01] H. Jaeger. “The “echo state” approach to analysing and training recurrent neural networks-with an erratum note”. In: *Bonn, Germany: German National Research Center for Information Technology GMD Technical Report* 148.34 (2001), p. 13.
- [Lor63] E. N. Lorenz. “Deterministic Nonperiodic Flow”. In: *Journal of the Atmospheric Sciences* 20.2 (Mar. 1963), pp. 130–141. DOI: 10.1175/1520-0469(1963)020<0130:dnf>2.0.co;2.
- [Ore+20] B. N. Oreshkin, D. Carpo, N. Chapados, and Y. Bengio. “N-BEATS: Neural basis expansion analysis for interpretable time series forecasting”. In: *International Conference on Learning Representations*. 2020.
- [Ott02] E. Ott. *Chaos in dynamical systems*. Second. Cambridge University Press, Cambridge, 2002, pp. xii+478. DOI: 10.1017/CB09780511803260.
- [Pat+18] J. Pathak, A. Wikner, R. Fussell, S. Chandra, B. R. Hunt, M. Girvan, and E. Ott. “Hybrid forecasting of chaotic processes: Using machine learning in conjunction with a knowledge-based model”. In: *Chaos: An Interdisciplinary Journal of Nonlinear Science* 28.4 (2018).
- [R C24] R Core Team. *R: A Language and Environment for Statistical Computing*. R Foundation for Statistical Computing. Vienna, Austria, 2024.
- [Ren+09] H. Ren, J. Chou, J. Huang, and P. Zhang. “Theoretical basis and application of an analogue-dynamical model in the Lorenz system”. In: *Adv. Atmos. Sci.* 26.1 (Jan. 2009), pp. 67–77.
- [RH17] J. Ramsay and G. Hooker. *Dynamic data analysis*. Springer Series in Statistics. Modeling data with differential equations. Springer, New York, 2017, pp. xvii+230. DOI: 10.1007/978-1-4939-7190-9.
- [RHW86] D. E. Rumelhart, G. E. Hinton, and R. J. Williams. “Learning internal representations by error propagation, parallel distributed processing, explorations in the microstructure of cognition, ed. de rumelhart and j. mcclelland. vol. 1. 1986”. In: *Biometrika* 71.599-607 (1986), p. 6.
- [RR08] A. Rahimi and B. Recht. “Uniform approximation of functions with random bases”. In: *2008 46th Annual Allerton Conference on Communication, Control, and Computing*. 2008, pp. 555–561. DOI: 10.1109/ALLERTON.2008.4797607.
- [RW05] C. E. Rasmussen and C. K. I. Williams. *Gaussian Processes for Machine Learning*. The MIT Press, Nov. 2005. DOI: 10.7551/mitpress/3206.001.0001.
- [RW94] D. Ruppert and M. P. Wand. “Multivariate locally weighted least squares regression”. In: *Ann. Statist.* 22.3 (1994), pp. 1346–1370. DOI: 10.1214/aos/1176325632.
- [Sch24] C. Schötz. *Nonparametric Estimation of Ordinary Differential Equations: Snake and Stubble*. 2024. DOI: 10.48550/arXiv.2407.14989. arXiv: 2407.14989 [math.ST].
- [SFC22] S. Shahi, F. H. Fenton, and E. M. Cherry. “Prediction of chaotic time series using recurrent neural networks and reservoir computing techniques: A comparative study”. In: *Machine Learning with Applications* 8 (2022), p. 100300. DOI: 10.1016/j.mlwa.2022.100300.
- [She20] A. Sherstinsky. “Fundamentals of Recurrent Neural Network (RNN) and Long Short-Term Memory (LSTM) network”. In: *Physica D: Nonlinear Phenomena* 404 (2020), p. 132306. DOI: 10.1016/j.physd.2019.132306.

- [SS24] C. Schötz and M. Siebel. *Lower Bounds for Nonparametric Estimation of Ordinary Differential Equations*. 2024. DOI: 10.48550/arXiv.2407.14993. arXiv: 2407.14993 [math.ST].
- [Str24] S. Strogatz. *Nonlinear Dynamics and Chaos. With Applications to Physics, Biology, Chemistry, and Engineering*. Third edition. New York: Chapman and Hall/CRC, 2024. DOI: 10.1201/9780429398490.
- [Vas+17] A. Vaswani, N. Shazeer, N. Parmar, J. Uszkoreit, L. Jones, A. N. Gomez, Ł. Kaiser, and I. Polosukhin. “Attention is All you Need”. In: *Advances in Neural Information Processing Systems*. Ed. by I. Guyon, U. V. Luxburg, S. Bengio, H. Wallach, R. Fergus, S. Vishwanathan, and R. Garnett. Vol. 30. Curran Associates, Inc., 2017.
- [Vla+20] P.-R. Vlachas, J. Pathak, B. R. Hunt, T. P. Sapsis, M. Girvan, E. Ott, and P. Koumoutsakos. “Backpropagation algorithms and reservoir computing in recurrent neural networks for the forecasting of complex spatiotemporal dynamics”. In: *Neural Networks* 126 (2020), pp. 191–217.
- [Wen+23] Q. Wen, T. Zhou, C. Zhang, W. Chen, Z. Ma, J. Yan, and L. Sun. “Transformers in Time Series: A Survey”. In: *Proceedings of the Thirty-Second International Joint Conference on Artificial Intelligence, IJCAI-23*. Ed. by E. Elkind. Survey Track. International Joint Conferences on Artificial Intelligence Organization, Aug. 2023, pp. 6778–6786. DOI: 10.24963/ijcai.2023/759.
- [Zen+23] A. Zeng, M. Chen, L. Zhang, and Q. Xu. “Are transformers effective for time series forecasting?” In: *Proceedings of the AAAI conference on artificial intelligence*. Vol. 37. 9. 2023, pp. 11121–11128.

*DeebLorenz*, CME, Values

Method	Median	Constant $\Delta t$						Random $\Delta t$					
		Noisefree			Noisy			Noisefree			Noisy		
		S	R	N	S	R	N	S	R	N	S	R	N
GpGp	0.60	0.18	0.40	0.40	0.68	0.77	0.71	0.22	0.52	0.52	0.69	0.78	0.80
SpPo	0.65	0.0033	0.22	0.30	0.54	0.63	0.67	0.37	0.67	0.68	0.99	0.98	0.98
SpPo4	0.66	0.0023	0.22	0.51	0.66	0.71	0.66	0.37	0.67	0.64	0.98	0.98	0.98
LinDT	0.66	0.000078	0.11	0.18	0.60	0.71	0.62	0.48	0.83	0.80	0.99	0.99	0.97
SINDy	0.66	0.0088	0.27	0.37	0.67	0.74	0.66	0.39	0.71	0.65	0.99	0.98	0.98
SINDyN	0.67	0.014	0.30	0.64	0.67	0.74	0.68	0.40	0.73	0.66	0.99	0.98	0.98
EsnDT	0.70	0.044	0.35	0.34	0.63	0.72	0.66	0.67	0.85	0.84	0.75	0.88	0.87
LinST	0.71	0.00019	0.057	0.23	0.60	0.71	0.63	0.71	0.87	0.90	0.76	0.83	0.90
SpGp	0.72	0.24	0.37	0.38	0.77	0.82	0.80	0.45	0.68	0.62	0.97	0.93	0.95
RaFeDT	0.73	0.052	0.29	0.28	0.65	0.77	0.70	0.69	0.84	0.81	0.75	0.88	0.85
EsnD	0.73	0.046	0.34	0.31	0.65	0.73	0.68	0.74	0.85	0.84	0.78	0.89	0.86
LinD	0.74	0.000043	0.094	0.18	0.63	0.71	0.67	0.76	0.87	0.84	0.99	0.99	0.99
PgGpDT	0.74	0.014	0.11	0.16	0.76	0.79	0.81	0.47	0.72	0.72	0.99	0.99	0.98
RaFeST	0.75	0.073	0.28	0.27	0.65	0.77	0.73	0.90	0.96	0.93	0.74	0.90	0.90
RaFeD	0.76	0.052	0.29	0.27	0.64	0.77	0.70	0.74	0.87	0.83	0.80	0.90	0.87
SpPo2	0.76	0.0099	0.28	0.87	0.54	0.63	0.87	0.33	0.65	0.87	0.98	0.98	0.98
LinPo4T	0.77	0.24	0.47	0.58	0.75	0.80	0.77	0.55	0.78	0.78	0.99	0.99	0.98
LinPo4	0.78	0.019	0.35	0.56	0.75	0.80	0.76	0.72	0.86	0.83	0.99	0.99	0.98
PgLlDT	0.78	0.61	0.69	0.69	0.75	0.80	0.77	0.68	0.86	0.81	1.0	0.99	0.99
Analog	0.79	0.74	0.83	0.79	0.76	0.83	0.80	0.76	0.84	0.78	0.77	0.85	0.79
PgLlD	0.79	0.56	0.69	0.66	0.75	0.80	0.77	0.77	0.88	0.85	1.0	0.99	0.99
SpNn	0.80	0.67	0.78	0.70	0.83	0.84	0.81	0.68	0.78	0.71	0.94	0.94	0.94
EsnST	0.80	0.12	0.31	0.34	0.61	0.74	0.66	0.91	0.96	0.93	0.86	0.93	0.92
LinS	0.81	0.00019	0.057	0.23	0.63	0.71	0.67	0.91	0.95	0.94	0.91	0.96	0.94
LinPo6T	0.81	0.54	0.64	0.80	0.74	0.79	0.85	0.61	0.82	0.87	1.0	0.99	0.98
PgGpST	0.82	0.048	0.24	0.22	0.81	0.82	0.80	0.76	0.89	0.89	0.88	0.91	0.90
PgNetDT	0.82	0.56	0.69	0.62	0.81	0.86	0.84	0.68	0.82	0.79	0.99	0.98	0.98
PgGpD	0.82	0.014	0.11	0.16	0.75	0.83	0.81	0.78	0.88	0.86	0.99	0.97	0.99
EsnS	0.82	0.067	0.35	0.32	0.65	0.73	0.66	0.92	0.97	0.94	0.91	0.96	0.94
Node1	0.82	0.71	0.82	0.79	0.85	0.86	0.87	0.70	0.82	0.81	0.83	0.87	0.86
RaFeS	0.82	0.072	0.31	0.26	0.61	0.74	0.73	0.91	0.96	0.94	0.92	0.96	0.93
LlNn	0.83	0.67	0.80	0.74	0.77	0.84	0.82	0.80	0.91	0.88	0.84	0.92	0.91
PwLlNn	0.83	0.70	0.82	0.75	0.80	0.85	0.83	0.75	0.88	0.84	0.90	0.93	0.91
LinPo6	0.84	0.0000066	0.047	0.31	0.75	0.80	0.77	0.93	0.91	0.88	1.0	1.0	0.99
PgNetD	0.84	0.54	0.72	0.64	0.80	0.86	0.82	0.79	0.90	0.87	0.99	0.99	0.98
PgLlST	0.85	0.50	0.67	0.62	0.76	0.80	0.77	0.91	0.96	0.94	0.90	0.95	0.93
PgGpS	0.86	0.048	0.24	0.22	0.81	0.82	0.80	0.89	0.95	0.93	0.89	0.96	0.93
PgLlS	0.86	0.56	0.69	0.65	0.75	0.80	0.77	0.94	0.97	0.95	0.92	0.96	0.93
PgNetST	0.88	0.67	0.77	0.76	0.88	0.89	0.87	0.83	0.90	0.88	0.89	0.91	0.91
Node32	0.89	0.68	0.78	0.79	0.79	0.85	0.85	0.96	0.97	0.96	0.94	0.97	0.95
GruT	0.91	0.79	0.86	0.86	0.87	0.91	0.89	0.94	0.96	0.95	0.91	0.95	0.92
PgNetS	0.92	0.65	0.77	0.75	0.88	0.90	0.88	0.93	0.96	0.94	0.93	0.96	0.94
TrafoT	0.92	0.85	0.91	0.88	0.86	0.90	0.89	0.94	0.96	0.95	0.94	0.96	0.95
Trafo	0.92	0.85	0.90	0.89	0.84	0.90	0.89	0.95	0.96	0.95	0.95	0.96	0.96
Gru	0.93	0.78	0.85	0.84	0.87	0.91	0.89	0.94	0.97	0.95	0.95	0.96	0.96
RnnT	0.94	0.85	0.91	0.90	0.92	0.93	0.92	0.95	0.97	0.97	0.95	0.97	0.96
Rnn	0.95	0.85	0.91	0.91	0.92	0.93	0.93	0.97	0.97	0.96	0.96	0.97	0.96
LstmT	0.96	0.88	0.92	0.91	0.92	0.94	0.92	0.97	0.98	0.97	0.98	0.98	0.97
Lstm	0.97	0.86	0.92	0.91	0.92	0.97	0.92	0.97	0.98	0.97	0.97	0.98	0.97
ConstL	0.99	0.99	0.99	0.98	0.99	0.99	0.98	0.99	0.99	0.98	0.99	0.99	0.98
ConstM	1.0	1.0	1.0	0.99	1.0	1.0	0.99	1.0	1.0	0.99	1.0	1.0	0.99

Table 7: Mean Cumulative Maximum Error (CME) for the three systems of *DeebLorenz*: LORENZ63STD (S, green), LORENZ63RANDOM (R, red), LORENZ63NONPAR (N, blue).

*DeebLorenz*, sMAPE, Values

Method	Median	Constant $\Delta t$						Random $\Delta t$					
		Noisefree			Noisy			Noisefree			Noisy		
		S	R	N	S	R	N	S	R	N	S	R	N
GpGp	38	9.4	23	24	42	47	42	13	31	35	46	50	59
SpPo	39	0.072	12	16	33	38	39	21	40	40	75	79	66
SpPo4	39	0.058	12	31	40	44	40	20	39	39	76	76	66
LinDT	40	0.0017	4.8	9.2	38	43	37	28	54	48	66	130	56
SINDyN	41	0.39	16	37	42	44	40	23	45	38	75	75	63
SINDy	42	0.20	14	21	57	48	39	22	45	40	110	120	100
EsnDT	44	1.5	19	19	40	45	38	43	63	55	49	63	84
EsnD	46	2.0	18	18	39	44	39	48	55	51	55	62	56
LinST	46	0.0039	2.6	11	38	43	37	48	60	55	51	53	56
RaFeDT	46	1.6	15	16	39	48	42	45	53	61	49	61	54
SpPo2	46	0.24	15	54	33	38	54	18	39	54	86	79	75
LinD	47	0.00090	4.6	9.2	40	43	40	51	57	51	150	66	52
LinPo4T	47	12	27	35	49	51	45	33	48	47	66	64	54
PgGpDT	47	0.28	5.5	8.2	53	49	48	28	45	46	85	82	68
SpGp	48	13	21	23	52	51	52	28	43	44	81	77	76
RaFeST	48	2.0	14	15	39	47	43	77	150	130	50	120	91
LinS	49	0.0039	2.6	11	40	44	39	65	68	53	64	67	53
RaFeD	49	1.6	15	15	41	47	40	52	55	50	56	62	56
SpNn	49	42	47	40	56	52	49	43	48	42	75	72	65
EsnS	49	2.2	17	16	39	44	39	69	120	68	80	68	54
LinPo4	49	0.50	20	33	49	50	45	48	55	48	65	64	54
PgLlDT	49	40	41	41	51	51	46	44	54	47	170	180	170
RaFeS	49	2.0	16	15	37	44	43	68	66	54	66	68	56
Analog	50	49	53	46	49	52	46	51	52	44	51	52	46
LinPo6T	50	34	38	47	50	49	50	38	51	51	65	64	54
LinPo6	51	0.00014	2.1	17	52	49	45	63	61	49	65	64	53
PgNetDT	52	35	41	36	56	56	52	43	52	47	120	120	110
PgLlST	52	29	41	36	50	50	46	67	93	99	67	70	54
PgLlD	53	34	43	38	51	50	46	54	61	57	170	180	170
Node1	53	47	50	48	60	55	54	46	53	49	58	56	53
EsnST	53	5.1	15	17	37	45	38	65	84	68	62	110	100
Node32	53	43	48	47	53	53	51	69	64	54	68	65	53
PgLlS	53	36	42	37	51	50	46	130	140	130	67	69	56
Pw1Nn	54	45	52	45	54	54	50	49	57	54	70	69	66
L1Nn	54	42	50	43	51	53	49	55	70	67	58	67	63
PgGpD	55	0.28	5.5	8.2	50	72	48	54	59	55	74	110	74
PgNetD	55	32	44	38	56	55	51	53	61	55	120	120	100
PgGpS	55	1.7	12	12	54	57	48	63	70	55	62	73	56
PgGpST	56	1.7	12	12	54	57	48	57	65	56	62	81	71
PgNetST	57	43	47	45	65	61	56	57	62	55	65	66	57
Gru	60	52	55	52	62	62	58	68	68	58	69	67	57
PgNetS	60	42	48	46	65	63	58	67	67	55	67	67	55
Trafo	61	58	61	55	60	61	55	73	70	59	72	70	62
GruT	62	55	57	54	63	62	59	70	67	61	66	69	61
TrafoT	62	59	62	54	61	62	56	71	72	62	72	72	60
ConstM	64	65	64	52	65	64	52	65	64	52	65	64	53
LstmT	64	64	62	56	67	64	55	73	69	57	67	68	58
Lstm	64	63	62	54	66	70	56	73	68	56	70	70	54
RnnT	65	61	63	61	67	67	61	69	69	63	72	70	58
Rnn	66	62	65	63	67	67	62	72	69	59	71	69	59
ConstL	73	74	73	64	74	73	64	74	73	64	74	74	64

Table 8: Mean sMAPE for the three systems of *DeebLorenz*: LORENZ63STD (S, green), LORENZ63RANDOM (R, red), LORENZ63NONPAR (N, blue).

*DeebLorenz*,  $t_{\text{valid}}$ , Values

Method	Median	Constant $\Delta t$						Random $\Delta t$					
		Noisefree			Noisy			Noisefree			Noisy		
		S	R	N	S	R	N	S	R	N	S	R	N
ConstM	0.0	0.0	0.0	0.0	0.0	0.0	0.0	0.0	0.0	0.0	0.0	0.0	0.0
ConstL	0.0	0.0	0.0	0.0	0.0	0.0	0.0	0.0	0.0	0.0	0.0	0.0	0.0
Lstm	0.2	0.9	0.6	0.6	0.6	0.2	0.5	0.1	0.1	0.1	0.1	0.1	0.1
LstmT	0.2	0.7	0.6	0.7	0.5	0.4	0.5	0.1	0.1	0.1	0.1	0.1	0.1
Rnn	0.3	1.0	0.7	0.7	0.4	0.5	0.5	0.2	0.1	0.2	0.2	0.1	0.2
RnnT	0.3	1.0	0.7	0.7	0.4	0.5	0.5	0.2	0.1	0.2	0.2	0.2	0.2
Gru	0.4	1.7	1.2	1.2	0.8	0.6	0.8	0.2	0.2	0.2	0.2	0.2	0.2
Trafo	0.5	1.0	0.7	0.8	1.0	0.7	0.8	0.2	0.2	0.2	0.2	0.2	0.1
TrafoT	0.5	1.0	0.6	0.8	0.9	0.7	0.7	0.3	0.2	0.2	0.3	0.2	0.2
GruT	0.5	1.6	1.0	1.1	0.8	0.6	0.8	0.3	0.2	0.3	0.4	0.3	0.4
PgNetS	0.6	2.6	1.8	1.8	0.7	0.8	0.8	0.3	0.2	0.3	0.4	0.2	0.3
Node32	0.6	2.5	1.8	1.6	1.4	1.1	1.2	0.2	0.1	0.2	0.2	0.2	0.2
PgNetST	0.8	2.4	1.8	1.9	0.7	0.8	0.9	1.2	0.7	0.9	0.6	0.6	0.7
PgL1S	0.9	3.7	2.6	2.9	1.7	1.4	1.6	0.3	0.2	0.2	0.4	0.2	0.3
PgGpS	1.0	9.4	7.2	7.4	1.3	1.4	1.5	0.6	0.3	0.3	0.6	0.2	0.4
PgL1ST	1.0	4.0	2.8	3.3	1.8	1.4	1.6	0.5	0.3	0.4	0.7	0.3	0.4
Pw1Nn	1.1	2.4	1.3	1.9	1.3	1.1	1.2	1.9	0.9	1.1	0.6	0.5	0.7
L1Nn	1.2	2.6	1.5	2.0	1.6	1.1	1.2	1.4	0.6	0.9	1.1	0.5	0.7
PgNetD	1.2	3.8	2.4	2.9	1.4	1.1	1.2	1.5	0.8	0.9	0.0	0.1	0.1
RaFeS	1.2	8.9	6.7	7.1	2.8	2.1	2.0	0.3	0.2	0.3	0.4	0.2	0.3
LinPo6	1.3	10.0	9.4	6.7	1.8	1.6	1.8	0.6	0.7	0.9	0.0	0.0	0.0
Node1	1.3	2.3	1.3	1.5	1.1	1.0	1.0	2.2	1.4	1.4	1.3	1.0	1.0
PgGpST	1.4	9.4	7.2	7.4	1.3	1.4	1.5	1.9	0.8	0.9	0.7	0.6	0.8
PgNetDT	1.4	3.6	2.5	3.1	1.3	1.0	1.2	2.7	1.4	1.5	0.0	0.1	0.1
PgGpD	1.4	9.9	8.7	8.1	1.8	1.4	1.4	1.8	0.8	1.1	0.0	0.1	0.0
EsnS	1.4	9.3	6.3	6.9	2.6	2.2	2.5	0.3	0.2	0.3	0.5	0.2	0.3
LinPo6T	1.4	3.8	3.0	1.5	1.8	1.5	1.1	2.9	1.4	0.8	0.0	0.0	0.1
SpNn	1.4	2.6	1.7	2.5	1.1	1.0	1.2	2.6	1.7	2.4	0.2	0.3	0.3
LinS	1.4	10.0	9.3	7.5	2.9	2.4	2.5	0.4	0.3	0.3	0.5	0.2	0.3
PgL1D	1.5	3.7	2.6	3.0	1.7	1.4	1.6	1.7	0.9	1.1	0.0	0.1	0.1
EsnST	1.5	8.5	6.7	6.5	2.9	2.0	2.5	0.5	0.3	0.3	1.0	0.4	0.5
PgL1DT	1.5	3.1	2.6	2.4	1.7	1.4	1.6	2.4	1.1	1.4	0.0	0.1	0.1
Analog	1.5	1.8	1.2	1.6	1.7	1.3	1.5	1.8	1.1	1.5	1.7	1.0	1.4
LinPo4	1.6	9.8	6.1	3.8	1.7	1.6	1.8	2.3	1.0	1.2	0.0	0.1	0.1
LinPo4T	1.7	6.6	4.8	3.5	1.7	1.6	1.8	3.7	1.7	1.7	0.0	0.1	0.1
RaFeD	1.8	9.2	6.8	7.0	2.8	1.8	2.0	1.9	0.9	1.2	1.5	0.7	0.8
RaFeST	1.9	8.9	7.0	7.0	2.7	1.9	2.0	0.6	0.3	0.5	1.8	0.6	0.7
RaFeDT	1.9	9.2	6.7	6.9	2.7	1.8	2.0	2.3	1.3	1.5	1.7	0.8	0.9
PgGpDT	1.9	9.9	8.7	8.1	1.6	1.5	1.4	4.5	2.3	2.2	0.0	0.0	0.0
LinD	2.0	10.0	8.8	7.8	2.9	2.3	2.5	1.6	0.8	1.2	0.0	0.1	0.0
SpPo2	2.0	9.9	6.7	0.9	3.7	3.1	0.9	5.8	3.1	0.9	0.1	0.1	0.1
EsnD	2.1	9.4	6.2	6.5	2.6	2.4	2.3	1.9	1.1	1.1	1.5	0.8	0.9
SpGp	2.2	7.0	5.8	5.9	1.7	1.4	1.4	4.8	2.7	3.3	0.1	0.5	0.3
LinST	2.2	10.0	9.3	7.5	3.2	2.4	2.8	2.1	0.9	0.7	1.6	1.2	0.6
EsnDT	2.4	9.4	6.1	6.2	2.8	2.3	2.5	2.6	1.1	1.2	1.6	0.8	0.9
SINDy	2.6	9.9	6.9	5.9	2.6	2.1	2.6	5.3	2.4	2.8	0.1	0.1	0.1
SINDyN	2.6	9.9	6.6	3.0	2.7	2.1	2.5	5.2	2.3	2.8	0.1	0.1	0.1
SpPo4	2.8	10.0	7.5	4.5	2.8	2.4	2.5	5.5	2.8	3.0	0.1	0.1	0.1
LinDT	2.8	10.0	8.7	7.8	3.2	2.4	3.2	4.3	1.4	1.5	0.1	0.0	0.1
SpPo	3.0	10.0	7.5	6.7	3.7	3.1	2.7	5.5	2.9	2.7	0.1	0.1	0.1
GpGp	3.4	7.7	5.5	5.5	2.5	1.8	2.2	7.1	4.3	4.4	2.3	1.7	1.5

Table 9: Mean  $t_{\text{valid}}$  for the three systems of *DeebLorenz*: LORENZ63STD (S, green), LORENZ63RANDOM (R, red), LORENZ63NONPAR (N, blue).

*DeebLorenz*, CME, Ranks

Method	Median	Constant $\Delta t$						Random $\Delta t$					
		Noisefree			Noisy			Noisefree			Noisy		
		S	R	N	S	R	N	S	R	N	S	R	N
LinST	4.5	4	2	7	4	3	2	18	22	31	5	2	10
LinDT	7.0	3	5	3	3	4	1	9	14	12	38	48	33
SpPo	7.5	7	8	13	2	1	9	4	3	6	35	33	36
SpPo4	7.5	6	9	22	15	5	5	3	4	3	33	32	37
GpGp	8.5	24	25	21	18	18	15	1	1	1	1	1	2
EsnDT	10.5	14	22	17	9	8	4	12	18	18	4	5	7
SINDy	12.0	8	12	19	17	12	6	5	6	4	36	35	35
LinS	12.5	5	3	8	8	6	8	34	33	38	17	20	22
RaFeD	14.0	18	15	11	10	17	13	21	21	17	8	8	6
RaFeDT	14.0	19	16	12	12	15	14	16	15	14	3	6	3
EsnD	14.5	15	20	15	14	9	11	20	17	20	7	7	5
LinD	14.5	2	4	4	7	7	10	24	23	19	44	41	50
RaFeST	14.5	22	13	10	11	16	16	32	36	33	2	9	8
SINDyN	14.5	12	17	27	16	13	12	6	8	5	37	37	34
PgGpDT	15.0	10	6	1	28	20	29	8	7	8	43	45	42
EsnST	16.5	23	18	18	6	14	3	36	37	34	11	15	14
PgGpST	19.5	16	10	5	35	29	26	23	27	30	12	10	9
EsnS	20.0	20	21	16	13	10	7	37	42	36	18	23	20
RaFeS	20.0	21	19	9	5	11	17	33	35	35	21	22	19
SpPo2	20.0	9	14	43	1	1	39	2	2	26	34	34	38
LinPo4	21.5	13	23	23	20	23	18	19	20	16	46	42	44
LinPo4T	23.0	26	26	24	21	22	19	10	10	10	45	43	45
SpGp	24.5	25	24	20	30	28	28	7	5	2	31	14	26
Analog	25.0	41	41	37	29	31	25	25	16	9	6	3	1
PgGpS	25.5	16	10	5	35	29	26	31	32	32	13	25	17
PgL1ST	26.0	27	28	25	27	21	23	35	34	37	16	18	16
LinPo6	26.5	1	1	14	23	24	24	38	31	29	51	50	46
PgGpD	26.5	10	6	1	22	32	29	27	26	23	41	31	47
Node1	27.0	40	39	38	40	37	38	17	11	13	9	4	4
PgL1S	27.5	32	29	29	24	26	22	41	44	44	20	21	18
LinPo6T	28.0	29	27	40	19	19	36	11	12	24	49	49	39
PgL1D	28.0	30	31	30	25	25	21	26	25	22	50	46	49
SpNn	28.0	36	36	32	38	33	31	14	9	7	25	16	21
PgL1DT	28.5	33	30	31	26	27	20	15	19	15	47	47	48
Pw1Nn	29.0	39	40	35	34	36	34	22	24	21	15	13	13
L1Nn	30.5	35	38	33	31	34	32	29	30	28	10	12	12
PgNetST	32.0	37	34	36	45	40	40	30	28	27	14	11	11
PgNetD	33.0	28	33	28	33	38	33	28	29	25	39	40	40
PgNetDT	33.5	31	32	26	37	39	35	13	13	11	40	39	43
Node32	37.0	38	37	39	32	35	37	46	45	45	24	29	25
PgNetS	37.0	34	35	34	44	42	41	39	39	39	22	24	23
Trafo	40.5	44	44	45	39	41	42	45	40	40	27	26	30
TrafoT	41.5	47	46	44	41	43	43	40	41	42	23	19	24
Gru	42.0	42	42	41	42	44	44	43	43	43	26	27	27
GruT	42.0	43	43	42	43	45	45	42	38	41	19	17	15
RnnT	45.5	45	45	46	48	46	48	44	46	47	28	28	29
Rnn	47.0	46	47	49	47	47	49	47	47	46	29	30	28
Lstm	48.0	48	49	48	46	49	46	48	49	49	30	38	31
LstmT	48.0	49	48	47	49	48	47	49	48	48	32	36	32
ConstL	50.0	50	50	50	50	50	50	50	50	50	42	44	41
ConstM	51.0	51	51	51	51	51	51	51	51	51	48	51	51

Table 10: Ranking according to mean Cumulative Maximum Error (CME) for the three systems of *DeebLorenz*: LORENZ63STD (S, green), LORENZ63RANDOM (R, red), LORENZ63NONPAR (N, blue).



*DeebLorenz*, sMAPE, Ranks

Method	Median	Constant $\Delta t$							Random $\Delta t$						
		Noisefree			Noisy				Noisefree			Noisy			
		S	R	N	S	R	N	S	R	N	S	R	N		
LinST	5.5	4	2	6	6	5	1	20	24	33	5	3	18		
LinDT	6.5	3	5	4	5	3	2	8	16	13	23	49	16		
SpPo	7.5	7	8	14	1	1	8	4	4	5	39	39	36		
LinS	10.0	5	3	5	11	8	9	35	38	22	14	20	4		
SpPo4	10.5	6	11	22	14	9	10	3	2	3	41	37	37		
LinD	11.5	2	4	3	12	4	11	23	22	18	49	15	2		
EsnDT	13.5	14	22	18	13	13	4	12	29	29	3	8	44		
PgGpDT	14.5	10	6	1	31	19	28	9	8	9	44	42	39		
RaFeDT	14.5	16	14	12	8	17	15	16	15	42	2	5	9		
SINDyN	14.5	12	19	27	17	11	12	6	6	2	40	36	33		
GpGp	15.0	24	25	21	16	16	14	1	1	1	1	1	27		
RaFeD	15.0	15	17	11	15	15	13	24	19	17	8	7	22		
SINDy	15.0	8	12	19	38	18	7	5	7	4	46	48	48		
LinPo6	16.0	1	1	16	28	21	18	32	25	15	16	10	5		
EsnD	17.5	19	21	17	9	6	6	19	18	20	7	6	21		
RaFeST	18.5	20	13	9	7	14	17	50	51	50	4	45	45		
EsnST	19.0	23	15	15	4	12	3	34	47	48	11	44	46		
LinPo4	19.0	13	23	23	20	25	19	18	20	14	19	13	10		
Analog	19.5	41	41	37	18	29	21	22	13	8	6	2	1		
LinPo4T	19.5	25	26	24	19	26	20	10	9	10	20	12	11		
LinPo6T	19.5	29	27	38	21	20	33	11	11	19	17	11	13		
SpPo2	20.0	9	16	45	2	1	39	2	3	24	45	40	42		
EsnS	20.5	22	20	13	10	7	5	40	49	47	42	21	8		
RaFeS	20.5	21	18	10	3	10	16	38	33	25	21	22	20		
Node1	26.0	40	39	40	39	35	40	17	14	16	9	4	7		
PgL1ST	26.0	27	29	25	22	24	23	37	48	49	24	29	14		
PgGpS	26.5	17	9	7	32	37	26	31	42	27	13	34	17		
PgGpD	27.0	10	6	1	23	50	28	26	23	32	37	43	41		
SpGp	27.0	26	24	20	29	28	36	7	5	7	43	38	43		
PgL1S	27.5	32	31	28	26	22	25	51	50	51	26	27	19		
PgL1DT	28.5	33	30	32	27	27	22	15	17	12	51	51	50		
PgL1D	30.0	30	32	30	25	23	24	27	26	37	50	50	51		
Node32	31.0	38	36	39	30	31	35	41	31	23	28	14	6		
PgGpST	31.0	17	9	7	32	37	26	30	32	34	12	41	40		
L1Nn	32.0	35	38	33	24	32	30	28	43	46	10	19	32		
SpNn	32.0	36	34	31	36	30	31	13	10	6	38	33	35		
Pw1Nn	32.5	39	40	34	34	33	32	21	21	26	31	26	38		
PgNetDT	33.0	31	28	26	35	36	37	14	12	11	48	47	49		
PgNetST	33.0	37	35	35	46	39	45	29	28	31	18	16	24		
PgNetD	33.5	28	33	29	37	34	34	25	27	30	47	46	47		
PgNetS	35.0	34	37	36	45	44	46	36	34	28	25	17	15		
ConstM	35.5	50	49	42	44	45	38	33	30	21	15	9	3		
Gru	40.0	42	42	41	42	42	47	39	36	38	29	18	23		
Trafo	41.0	44	44	47	40	40	42	47	44	39	34	30	31		
GruT	42.0	43	43	43	43	41	48	43	35	41	22	25	30		
LstmT	43.0	49	45	48	48	46	41	46	41	36	27	23	26		
TrafoT	43.0	45	46	46	41	43	43	44	45	43	35	32	29		
Lstm	44.0	48	47	44	47	49	44	48	37	35	30	28	12		
RnnT	45.0	46	48	49	49	47	49	42	40	44	33	31	25		
Rnn	46.0	47	50	50	50	48	50	45	39	40	32	24	28		
ConstL	50.0	51	51	51	51	51	51	49	46	45	36	35	34		

Table 11: Ranking according to mean sMAPE for the three systems of *DeebLorenz*: LORENZ63STD (S, green), LORENZ63RANDOM (R, red), LORENZ63NONPAR (N, blue).

*DeebLorenz*,  $t_{\text{valid}}$ , Ranks

Method	Median	Constant $\Delta t$						Random $\Delta t$					
		Noisefree			Noisy			Noisefree			Noisy		
		S	R	N	S	R	N	S	R	N	S	R	N
LinST	4.5	1	2	5	4	4	2	19	23	31	5	2	13
SpPo	6.5	7	8	14	1	1	3	3	3	6	34	32	32
GpGp	7.0	24	25	21	18	18	13	1	1	1	1	1	1
LinDT	7.0	1	5	3	3	5	1	9	13	13	38	49	31
SpPo4	7.5	6	9	22	11	3	6	4	4	3	32	36	32
EsnDT	11.5	15	23	18	10	9	9	13	17	18	6	5	5
LinS	12.0	1	2	5	6	7	7	36	34	38	17	21	19
SINDy	13.0	8	13	19	16	13	4	5	6	4	36	35	36
SINDyN	13.0	12	19	27	14	11	5	6	8	5	35	34	35
LinD	13.5	1	4	3	5	8	8	27	25	19	47	37	50
RaFeST	13.5	21	12	10	12	15	15	32	33	32	2	11	9
RaFeDT	14.0	20	17	12	13	16	16	16	15	12	3	7	6
EsnD	14.5	14	21	17	15	6	12	20	16	21	8	6	4
EsnST	15.0	23	15	16	7	14	9	35	36	35	11	15	14
RaFeD	15.0	19	14	11	9	17	17	21	21	16	7	8	7
PgGpDT	16.5	10	6	1	30	23	29	8	7	8	49	50	47
EsnS	19.0	18	20	13	17	10	11	39	41	37	18	23	20
PgGpST	19.0	16	10	7	36	25	26	22	27	25	12	9	8
RaFeS	21.0	22	18	9	8	12	14	37	40	34	21	22	21
LinPo4	21.5	13	22	23	23	21	19	17	20	17	46	45	39
SpPo2	21.5	9	16	43	2	1	39	2	2	27	37	32	37
SpGp	23.0	25	24	20	28	31	28	7	5	2	30	14	22
LinPo4T	23.5	26	26	24	23	20	18	10	9	9	45	44	41
LinPo6	23.5	1	1	15	21	19	20	31	29	26	50	48	46
PgL1ST	24.5	27	28	25	22	24	24	34	32	33	13	17	16
Analog	25.0	41	41	38	29	32	25	25	18	10	4	3	2
PgGpD	25.0	10	6	1	20	30	29	24	26	23	42	31	49
PgGpS	25.0	16	10	7	36	25	26	33	35	36	15	25	17
Node1	27.5	40	40	39	39	37	38	18	12	15	9	4	3
PgL1D	27.5	30	31	28	26	27	21	26	22	20	44	43	45
PgL1S	28.0	31	29	29	26	27	21	40	43	41	20	20	18
Pw1Nn	28.0	38	39	34	34	36	32	23	24	22	14	13	12
LinPo6T	29.5	29	27	40	19	22	37	11	14	30	48	46	40
PgL1DT	29.5	33	30	32	25	29	23	15	19	14	43	42	44
SpNn	29.5	35	37	31	38	38	33	14	10	7	28	16	23
L1Nn	31.0	36	38	33	31	33	35	29	31	29	10	12	10
PgNetD	32.0	28	33	30	33	34	31	28	28	24	39	41	42
PgNetST	32.0	39	34	35	45	41	40	30	30	28	16	10	11
PgNetDT	33.5	32	32	26	35	39	36	12	11	11	40	39	43
Node32	35.5	37	36	37	32	35	34	46	47	45	26	29	26
PgNetS	36.5	34	35	36	44	40	41	38	37	40	22	24	24
TrafoT	41.5	44	47	44	41	42	45	41	39	43	23	19	25
GruT	42.0	43	43	42	42	45	43	42	38	39	19	18	15
Trafo	42.0	45	44	45	40	43	42	45	42	42	27	28	30
Gru	42.5	42	42	41	43	44	44	43	44	44	24	27	28
RnnT	45.5	46	45	46	48	46	48	44	45	47	25	26	27
Rnn	46.5	47	46	48	49	47	49	47	46	46	29	30	29
LstmT	47.5	49	48	47	47	48	47	49	48	48	33	38	38
Lstm	48.0	48	49	49	46	49	46	48	49	49	31	40	34
ConstL	50.0	50	50	50	50	50	50	50	50	50	41	47	48
ConstM	51.0	51	51	51	51	51	51	51	51	51	51	51	51

Table 12: Ranking according to mean  $t_{\text{valid}}$  for the three systems of *DeebLorenz*: LORENZ63STD (S, green), LORENZ63RANDOM (R, red), LORENZ63NONPAR (N, blue).

Ranks for CME, sMAPE,  $t_{\text{valid}}$ 

Method	Constant $\Delta t$									Random $\Delta t$								
	Noisefree			Noisy			Noisefree			Noisefree			Noisy			Noisefree		
	S	R	N	S	R	N	S	R	N	S	R	N	S	R	N	S	R	N
Analog	41,41,41	41,41,41	37,37,38	29,18,29	31,29,32	25,21,25	25,22,25	16,13,18	9,8,10	6,6,4	3,2,3	1,1,2						
ConstL	50,51,50	50,51,50	50,51,50	50,51,50	50,51,50	50,51,50	50,49,50	50,46,50	50,45,50	42,36,41	44,35,47	41,34,48						
ConstM	51,50,51	51,49,51	51,42,51	51,44,51	51,45,51	51,38,51	51,33,51	51,30,51	51,21,51	48,15,51	51,9,51	51,3,51						
EsnD	15,19,14	20,21,21	15,17,17	14,9,15	9,6,6	11,6,12	20,19,20	17,18,16	20,20,21	7,7,8	7,6,6	5,21,4						
EsnDT	14,14,15	22,22,23	17,18,18	9,13,10	8,13,9	4,4,9	12,12,13	18,29,17	18,29,18	4,3,6	5,8,5	7,44,5						
EsnS	20,22,18	21,20,20	16,13,13	13,10,17	10,7,10	7,5,11	37,40,39	42,49,41	36,47,37	18,42,18	23,21,23	20,8,20						
EsnST	23,23,23	18,15,15	18,15,16	6,4,7	14,12,14	3,3,9	36,34,35	37,47,36	34,48,35	11,11,11	15,44,15	14,46,14						
GpGp	24,24,24	25,25,25	21,21,21	18,16,18	18,16,18	15,14,13	1,1,1	1,1,1	1,1,1	1,1,1	1,1,1	2,27,1						
PgGpD	10,10,10	6,6,6	1,1,1	22,23,20	32,50,30	29,28,29	27,26,24	26,23,26	23,32,23	41,37,42	31,43,31	47,41,49						
PgGpDT	10,10,10	6,6,6	1,1,1	28,31,30	20,19,23	29,28,29	8,9,8	7,8,7	8,9,8	43,44,49	45,42,50	42,39,47						
PgGpS	16,17,16	10,9,10	5,7,7	35,32,36	29,37,25	26,26,26	31,31,33	32,42,35	32,27,36	13,13,15	25,34,25	17,17,17						
PgGpST	16,17,16	10,9,10	5,7,7	35,32,36	29,37,25	26,26,26	23,30,22	27,32,27	30,34,25	12,12,12	10,41,9	9,40,8						
Gru	42,42,42	42,42,42	41,41,41	42,42,43	44,42,44	44,47,44	43,39,43	43,36,44	43,38,44	26,29,24	27,18,27	27,23,28						
GruT	43,43,43	43,43,43	42,43,42	43,43,42	45,41,45	45,48,43	42,43,42	38,35,38	41,41,39	19,22,19	17,25,18	15,30,15						
LinD	2,2,1	4,4,4	4,3,3	7,12,5	7,4,8	10,11,8	24,23,27	23,22,25	19,18,19	44,49,47	41,15,37	50,2,50						
LinDT	3,3,1	5,5,5	3,4,3	3,5,3	4,3,5	1,2,1	9,8,9	14,16,13	12,13,13	38,23,38	48,49,49	33,16,31						
LinPo4	13,13,13	23,23,22	23,23,23	20,20,23	23,25,21	18,19,19	19,18,17	20,20,20	16,14,17	46,19,46	42,13,45	44,10,39						
LinPo4T	26,25,26	26,26,26	24,24,24	21,19,23	22,26,20	19,20,18	10,10,10	10,9,9	10,10,9	45,20,45	43,12,44	45,11,41						
LinPo6	1,1,1	1,1,1	14,16,15	23,28,21	24,21,19	24,18,20	38,32,31	31,25,29	29,15,26	51,16,50	50,10,48	46,5,46						
LinPo6T	29,29,29	27,27,27	40,38,40	19,21,19	19,20,22	36,33,37	11,11,11	12,11,14	24,19,30	49,17,48	49,11,46	39,13,40						
LinS	5,5,1	3,3,2	8,5,5	8,11,6	6,8,7	8,9,7	34,35,36	33,38,34	38,22,38	17,14,17	20,20,21	22,4,19						
LinST	4,4,1	2,2,2	7,6,5	4,6,4	3,5,4	2,1,2	18,20,19	22,24,23	31,33,31	5,5,5	2,3,2	10,18,13						
LlNn	35,35,36	38,38,38	33,33,33	31,24,31	34,32,33	32,30,35	29,28,29	30,43,31	28,46,29	10,10,10	12,19,12	12,32,10						
PgLlD	30,30,30	31,32,31	30,30,28	25,25,26	25,23,27	21,24,21	26,27,26	25,26,22	22,37,20	50,50,44	46,50,43	49,51,45						
PgLlDT	33,33,33	30,30,30	31,32,32	26,27,25	27,27,29	20,22,23	15,15,15	19,17,19	15,12,14	47,51,43	47,51,42	48,50,44						
PgLlS	32,32,31	29,31,29	29,28,29	24,26,26	26,22,27	22,25,21	41,51,40	44,50,43	44,51,41	20,26,20	21,27,20	18,19,18						
PgLlST	27,27,27	28,29,28	25,25,25	27,22,22	21,24,24	23,23,24	35,37,34	34,48,32	37,49,33	16,24,13	18,29,17	16,14,16						
Lstm	48,48,48	49,47,49	48,44,49	46,47,46	49,49,49	46,44,46	48,48,48	49,37,49	49,35,49	30,30,31	38,28,40	31,12,34						
LstmT	49,49,49	48,45,48	47,48,47	49,48,47	48,46,48	47,41,47	49,46,49	48,41,48	48,36,48	32,27,33	36,23,38	32,26,38						
PgNetD	28,28,28	33,33,33	28,29,30	33,37,33	38,34,34	33,34,31	28,25,28	29,27,28	25,30,24	39,47,39	40,46,41	40,47,42						
PgNetDT	31,31,32	32,28,32	26,26,26	37,35,35	39,36,39	35,37,36	13,14,12	13,12,11	11,11,11	40,48,40	39,47,39	43,49,43						
PgNetS	34,34,34	35,37,35	34,36,36	44,45,44	42,44,40	41,46,41	39,36,38	39,34,37	39,28,40	22,25,22	24,17,24	23,15,24						
PgNetST	37,37,39	34,35,34	36,35,35	45,46,45	40,39,41	40,45,40	30,29,30	28,28,30	27,31,28	14,18,16	11,16,10	11,24,11						
Node1	40,40,40	39,39,40	38,40,39	40,39,39	37,35,37	38,40,38	17,17,18	11,14,12	13,16,15	9,9,9	4,4,4	4,7,3						
Node32	38,38,37	37,36,36	39,39,37	32,30,32	35,31,35	37,35,34	46,41,46	45,31,47	45,23,45	24,28,26	29,14,29	25,6,26						
PwLlNn	39,39,38	40,40,39	35,34,34	34,34,34	36,33,36	34,32,32	22,21,23	24,21,24	21,26,22	15,31,14	13,26,13	13,38,12						
RaFeD	18,15,19	15,17,14	11,11,11	10,15,9	17,15,17	13,13,17	21,24,21	21,19,21	17,17,16	8,8,7	8,7,8	6,22,7						
RaFeDT	19,16,20	16,14,17	12,12,12	12,8,13	15,17,16	14,15,16	16,16,16	15,15,15	14,42,12	3,2,3	6,5,7	3,9,6						
RaFeS	21,21,22	19,18,18	9,10,9	5,3,8	11,10,12	17,16,14	33,38,37	35,33,40	35,25,34	21,21,21	22,22,22	19,20,21						
RaFeST	22,20,21	13,13,12	10,9,10	11,7,12	16,14,15	16,17,15	32,50,32	36,51,33	33,50,32	2,4,2	9,45,11	8,45,9						
Rnn	46,47,47	47,50,46	49,50,48	47,50,49	47,48,47	49,50,49	47,45,47	47,39,46	46,40,46	29,32,29	30,24,30	28,28,29						
RnnT	45,46,46	45,48,45	46,49,46	48,49,48	46,47,46	48,49,48	44,42,44	46,40,45	47,44,47	28,33,25	28,31,26	29,25,27						
SpGp	25,26,25	24,24,24	20,20,20	30,29,28	28,28,31	28,36,28	7,7,7	5,5,5	2,7,2	31,43,30	14,38,14	26,43,22						
SpNn	36,36,35	36,34,37	32,31,31	38,36,38	33,30,38	31,31,33	14,13,14	9,10,10	7,6,7	25,38,28	16,33,16	21,35,23						
SpPo	7,7,7	8,8,8	13,14,14	2,1,1	1,1,1	9,8,3	4,4,3	3,4,3	6,5,6	35,39,34	33,39,32	36,36,32						
SpPo2	9,9,9	14,16,16	43,45,43	1,2,2	1,1,1	39,39,39	2,2,2	2,3,2	26,24,27	34,45,37	34,40,32	38,42,37						
SpPo4	6,6,6	9,11,9	22,22,22	15,14,11	5,9,3	5,10,6	3,3,4	4,2,4	3,3,3	33,41,32	32,37,36	37,37,32						
SINDy	8,8,8	12,12,13	19,19,19	17,38,16	12,18,13	6,7,4	5,5,5	6,7,6	4,4,4	36,46,36	35,48,35	35,48,36						
SINDyN	12,12,12	17,19,19	27,27,27	16,17,14	13,11,11	12,12,5	6,6,6	8,6,8	5,2,5	37,40,35	37,36,34	34,33,35						
Trafo	44,44,45	44,44,44	45,47,45	39,40,40	41,40,43	42,42,42	45,47,45	40,44,42	40,39,42	27,34,27	26,30,28	30,31,30						
TrafoT	47,45,44	46,46,47	44,46,44	41,41,41	43,43,42	43,43,45	40,44,41	41,45,39	42,43,43	23,35,23	19,32,19	24,29,25						

Table 13: Ranks of all error metrics for the three systems of *DeebLorenz*: LORENZ63STD (S, green), LORENZ63RANDOM (R, red), LORENZ63NONPAR (N, blue). The cells with the largest differences in ranks are shown in lighter color.

*Dysts*, Noisefree

Method	Validation			Test		
	CME	sMAPE	$t_{\text{valid}}$	CME	sMAPE	$t_{\text{valid}}$
Analog	0.61	37	0.10	0.60	34	0.13
ConstL	0.95	110	0.010	0.96	110	0.010
ConstM	1.0	110	0	1.0	100	0
EsnD	0.0047	0.16	1.0	0.022	0.67	1.0
EsnS	0.0040	0.12	1.0	0.030	0.96	1.0
GpGp	0.26	13	0.33	0.64	36	0.20
Gru	0.28	13	0.42	0.40	18	0.37
LinD	0.0013	0.066	1.0	0.0079	0.41	1.0
LinPo4	0.033	1.5	1.0	0.040	1.1	1.0
LinPo6	0.47	19	0.49	0.19	12	0.55
LinS	0.0011	0.035	1.0	0.0054	0.23	1.0
LlNn	0.64	38	0.12	0.73	48	0.085
Lstm	0.77	56	0.055	0.91	85	0
Node1	0.18	8.9	0.59	0.42	14	0.39
Node32	0.26	12	0.46	0.44	24	0.28
PgGpD	0.052	1.9	0.98	0.22	8.1	0.55
PgGpS	0.13	5.3	0.74	0.44	20	0.35
PgLlD	0.32	20	0.41	0.61	40	0.29
PgLlS	0.31	12	0.41	0.57	35	0.23
PgNetD	0.15	8.3	0.65	0.26	12	0.46
PgNetS	0.27	14	0.45	0.46	19	0.32
PwlNn	0.61	33	0.13	0.60	35	0.16
RaFeD	0.0036	0.14	1.0	0.022	0.92	1.0
RaFeS	0.0039	0.19	1.0	0.029	0.84	1.0
Rnn	0.49	27	0.23	0.62	39	0.19
SINDy	0.010	0.37	1.0	0.035	1.4	1.0
SINDyN	0.058	2.3	0.96	0.12	6.0	0.76
SpGp	0.26	14	0.37	0.54	28	0.28
SpNn	0.63	38	0.13	0.62	36	0.16
SpPo	0.0022	0.061	1.0	0.0041	0.18	1.0
SpPo2	0.21	4.0	0.45	0.21	3.8	0.71
SpPo4	0.012	0.35	1.0	0.0079	0.40	1.0
Trafo	0.45	26	0.13	0.63	40	0.15
_BlRNN				0.90	90	0.025
_DLin				0.90	76	0.025
_Esn				0.79	93	0.12
_Kalma				0.98	120	0
_LinRe				0.84	64	0.060
_NBEAT				0.56	27	0.13
_NHITS				0.70	38	0.10
_NLin				0.88	74	0.020
_Node				0.77	44	0.045
_Nvar				0.80	51	0.065
_RaFo				0.69	49	0.060
_RNN				0.76	52	0.090
_TCN				0.94	110	0.015
_Trafo				0.81	58	0.015
_XGB				0.81	71	0.050

*Dysts*, Noisy

Method	Validation			Test		
	CME	sMAPE	$t_{\text{valid}}$	CME	sMAPE	$t_{\text{valid}}$
Analog	0.76	52	0.010	0.81	57	0.0050
ConstL	0.96	94	0.010	0.96	100	0.010
ConstM	1.0	100	0	1.0	110	0
EsnD	0.36	17	0.18	0.73	54	0.095
EsnS	0.38	17	0.19	0.76	52	0.090
GpGp	0.63	41	0.050	0.90	85	0.020
Gru	0.63	44	0.10	0.75	54	0.095
LinD	0.49	25	0.18	0.77	58	0.065
LinPo4	0.84	68	0.045	0.84	65	0.045
LinPo6	0.89	77	0.030	0.91	78	0.025
LinS	0.46	25	0.16	0.77	57	0.055
LlNn	0.79	54	0.045	0.88	75	0.025
Lstm	0.81	73	0.035	0.96	110	0
Node1	0.61	43	0.095	0.77	56	0.085
Node32	0.69	44	0.075	0.80	60	0.065
PgGpD	0.67	45	0.060	0.88	72	0.030
PgGpS	0.67	43	0.055	0.86	68	0.030
PgLlD	0.63	49	0.085	0.80	68	0.065
PgLlS	0.63	44	0.070	0.81	66	0.060
PgNetD	0.73	47	0.070	0.80	55	0.080
PgNetS	0.74	59	0.085	0.80	63	0.050
PwlNn	0.80	55	0.050	0.83	65	0.050
RaFeD	0.45	19	0.11	0.84	69	0.050
RaFeS	0.45	19	0.11	0.80	72	0.050
Rnn	0.71	49	0.085	0.77	60	0.070
SINDy	0.86	100	0.045	0.87	96	0.035
SINDyN	0.83	60	0.055	0.87	70	0.035
SpGp	0.81	51	0.035	0.92	82	0.020
SpNn	0.81	60	0.040	0.85	63	0.035
SpPo	0.65	40	0.095	0.78	52	0.065
SpPo2	0.79	54	0.055	0.79	51	0.050
SpPo4	0.81	67	0.060	0.85	62	0.045
Trafo	0.63	43	0.030	0.77	57	0.040

Table 14: Median error metrics of tuned methods on validation and testing datasets for the *Dysts* database. Here,  $t_{\text{valid}}$  is normalized so that the best value is 1 to make different systems comparable.

Relative Differences in CME When Adding the Timestep to the Input ( $\emptyset \rightarrow T$ )

Method		Constant $\Delta t$						Random $\Delta t$					
		Noisefree			Noisy			Noisefree			Noisy		
		S	R	N	S	R	N	S	R	N	S	R	N
	$T < \emptyset$	22%	50%	39%	28%	61%	44%	94%	83%	89%	83%	78%	72%
EsnD	67%	0.05	-0.03	-0.07	0.03	0.00	0.03	0.10	-0.01	0.01	0.03	0.01	-0.01
EsnS	75%	-0.57	0.12	-0.05	0.05	-0.02	0.01	0.00	0.01	0.01	0.06	0.03	0.02
Gru	50%	-0.02	-0.02	-0.02	0.00	0.00	0.00	0.00	0.01	0.00	0.04	0.01	0.03
LinD	75%	-0.57	-0.13	0.00	0.04	0.00	0.09	0.45	0.06	0.05	0.01	-0.01	0.02
LinPo4	42%	-1.70	-0.29	-0.03	0.00	0.00	0.00	0.26	0.09	0.06	0.00	0.00	0.00
LinPo6	67%	-2.00	-1.73	-0.89	0.01	0.01	-0.09	0.41	0.11	0.01	0.00	0.00	0.01
LinS	100%	0.00	0.00	0.00	0.04	0.00	0.05	0.24	0.09	0.05	0.18	0.15	0.04
Lstm	50%	-0.02	0.00	0.00	0.00	0.03	0.00	0.00	0.00	0.00	-0.01	0.00	0.00
PgGpD	42%	0.00	0.00	0.00	-0.01	0.04	0.00	0.49	0.20	0.17	0.00	-0.02	0.01
PgGpS	50%	0.00	0.00	0.00	0.00	0.00	0.00	0.16	0.06	0.05	0.01	0.05	0.04
PgLlD	58%	-0.10	0.00	-0.04	0.00	0.00	0.00	0.12	0.03	0.04	0.00	0.00	0.00
PgLlS	83%	0.12	0.03	0.05	-0.01	0.00	0.00	0.03	0.01	0.01	0.02	0.01	0.01
PgNetD	50%	-0.05	0.04	0.03	-0.02	-0.01	-0.02	0.16	0.09	0.10	0.00	0.00	0.00
PgNetS	75%	-0.03	0.01	-0.01	0.00	0.01	0.01	0.12	0.06	0.07	0.04	0.05	0.04
RaFeD	58%	-0.01	-0.01	-0.03	0.00	0.00	0.00	0.08	0.04	0.02	0.06	0.02	0.02
RaFeS	58%	0.00	0.09	-0.01	-0.05	-0.04	0.00	0.01	0.00	0.00	0.22	0.06	0.04
Rnn	75%	0.00	0.00	0.01	0.00	0.00	0.01	0.02	0.00	-0.01	0.01	0.00	0.00
Trafo	42%	0.00	-0.01	0.01	-0.03	-0.01	0.00	0.02	0.00	0.00	0.01	0.01	0.02

Table 15: Relative differences,  $2(\emptyset - T)/(\emptyset + T)$ , in CME between default ( $\emptyset$ ) and timestep input ( $T$ ) variants of propagator estimators on the three systems of *DeebLorenz* — LORENZ63STD (S, green), LORENZ63RANDOM (R, red), LORENZ63NONPAR (N, blue).

Relative Differences in CME Between State ( $S$ ) and Diff. Quotient Target ( $D$ )

Method		<i>Dysts</i>		<i>DeebLorenz</i>											
		Constant $\Delta t$		Constant $\Delta t$						Random $\Delta t$					
		Noisefree	Noisy	Noisefree			Noisy			Noisefree			Noisy		
		Median	Median	S	R	N	S	R	N	S	R	N	S	R	N
	$D < S$	67%	33%	92%	50%	67%	58%	58%	58%	100%	100%	100%	25%	33%	33%
Esn	86%	0.31	0.04	0.36	0.02	0.02	0.00	0.01	-0.02	0.22	0.13	0.11	0.16	0.08	0.08
EsnT	75%			0.93	-0.13	0.00	-0.03	0.02	0.00	0.31	0.11	0.11	0.13	0.07	0.05
Lin	43%	-0.38	0.00	1.24	-0.48	0.24	0.00	0.00	-0.01	0.18	0.08	0.11	-0.09	-0.03	-0.05
LinT	58%			0.82	-0.60	0.24	0.00	0.00	0.03	0.39	0.05	0.12	-0.26	-0.19	-0.08
PgGp	57%	0.67	-0.02	1.12	0.75	0.28	0.07	0.00	-0.01	0.14	0.07	0.08	-0.10	-0.01	-0.06
PgGpT	67%			1.12	0.75	0.28	0.06	0.04	-0.01	0.47	0.21	0.20	-0.11	-0.08	-0.09
PgLl	50%	-0.08	0.01	0.01	0.00	-0.02	0.00	0.00	0.00	0.19	0.10	0.12	-0.08	-0.04	-0.06
PgLlT	42%			-0.20	-0.03	-0.11	0.00	0.00	0.00	0.28	0.11	0.15	-0.10	-0.04	-0.07
PgNet	71%	0.56	0.00	0.20	0.08	0.16	0.10	0.05	0.07	0.16	0.06	0.08	-0.06	-0.03	-0.04
PgNetT	75%			0.18	0.11	0.20	0.09	0.03	0.04	0.21	0.09	0.10	-0.10	-0.08	-0.08
RaFe	71%	0.28	-0.04	0.33	0.06	-0.04	-0.05	-0.04	0.03	0.20	0.09	0.12	0.14	0.06	0.07
RaFeT	67%			0.32	-0.04	-0.06	0.00	0.00	0.03	0.26	0.13	0.14	-0.02	0.02	0.05

Table 16: Relative differences,  $2(S - D)/(S + D)$ , in CME between state ( $S$ ) and difference quotient ( $D$ ) variants of propagator estimators on the three systems of *DeebLorenz* — LORENZ63STD (S, green), LORENZ63RANDOM (R, red), LORENZ63NONPAR (N, blue) — and median of the *Dysts* testing datasets.

*DeebLorenz* (100 repetitions), CME,  $t$ -test,  $p$ -values

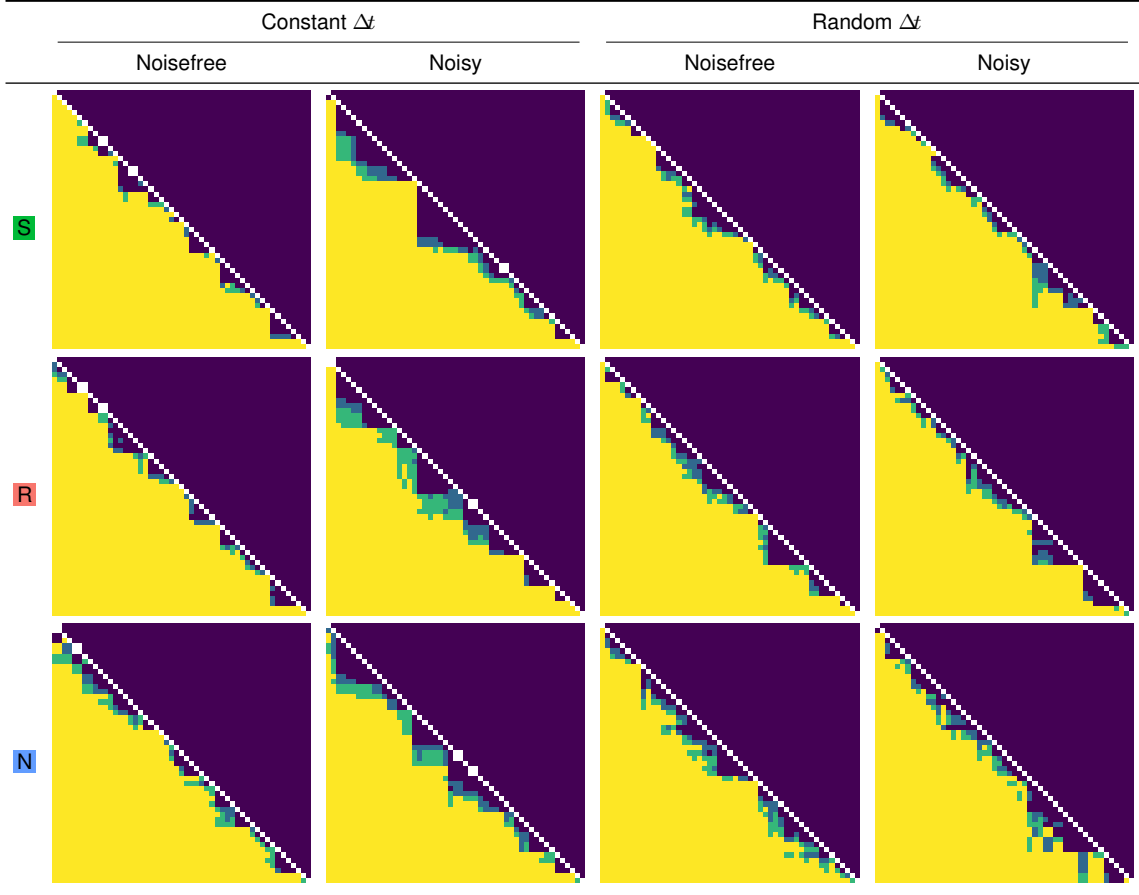


Figure 7: For *DeebLorenz*, the  $p$ -values for paired, one-sided  $t$ -tests of the null hypothesis  $\text{CME}(\text{ColumnMethod}) \geq \text{CME}(\text{RowMethod})$ . The colors from yellow to dark blue indicate  $p$ -values in the intervals  $[0, 0.001]$ ,  $(0.001, 0.01]$ ,  $(0.01, 0.05]$ ,  $(0.05, 1]$ . That is, a pixel in dark blue color indicates that the method corresponding to its column index is not significantly better than the method corresponding to its row index. If the color is yellow, then the difference is highly significant. The methods for the rows and columns are sorted by rank (see Table 10), with the best method at the top and on the left, respectively. The plots show that rankings are mostly statistically significant up to perturbations of a few positions.

*DeebLorenz* (10 repetitions), CME,  $t$ -test,  $p$ -values

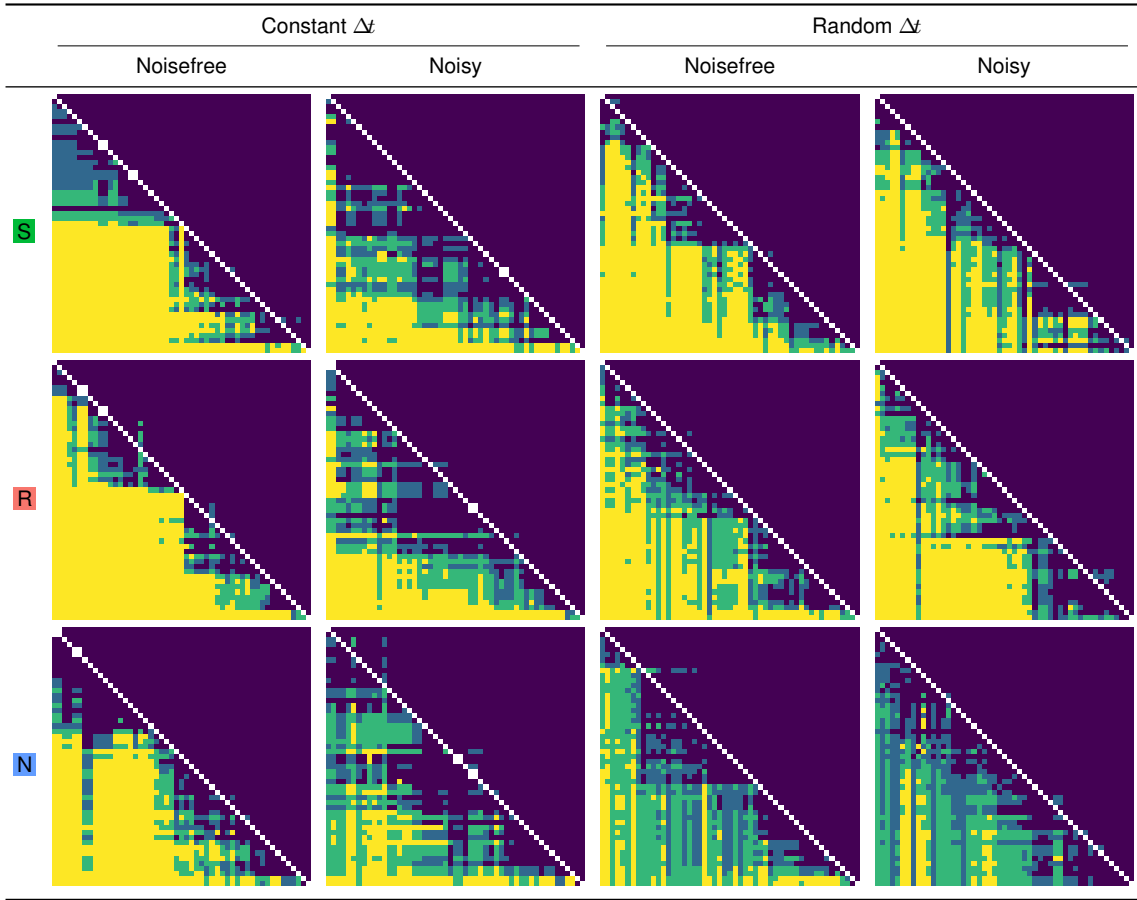


Figure 8: Same as Figure 7 but with only 10 instead of 100 repetitions. The methods are ordered as in Figure 7, i.e., according to Table 10. The  $p$ -values are larger than in Figure 7. This plot shows that doing only 10 repetitions leads to largely indistinguishable method performances.

Cumulative Maximum Error for Test Data of LORENZ63STD with Constant Timestep

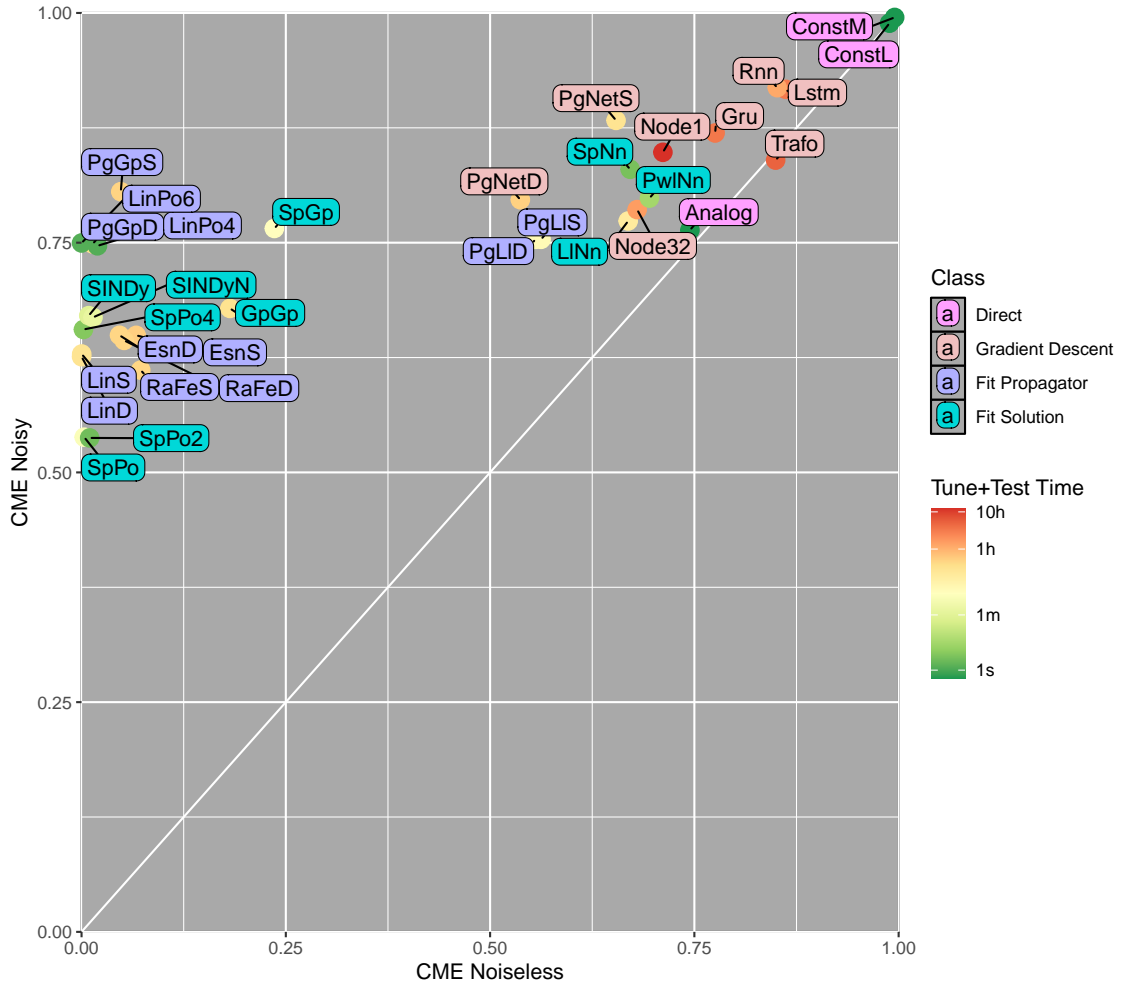


Figure 9: Same as Figure 4 but for LORENZ63STD with Constant Timestep.



Cumulative Maximum Error for Test Data of LORENZ63NONPAR with Constant Timestep

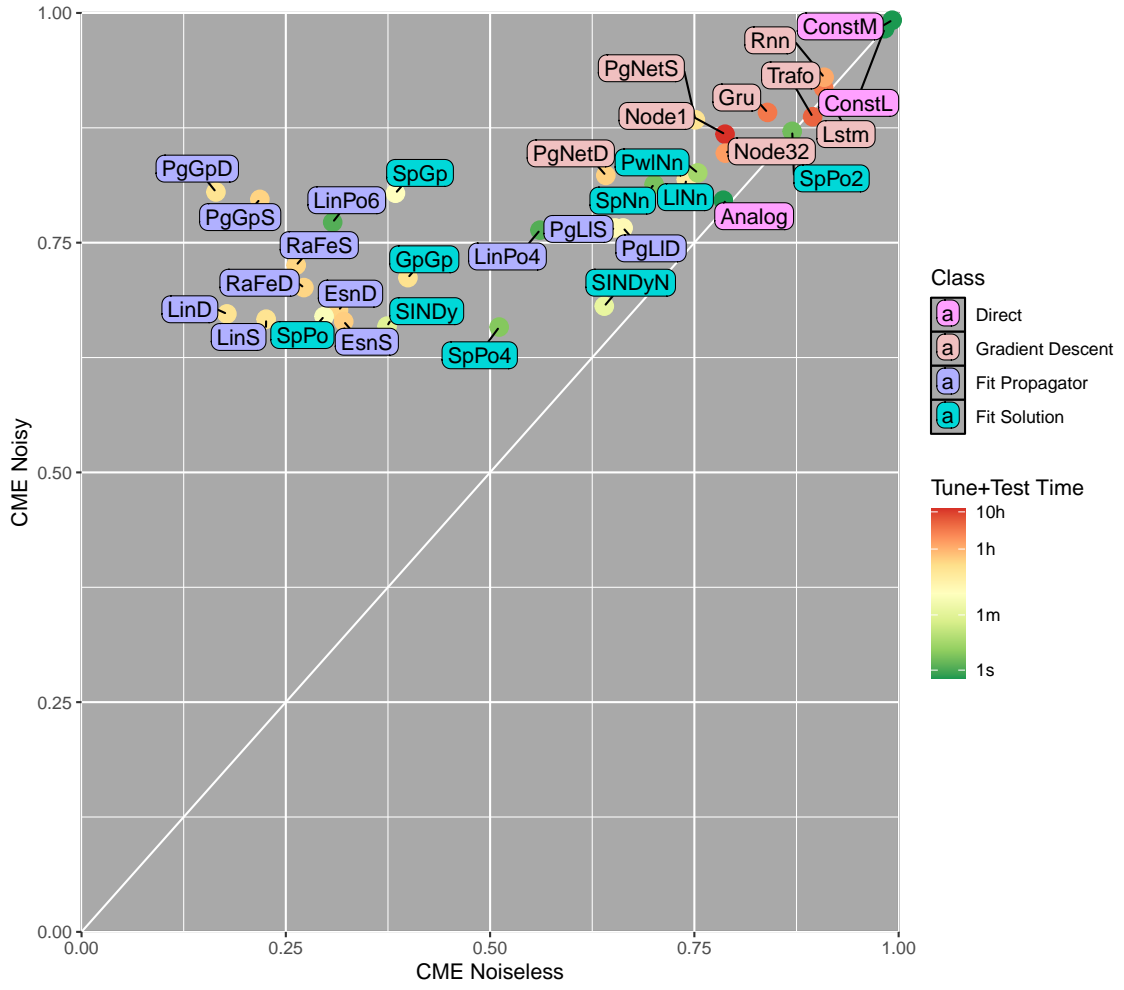


Figure 10: Same as Figure 4 but for LORENZ63NONPAR with Constant Timestep.

Cumulative Maximum Error for Test Data of LORENZ63STD with Random Timestep

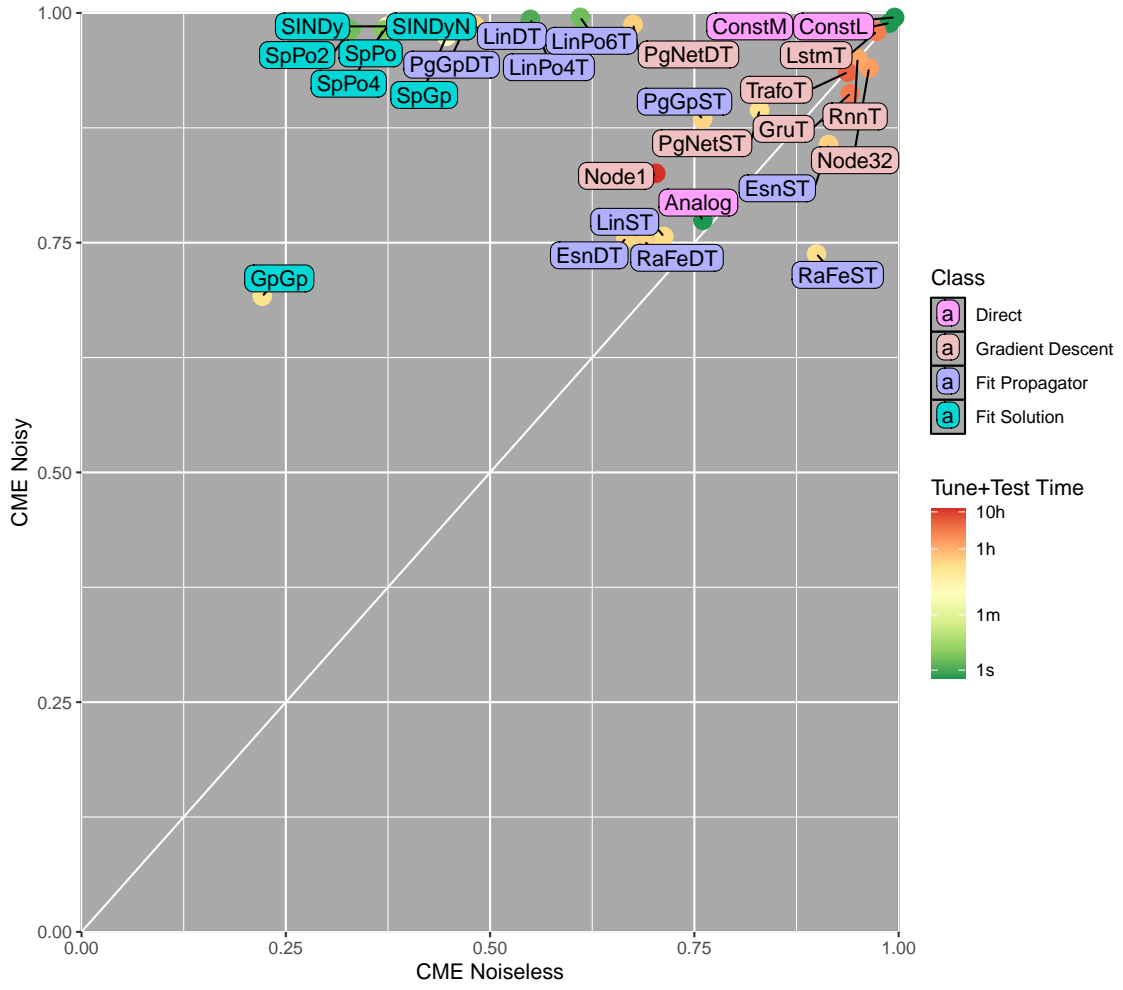


Figure 11: Same as Figure 4 but for LORENZ63STD with Random Timestep.

Cumulative Maximum Error for Test Data of LORENZ63RANDOM with Random Timestep

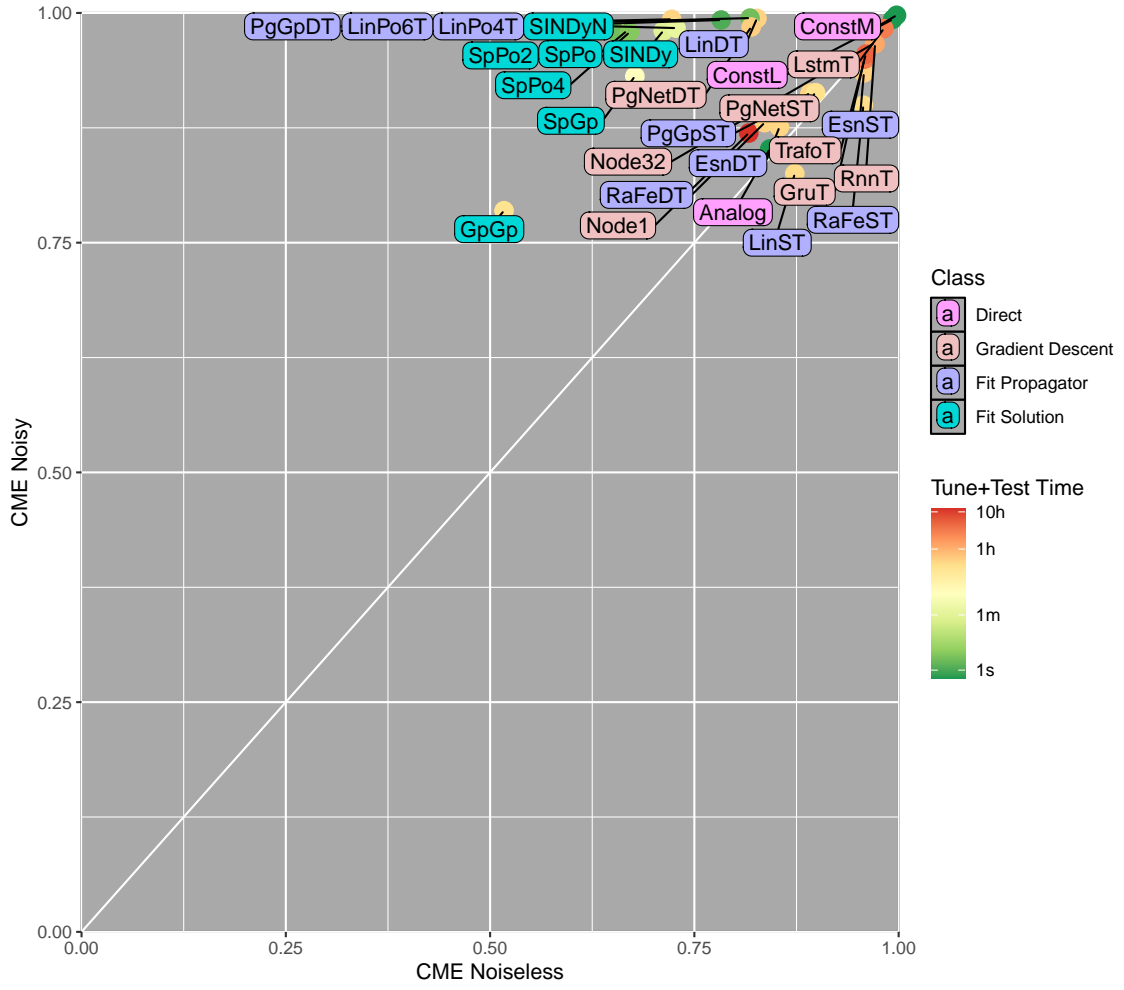


Figure 12: Same as Figure 4 but for LORENZ63RANDOM with Random Timestep.

Cumulative Maximum Error for Test Data of LORENZ63NONPAR with Random Timestep

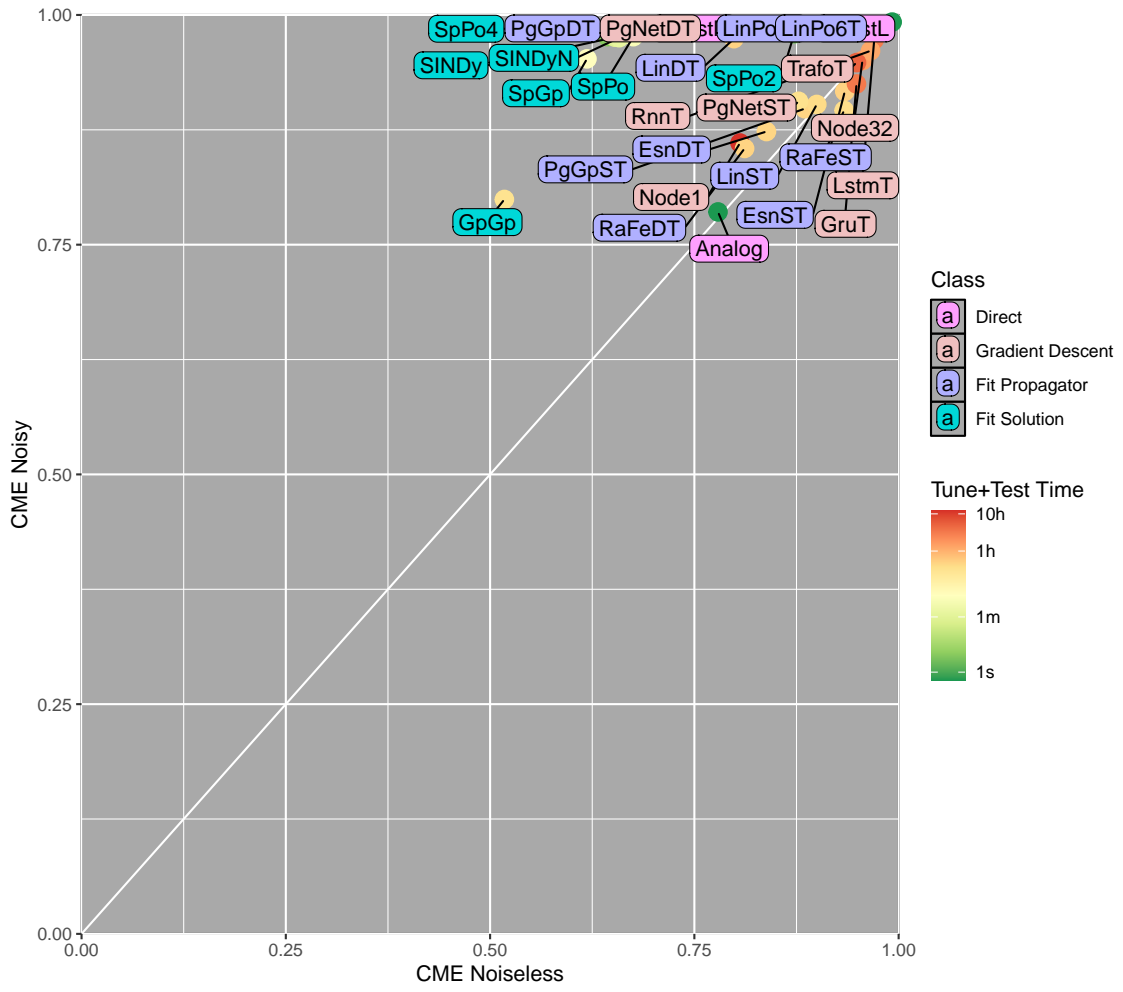


Figure 13: Same as Figure 4 but for LORENZ63NONPAR with Random Timestep.

Cumulative Maximum Error for Test Data of LORENZ63STD

Name	Class	Model	Variant	Noisefree						Noisy					
				$n = 10^3$		$n = 10^4$		$n = 10^5$		$n = 10^3$		$n = 10^4$		$n = 10^5$	
				#	CME	#	CME	#	CME	#	CME	#	CME	#	CME
LinPo6	Fit Prop.	Lin	Poly6	9	0.15	1	0.0000086	1	0.000024	19	0.85	14	0.76	14	0.74
LinD	Fit Prop.	Lin	D	1	0.010	2	0.000038	2	0.000056	4	0.65	4	0.58	4	0.56
LinS	Fit Prop.	Lin	S	2	0.021	3	0.00021	3	0.00024	3	0.65	3	0.58	3	0.56
SpPo4	Fit Solu.	Spline	Poly4	6	0.044	4	0.0034	6	0.0039	9	0.78	7	0.64	8	0.62
SpPo	Fit Solu.	Spline	Poly	4	0.021	5	0.0041	7	0.0039	1	0.61	2	0.53	1	0.54
SINDy	Fit Solu.	SINDy		7	0.050	6	0.011	9	0.011	14	0.83	10	0.66	6	0.60
PgGpD	Fit Prop.	GP	D	13	0.26	7	0.012	4	0.00047	13	0.83	19	0.77	16	0.75
SpPo2	Fit Solu.	Spline	Poly2	3	0.021	8	0.014	10	0.014	1	0.61	1	0.53	1	0.54
SINDyN	Fit Solu.	SINDy	norm	8	0.068	9	0.020	11	0.015	12	0.83	11	0.67	23	0.79
LinPo4	Fit Prop.	Lin	Poly4	5	0.038	10	0.026	12	0.025	10	0.80	13	0.75	15	0.74
PgGpS	Fit Prop.	GP	S	15	0.41	11	0.030	8	0.0090	15	0.83	22	0.78	20	0.77
RaFeD	Fit Prop.	RandFeat	D	12	0.19	12	0.054	15	0.072	7	0.70	6	0.64	7	0.61
EsnS	Fit Prop.	ESN	S	14	0.27	13	0.060	14	0.069	5	0.65	12	0.68	9	0.64
EsnD	Fit Prop.	ESN	D	11	0.18	14	0.065	17	0.12	6	0.69	8	0.66	10	0.64
RaFeS	Fit Prop.	RandFeat	S	10	0.18	15	0.084	16	0.074	8	0.71	5	0.62	5	0.58
GpGp	Fit Solu.	GP	GP	16	0.71	16	0.17	5	0.0030	11	0.82	9	0.66	11	0.65
SpGp	Fit Solu.	Spline	GP	19	0.75	17	0.20	13	0.034	18	0.84	18	0.77	13	0.73
PgNetD	Gr. Desc.	NeuralNet	D	17	0.72	18	0.51	21	0.51*	23	0.87	25	0.82	22	0.77*
PgL1S	Fit Prop.	LocalLin	S	23	0.82	19	0.56	19	0.34	16	0.84	16	0.76	18	0.76
PgL1D	Fit Prop.	LocalLin	D	22	0.82	20	0.56	18	0.34	17	0.84	15	0.76	17	0.76
Node32	Gr. Desc.	NODE	bs32	21	0.82	21	0.63	22	0.58*	22	0.87	20	0.78	21	0.77*
PgNetS	Gr. Desc.	NeuralNet	S	18	0.75	22	0.65	23	0.60*	24	0.87	28	0.87	29	0.85*
SpNn	Fit Solu.	Spline		24	0.84	23	0.66	20	0.49	25	0.87	24	0.82	27	0.82
PwLnn	Fit Solu.	PwLin	NN	25	0.84	24	0.69	25	0.65	20	0.86	21	0.78	25	0.81
Analog	Direct	Analog		27	0.89	25	0.75	24	0.63	26	0.89	17	0.76	12	0.71
L1Nn	Fit Solu.	LocalLin	NN	29	0.90	26	0.77	27	0.73	28	0.90	23	0.79	19	0.76
Gru	Gr. Desc.	GRU		20	0.79	27	0.77	26	0.67*	21	0.86	27	0.87	24	0.79*
Trafo	Gr. Desc.	Transformer		28	0.89	28	0.83	29	0.81*	27	0.89	26	0.84	26	0.81*
Rnn	Gr. Desc.	RNN		26	0.85	29	0.85	28	0.77*	29	0.90	29	0.92	28	0.83*
Lstm	Gr. Desc.	LSTM		30	0.90	30	0.88	30	0.90*	30	0.93	30	0.93	30	0.93*
ConstL	Direct	Const	Last	31	0.99	31	0.99	31	0.99	31	0.99	31	0.99	31	0.99
ConstM	Direct	Const	Mean	32	0.99	32	1.0	32	1.0	32	0.99	32	1.0	32	1.0

\*Batch size 1024. Trained on GPUs.

Table 17: Cumulative Maximum Errors (CME) for the test data of LORENZ63STD with data increased and reduced by a factor of 10. The setup  $n = 10^4$  is the default used for all other experiments in the database *DeebLorenz*. The precise error values shown here for  $n = 10^4$  may diverge slightly from those shown in Table 7 as new time series were sampled for this experiment. To make all results within this table comparable, shorter time series ( $n \in \{10^3, 10^4\}$ ) are created from the longest ones ( $n = 10^5$ ) by removing data points from the beginning of the time series, so that the forecasting task is evaluated on the exact same part of the time series for all  $n$ .

Some models, such as *EsnD*, do not improve when increasing the number of observations from  $n = 10^4$  to  $n = 10^5$ , indicating a saturation for the give model complexity. The reservoir size of *EsnD* was fixed to 400, which yields good results across all systems considered in the main part of the article. Increasing the reservoir size to 1000 indeed decreases the error for  $n = 10^5$  observations (CME of 0.031 for noise-free and 0.563 for noisy data).